*VIBRIO* EFFECTOR PROTEIN, VOPQ TARGETS
THE HOST LYSOSOME TO MANIPULATE AUTOPHAGY

APPROVED BY SUPERVISORY COMMITTEE

Kim Orth, Ph.D.

Benjamin Tu, Ph.D.

Michael Shiloh, Ph.D.

Joel Goodman, Ph.D.

DEDICATION

To my family

ACKNOWLEDGMENTS

First and foremost, I would like to thank my mentor Kim Orth. I could not have asked for a more strong, positive and smart mentor. You have been incredibly understanding and supportive throughout the years and have inspired my science. Your enthusiasm is unrivaled and helps keep science exciting and fun. Thank you for providing me with amazing opportunities and freedom to grow as a young scientist.

Thank you to my collaborators, Vincent Starai and Terry Bennett. Thank you, Vinny for your expertise and patience with this project. Your humor and encouragement has helped me stay positive even when I was struggling with the project. Thank you for welcoming me into your lab and teaching me the concepts and methods of vacuole fusion.

Thank you Dara Burdette and Phi Luong for the initial studies on VopQ. Phi, thank you for being there as a mentor even years after you graduated. Thanks to all the past and current lab members: Yi Heng-Hao, Lingling Zhang, Anne-Marie Krachler, Chris Broberg, Melanie Yarborough, Herman Gonzalez, Dor Salomon, Marcela Santos, Jessie Fernandez, Nicole De Nisco, Peng Li, Hyeilin Ham, TJ Calder, Andrew Woolery and Alex Klimko. Orth lab is a lively and inspiring place to work and I'm thankful to each member for shaping the lab.

Thank you to my committee members: Ben Tu, Joel Goodman and Michael Shiloh. Each of you made important contributions to my work and your guidance has definitely made graduate school easier to navigate. Ben, thank you for all the valuable input and discussions on my project. Joel, thank you for the career advice and help on my CV. Michael, thank you for helping me on my qualifying exam and translational work. I would like to thank the

UTSW community for providing such a great collaborative environment for science; special thanks to Eric Olson and the molecular biology department. Thank you, Helen Yin, for giving me the opportunity to be part of the Mechanism of Disease program. I'd like to thank all the labs that have provided valuable reagents and helpful discussions: Alto lab, Hooper lab, Rizo-Rey lab, Radhakrishnan Lab, Levine lab, Tu Lab, Li Lab and Jiang lab. Special thanks to Alto lab for microinjection equipment and helpful discussion during joint lab meeting. Thank you Sohini Mukherjee for training me on liposome assays and letting me use your equipment. Thank you Hui Zheng for performing the lipid bilayer assays and letting me use your FPLC. Thank you Lisa Kinch for the multiple VopQ bioinformatics analyses. Thank you Chad Brautigam for training me in Circular Dichroism. Thank you Diana Tomchick, Helen Aronovich and Zhe Chen for all the help in the crystallography core. Diana, you have been so generous with your time, thank you so much for all the suggestions and continual interest in my project.

Last but not least, I would like to thank my friends and family for all the support throughout my graduate studies. Thank you for putting up with my bad time management skills and understanding my unusual work hours. Thank you for the encouraging words and always believing in me. I could not have made it through graduate school without your company.

# *VIBRIO* EFFECTOR PROTEIN, VOPQ TARGETS THE HOST LYSOSOME TO MANIPULATE AUTOPHAGY

by

ANJU SREELATHA

DISSERTATION

Presented to the Faculty of the Graduate School of Biomedical Sciences

The University of Texas Southwestern Medical Center at Dallas

In Partial Fulfillment of the Requirements

For the Degree of

DOCTOR OF PHILOSOPHY

The University of Texas Southwestern Medical Center at Dallas

Dallas, Texas

August 2014

*VIBRIO* EFFECTOR PROTEIN, VOPQ TARGETS
THE HOST LYSOSOME TO MANIPULATE AUTOPHAGY

ANJU SREELATHA

The University of Texas Southwestern Medical Center at Dallas, 2014

Supervising Professor: Kim Orth, Ph.D.

*Vibrio parahaemolyticus* is a gram-negative marine bacterium that is the major cause of gastroenteritis due to the consumption of contaminated raw or undercooked seafood. *Vibrio parahaemolyticus* harbors two Type III secretion systems. The first, T3SS1, orchestrates a temporally regulated cell death mediated by autophagy, membrane blebbing, followed by cell rounding and eventual lysis of the host cell. One T3SS1 effector protein, VopQ is both necessary and sufficient to induce rapid autophagy during the first hour of infection. Herein, I characterize the biochemical activity of the virulence factor VopQ, a novel *Vibrio parahaemolyticus* protein with no homology to any proteins outside of the *Vibrio* species. VopQ binds to the conserved $V_o$ domain of the V-ATPase that is enriched on the lysosomal

membrane and causes deacidification of the lysosomes within minutes of entry into the host cell. VopQ forms an ~18 angstrom gated channel that facilitates outward-rectified flux of ions across lipid bilayers. These studies show how a bacterial pathogen uses a novel, targeted pore forming effector to alter autophagic flux by manipulating the partitioning of small molecules and ions. Additionally, we demonstrate that VopQ is also a potent inhibitor of vesicular membrane fusion using *in vitro* membrane fusion. The inhibition of membrane fusion appears to be independent of VopQ's pore-forming activity. VopQ inhibits the final step of membrane fusion by inhibiting trans-SNARE complex formation. In order to delineate the two inhibitory functions of VopQ, deacidification and membrane fusion, I use mutational, biochemical and crystallographic studies. Elucidating the molecular mechanism of VopQ not only provides a better understanding of *Vibrio parahaemolyticus* pathology but also offers new insight into the host cell mechanisms of autophagy and vesicle fusion.

TABLE OF CONTENTS

PRIOR PUBLICATIONS

Ham H*, **Sreelatha A***, Orth K (2011) Manipulation of host membranes by bacterial effectors. Nat Rev Microbiol 9: 635-646. *co-first authors. PMID: 21765451

**Sreelatha A**, Bennett TL, Zheng H, Jiang QX, Orth K, Starai VJ (2013) Vibrio effector protein, VopQ, forms a lysosomal gated channel that disrupts host ion homeostasis and autophagic flux. Proc Natl Acad Sci USA 110: 11559-11564. PMID: 23798441

**Sreelatha A**, Orth K, Starai VJ (2013) The pore-forming bacterial effector, VopQ, halts autophagic turnover. Autophagy 9: 2169-2170. PMID: 24145145

Lewallen DM, **Sreelatha A**, Dharmarajan V, Madoux F, Chase P, et al. (2013) Inhibiting AMPylation: A Novel Screen To Identify the First Small Molecule Inhibitors of Protein AMPylation. ACS Chem Biol. PMID: 24274060

Munoz E, **Sreelatha A**, Garriga R, Baughman RH, Goux WJ (2013) Amyloidogenic peptide/single-walled carbon nanotube composites based on tau-protein-related peptides derived from AcPHF6: preparation and dispersive properties. J Phys Chem B 117: 7593-7604. PMID: 23745842

**Sreelatha A**, Bennett TL, O'Brien K, Jordan KD, Orth K, Starai VJ. Vibrio effector protein, VopQ, inhibits vacuole fusion. Manuscript in preparation.

## LIST OF FIGURES

## LIST OF TABLES

## LIST OF DEFINITIONS

2XYT – 2 times yeast tryptone

Å – angstrom

*atg* – autophagy gene

ATP– Adenosine triphosphate

CD – Circular dichroism

CNF – Cytotoxic necrotizing factor

CV – column volume

DDM – n-dodecyl β-D maltoside

DMEM – Dulbecco's Modified Eagle Medium

DOPS – 1,2-dioleoyl-sn-glycero-3-phospho-L-serine

DTT – dithiothreitol

*E. coli* – *Escherichia coli*

FBS – Fetal Bovine Serum

FD – FITC dextran

FITC – fluorescein isothiocyanate

FPLC– Fast protein liquid chromatography

GEF– Guanine nucleotide exchange factor

GFP – Green Fluorescent Protein

GST – Glutathione S-transferase

HEPES – *N*-(2-hydroxyethyl)piperazine-*N'*-(2-ethanesulfonic acid)

His – Histidine

IPTG – Isopropyl-beta-D-thiogalactopyranoside

kDa – kilodalton

LAMP – lysosome associated membrane protein

LB – Luria Bertani

LC3 – Microtubule-associate protein Light Chain 3

LDH – Lactate Dehydrogenase

MAPK – Mitogen activated protein kinase

MBP – Maltose binding protein

MLB – Marine LB

MOI – Multiplicity of infection

NSF– N-ethylmaleimide sensitive fusion protein

OD – Optical Density

OG – Octyl β-D-glucopyranoside

PBS – Phosphate-buffered saline

PCR – Polymerase chain reaction

PDB – Protein data bank

PI3K – Phosphatidylinositol 3-kinase

POPC – 1-palmytoyl-2-oleoyl-sn-glycero-3-phosphocholine

PX – Phox

p70S6K – p70 S6 kinase

SDS-PAGE – Sodium dodecyl sulfate-polyacrylamide gel electrophoresis

SNARE – Soluble NSF attachment protein receptor

SNAP – α- soluble NSF attachment protein

T3SS –Type three secretion system

TDH – Thermostable direct hemolysin

TOR – Target of rapamycin

TRH –TDH related hemolysin

TRD – Texas red dextran

V- ATPase – vacuolar ATPase

Vep – Vibrio effector protein

*V. parahaemolyticus – Vibrio parahaemolyticus*

Vop – Vibrio outer protein

YCD – Yeast complete dropout media

# CHAPTER ONE

## Introduction and Literature Review

### *Vibrio parahaemolyticus*

*Vibrio parahaemolyticus* is a Gram-negative halophilic bacterium found in marine and estuarine environments. It is the leading cause of seafood borne illness in the United States causing about 4500 cases per year (*1, 2*). Upon consumption of contaminated seafood, *V. parahaemolyticus* causes acute gastroenteritis leading to diarrhea, nausea, vomiting and fever (*3*). In some cases, *V. parahaemolyticus* can also infect open wounds and/or lead to septicemia. While most *V. parahaemolyticus* infections are self-limiting, it may be life threatening in patients who are immune compromised or have underlying conditions such as liver diseases.

The bacterium was first isolated in 1950 from Japanese patients who consumed contaminated fish, *shirasu (4-6)*. Since the initial outbreak, the reported cases have increased more than ten fold (*7*). In particular, *V. parahaemolyticus* infections are common in the summer months because the bacteria thrive in warm, saline waters (**Figure 1A**). Concomitantly, recent global increases in water temperatures have led to the spread of *V. parahaemolyticus* as far north as Alaska. In fact, human infection rates have increased more than 40% in the last five years alone (*8*)(**Figure 1B**).

Aside from human infections, *V. parahaemolyticus* also poses a threat to marine organisms such as shrimp and fish. *V. parahaemolyticus* causes acute hepatopancreatic

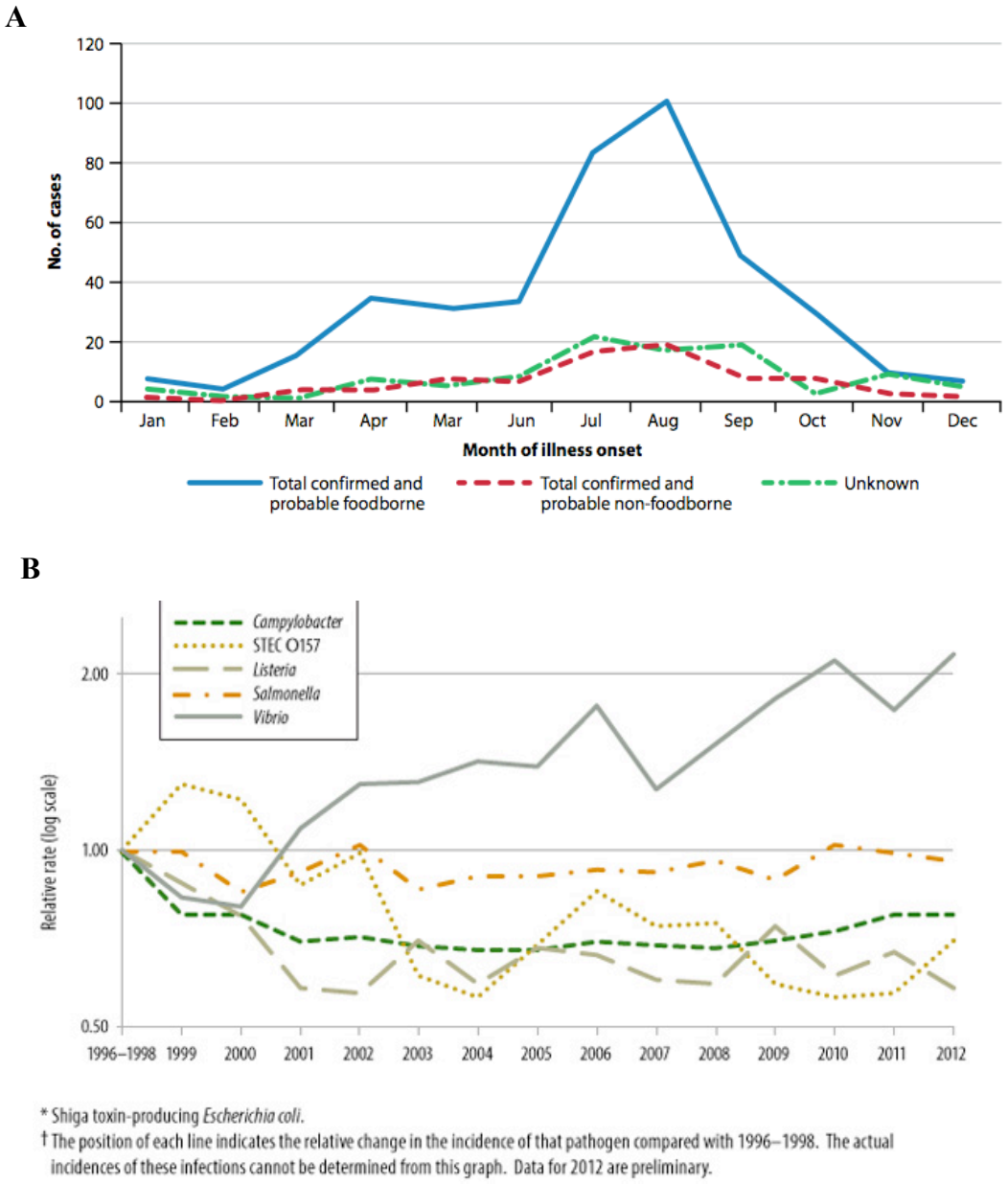


**Figure 1. Epidemiology for select bacterial pathogens. (A)** The number of *Vibrio* incidences in 2011 shows increased number of cases in the summer months of July and August. Figure reproduced from (*7*) **(B)** Relative rates of enteric infections over the course of 16 years show an increasing rate of Vibriosis. Figure reproduced from (*8*)

necrosis syndrome in shrimp leading to early mortality (*9, 10*). In 2013, more than a billion dollars was lost due to *V. parahaemolyticus* infections in shrimp farms in Southeast Asia. In sea bass, *V. parahaemolyticus* causes skin lesions, muscle hemorrhages and death (*11*). The health and economic burden of *V. parahaemolyticus* infections underscore the need for a better understanding of pathogenesis.

Pandemic strains of *V. parahaemolyticus* produce toxins such as Thermostable Direct Hemolysin (TDH) and TDH-Related Hemolysin (TRH), and harbor two type three secretion systems (T3SS)(*12*) (**Figure 2**). TDH is an exotoxin that forms a tetrameric pore of 23Å diameter with low ion selectivity on the host membrane (*13*). TDH induces cytotoxicity and enterotoxicity marked by fluid accumulation in the intestines (*14*). TRH, similar to TDH, also forms a pore leading to enterotoxicity (*15*). Strains with TDH are denoted as $KP^+$ (Kanagawa Phenomenon), which is the hemolytic activity observed on blood agar (*16*). However $KP^-$ *V. parahaemolyticus* strains are still cytotoxic due to the presence of the other virulence factors such as the T3SSs (*17*).

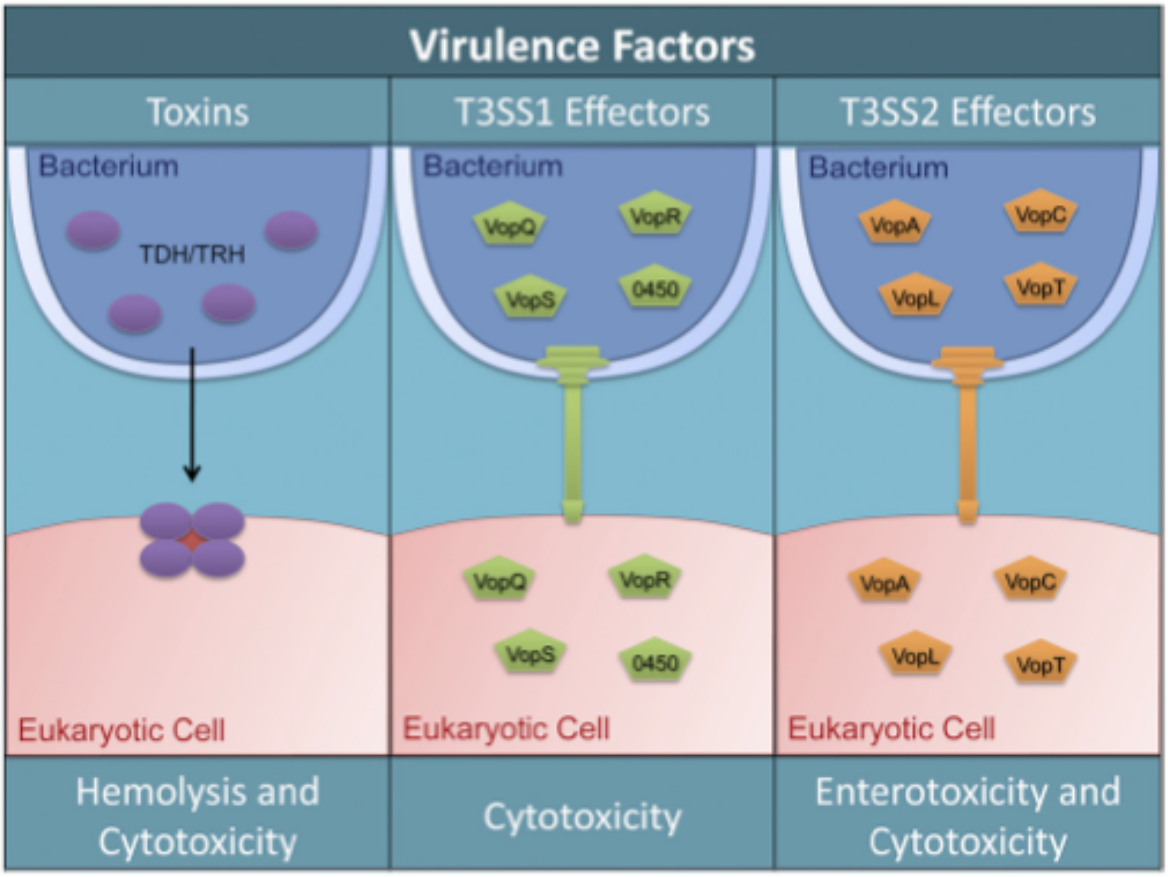


**Figure 2. *Vibrio parahaemolyticus* virulence factors.** *V. parahaemolyticus* produces two toxins and two T3SSs that contribute to rapid host cell death. TDH and TRH toxins causes hemolysis and cytotoxicity. The T3SS1 causes cytotoxicity and T3SS2, using its own unique repertoire of effectors causes enterotoxicity and cytotoxicity. Figure reproduced from (*18*)

**Type III Secretion System**

During infection, *V. parahaemolyticus* uses the T3SS to disrupt host cellular signaling and induce cytotoxicity (*19*). T3SS is a syringe-like apparatus used to translocate bacterial proteins, effectors, into the host cell. Effector proteins are bacterial equivalents of viral oncogenes in that they mimic endogenous eukaryotic activity. As such, effectors can be used as a tool in studying host-pathogen interaction and elucidating eukaryotic signaling. In the bacteria, these proteins are kept quiescent through a number of mechanisms such as the action of chaperones that can hold the effector in an inactive form in the bacteria. The first 100 amino acids, approximately, of a T3SS effector contains the chaperone-binding region. Effectors can also have an overlapping sequence encoded in the first 30-125 amino acids that both targets the effector to the T3SS in the bacteria and localizes the effector in the host cell.

*V. parahaemolyticus* has two type III secretion systems that are differentially regulated (*19*). Three strains of *V. parahaemolyticus* are widely used to study T3SSs, and are derived from a clinical isolate. POR1 lacks TDH and TRH, but harbors both T3SS1 and T3SS2, POR2 lacks T3SS1 but harbors T3SS2, while POR3 lacks T3SS2 and harbors T3SS1 (**Table 1**). T3SS1 is found in all strains; it is induced by low calcium and high temperatures and causes host cell cytotoxicity in tissue culture experiments (*12*). T3SS2 is associated with clinical pathogenic strains; it is induced by bile salts and contributes to the enterotoxicity in the animal host intestines (*20, 21*). T3SS2 appears to be a more recent acquisition by *V. parahaemolyticus* and is shared by a number of Vibrio species (*22*). The known effectors encoded on T3SS2 include VopT (vpa1327), VopA (vpa1346), VopL (vpa1370), VopC (vpa1321) and VopV (vpa1357). Several of these effectors have conserved domains and

targets **(Table 2)**. For example, VopT has an ADP ribosyltransferase domain that catalyzes transfer of ADP ribose to Ras GTPase (*23*). VopA is an acetyltransferase that inhibits the MAPK signaling by preventing phosphorylation of MAPKK (*24, 25*). VopL contains three WH2 domains that bind actin and act as nucleators for actin polymerization (*26*). Studies with VopL have shed light into eukaryotic actin dynamics and underscore the contribution of effectors in the study of eukaryotic signaling (*27-29*). VopC belongs to the family of Cytotoxic Necrotizing Factor (CNF) toxins that deamidate Rho GTPases thereby trapping the GTPase in its GTP-bound active form. This induces host actin cytoskeleton changes such as the formation of ruffles and filopodia aiding in bacterial invasion of the host cell (*30*). This discovery revealed for the first time that *V. parahaemolyticus* could survive and proliferate inside a host cell, bringing a new paradigm into the mechanisms that this pathogen uses during the infection of the host (*30*). There are likely more undiscovered effectors that contribute to the pathogenicity induced by this secretion system.

| Strains | TDH | T3SS1 | T3SS2 | Factors Present | Parental Strain | Ref |
|---|---|---|---|---|---|---|
| RIMD2210633 | + | + | + | TDH, T3SS1, T3SS2 | Clinical isolate | (*12*) |
| POR1 | – | + | + | T3SS1, T3SS2 | RIMD2210633 | (*14*) |
| POR2 | – | – | + | T3SS2 | POR1 | (*19*) |
| POR3 | – | + | – | T3SS1 | POR1 | (*19*) |

**Table 1.** *V. parahaemolyticus* strains used to dissect the contribution of virulence factors.

| Effector | Function | Ref |
|---|---|---|
| VopQ | Lysosomal gated channel | (*31*) |
| VopS | Rho GTPase AMPylater | (*32*) |
| VopR | Unknown | (*33*) |
| VPA0450 | PI(4,5)$P_2$ phosphatase | (*34*) |
| VopA/P | MAPK kinase acetyltransferase | (*24*) |
| VopC | Rho GTPase deamidase | (*30*) |
| VopL | Actin nucleator | (*26*) |
| VopT | ADP-ribosyltranferase | (*23*) |

**Table 2.** *V. parahaemolyticus* secretes a variety of effectors through T3SS1 and T3SS2 that manipulate autophagy, GTPase signaling and actin cytoskeleton.

Effectors from T3SS1 orchestrate a temporally regulated cell death. T3SS1 induces autophagy, membrane blebbing, and cell rounding eventually resulting in lysis of the host cell (**Figure 3**) (*35*). A number of effectors have been shown to be translocated by T3SS1, including VopQ (also known as VepA) (*vp1680*), VopR (*vp1683*), VopS (*vp1686*), and VPA0450 (*20*). VopS uses a Fic domain to AMPylate Rho GTPases resulting in collapse of the actin cytoskeleton and rounding of the host cells (*32*). VPA0450 encodes a phosphatidylinositol-5-phosphatase that hydrolyzes $PI(4,5)P_2$ on the plasma membrane. This causes membrane blebbing and accelerates lysis of the host cell (*34*). The molecular mechanism of VopR has not been characterized although recent studies show that VopR and other effectors contain a BPD (Bacterial Phosphoinositide-binding Domain) that localizes effectors to phosphatidylinositols in the host cell. This domain is speculated to help in the refolding of effectors when delivered to the host cell. VopR, VopS and VPA0450 share a N-terminal phosphoinositide-binding domain (*33*). Therefore it is reasonable to speculate that VopR targets a membrane lipid or protein similar to VopS and VPA450. VopQ is one of the initial effectors to act on the host cell by inducing autophagy within an hour of *V. parahaemolyticus* infection (*36*). Understanding the mechanism by which VopQ induces autophagy is essential in understanding *Vibrio* infection and could give new insights into the mechanisms of eukaryotic autophagy.

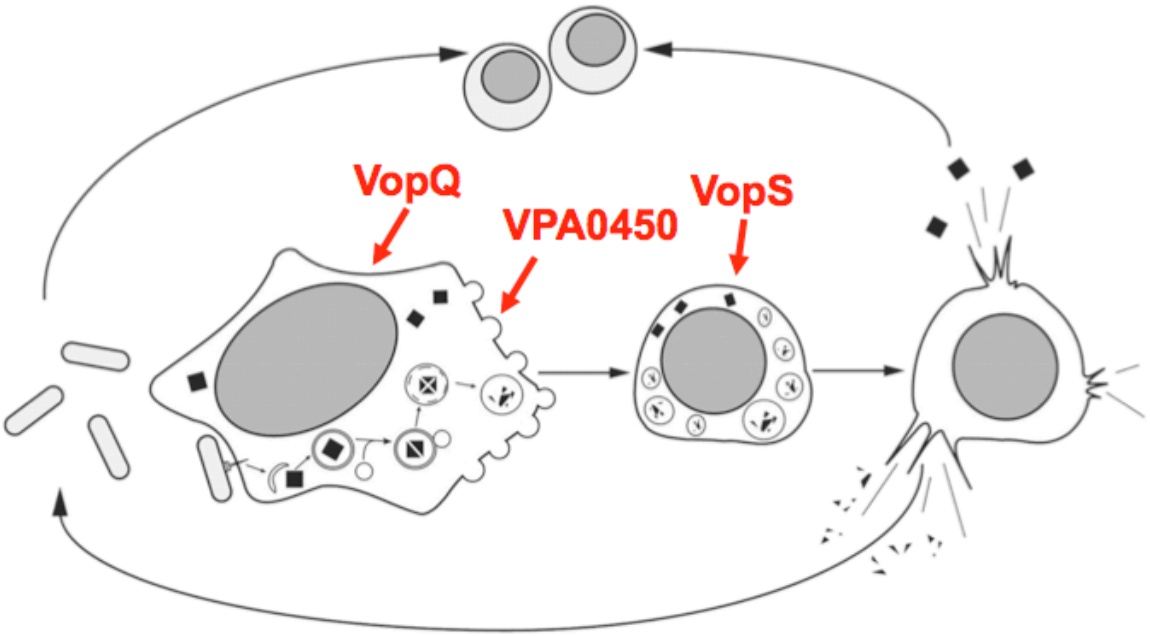


**Figure 3. T3SS1 orchestrates multifaceted cell death.** Upon infection, *V. parahaemolyticus* uses its T3SS1 to inject effectors into the host cell to induce autophagy (VopQ), membrane blebbing (VPA0450), cell rounding (VopS) and cell lysis. Figure adapted from (*35*) Copyright (2008) National Academy of Sciences, U.S.A.

**Autophagy**

Autophagy is a cellular process by which cells degrade and recycle cellular contents (*37*). Macroautophagy proceeds through four distinct steps: initiation, nucleation, maturation and fusion with the lysosome (*38*) (**Figure 4**). In the last decade, many genes involved in autophagy (*ATG* genes) have been identified using yeast genetic studies and mammalian autophagy screens (*39*). Upon starvation, Atg13 associates with Atg1 initiating the formation of the preautophagosomal structure. Following initiation, PI 3-kinase, Atg9, and Atg2 are recruited to the autophagosomal membrane along with other Atg proteins (nucleation). Maturation depends on two ubiquitin-like conjugation systems: Atg5-Atg12 and Atg8-phosphatidyethanolamine. Upon induction of autophagy, Atg8 is lipidated and conjugated to phosphatidylethanolamine. Similarly, the mammalian homologue of Atg8, LC3, resides in the cytosol under normal conditions (LC3-I), and is conjugated to phosphatidylethanolamine to form LC3-II in an Atg5-dependent manner upon induction of autophagy. During elongation and maturation, LC3-II localizes to autophagosomal membranes, which can be monitored using microscopy and western blot. LC3-II localization is a commonly used marker for the induction of autophagy (*40, 41*). In the final step of autophagy, the outer membrane of the autophagosome fuses with the lysosome to form the autolysosome.

Starvation-induced autophagy is regulated by two important signaling pathways originating from mTOR (mammalian Target Of Rapamycin) and PI 3-kinase (**Figure 5**). The protein kinase mTOR senses intracellular nutrient levels and serves as a negative regulator of autophagy. Under rich nutrient conditions, mTOR phosphorylates Atg13, thereby preventing its interaction with Atg1. PI 3-kinase acts upstream of mTOR, and also plays a

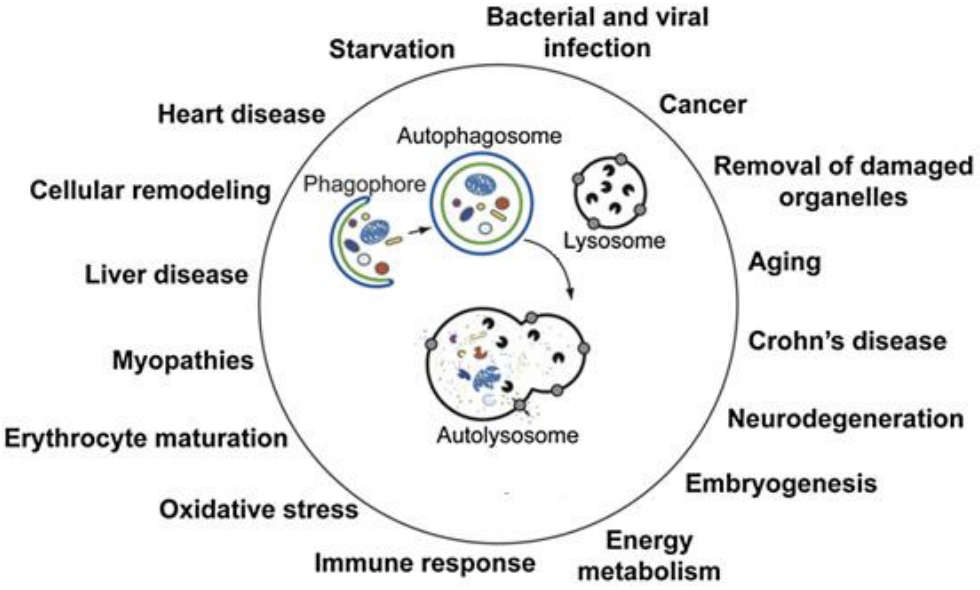


**Figure 4. Induction and progression of autophagy.** Autophagy begins with the formation of a double membrane that encapsulates part of the cytoplasm or organelles to form an autophagosome. The autophagosome then fuses with the lysosome to form the autolysosome. The contents are then degraded and used as nutrients for cellular processes. Autophagy plays a role in housekeeping as well as a response to nutrient deprivation, bacterial invasion, hypoxia and other stress conditions. Furthermore, autophagy has been linked to many diseases such as cancer, neurodegeneration and cardiomyopathy. Figure reproduced from (*40*)

role in formation of the autophagosome. PI 3-kinase complex recruits Atg5-Atg12 to the autophagosomal membrane to facilitate Atg8 lipidation. Many genes involved in the PI 3-kinase dependent autophagy pathway have been identified using genetic screens in *Saccharomyces cerevisiae,* in which autophagy is mainly a starvation response. However, little is known about a pathological autophagy response that is PI 3-kinase independent.

Autophagy is a vital innate immune mechanism that defends the host from intracellular pathogens (*42*). For example, the autophagy pathway degrades the intracellular pathogens *Mycobacterium tuberculosis* and *Listeria monocytogenes* by lysosomal fusion (*43, 44*). However, some pathogens have evolved strategies to subvert autophagy and use it to their own advantage by interrupting autophagosome maturation. This not only prevents their detection by the host defense, but may also provide nutrients for the bacteria to survive. Multiple studies have used bacterial effectors as a tool to study the vesicle trafficking and autophagic pathways (*45*). Therefore, characterizing the mechanism by which VopQ induces autophagy would not only be beneficial in understanding host-pathogen interaction, but could also be significant in advancing our understanding of the autophagic pathway. Autophagy is implicated in numerous diseases such as Alzheimer's disease, Parkinson's disease, liver diseases, cancer, and cardiomyopathy (*40*). Hence, studying VopQ-induced autophagy might reveal novel therapeutic strategies to treat these diseases.

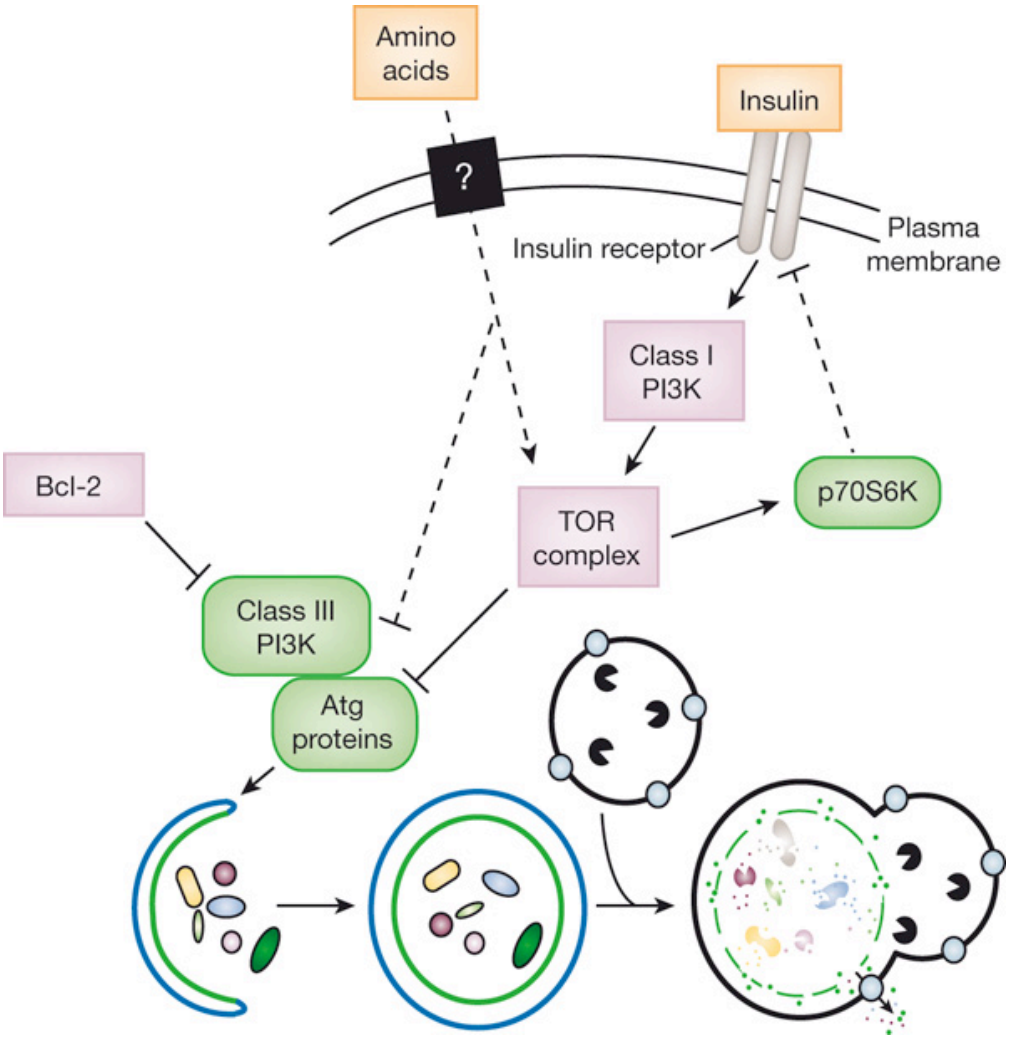


**Figure 5. Simplified model of the autophagy pathway.** Autophagy can be triggered by various factors such as nutrient deprivation or growth factors. Proteins labeled in green are stimulatory while proteins labeled in pink are inhibitory for autophagy. Figure reproduced from (*37*)

**Vesicle fusion**

Vesicles or "bubbles within the cell" play a role in key cellular processes such as autophagy, protein transport, exocytosis and endocytosis (**Figure 6**). Hence, imbalances in vesicle trafficking and fusion lead to a variety of diseases such as diabetes, neurological, and immunological disorders (*46*). The 2013 Nobel Prize was awarded to the three scientists, Randy Schekman, James Rothman and Thomas Sudhöf, who made pivotal discoveries in understanding membrane trafficking. Randy Schekman used yeast genetics to identify the genes involved in trafficking such as Rab-GTPases and dissect their functions (*47, 48*). James Rothman used the different approach of biochemical reconstitution to identify important proteins involved in vesicle fusion such as NSF and SNAP proteins (*49, 50*). Thomas Sudhöf studied the signaling behind this important process of vesicle transport in neurons and showed that calcium-sensitive proteins regulate the release of cargo from vesicles (*51, 52*). Together the three defined vesicle trafficking machinery and signaling that paved the way for studies on vesicle fusion.

Yeast vacuoles are an established model to study membrane fusion due to the ease of isolation and conserved fusion machinery (*53*). Vacuolar fusion proceeds through three distinct and biochemically separable steps: priming, docking, and fusion. During priming, the SNARE chaperones Sec17p and Sec18p (α-SNAP/NSF) disassemble cis-SNARE complexes in an ATP-dependent manner (**Figure 7**)(*54*). Docking requires the activities of the Rab-GTPase Ypt7p and the multi-subunit tethering complex, the HOPS (homotypic fusion and vacuole protein sorting) complex, to tether vacuoles, and enable the formation of the essential trans-SNARE complexes composed of Vam3p, Vti1p, Vam7p, and Nyv1p

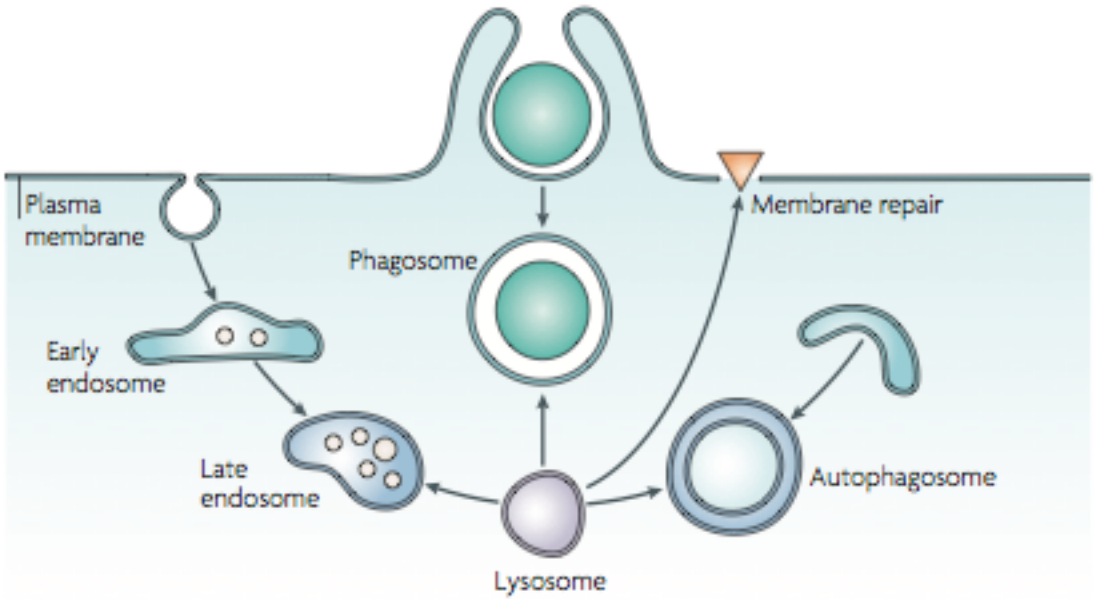


**Figure 6. Vesicle trafficking and fusion**. Cargo is endocytosed at the plasma membrane and encapsulated in the early endosome, which matures into the late endosome, and fuses with the lysosome. Autophagic cargo such as damaged organelles or pathogens are encapsulated in the autophagosome that also fuses with the degradative lysosome. Figure reproduced from (*55*)

across apposed membranes (*56-58*). During the final fusion step, trans-SNARE complexes catalyze the mixing of lipid bilayers, and luminal contents are exchanged.

Many proteins and regulatory lipids are involved in regulating membrane fusion. One such key protein is the V-ATPase (**Figure 8**) (*59*). The V-ATPase is a multisubunit protein complex that is composed of 2 sectors. The $V_1$ sector is composed of an eight-protein complex that hydrolyze ATP to provide energy for the $V_o$ sector. The $V_o$ sector is composed of six subunits that function as a proton pump to acidify intracellular organelles. The loss of the V-ATPase is lethal in eukaryotes highlighting the importance of this vital protein complex. However, yeast that lack subunits of the V-ATPase exhibit conditional lethality that is rescued in acidic media. Besides its acidification function, V-ATPase has been implicated in several pathways including autophagy and membrane fusion (*60*).

Several acidification independent roles of the V-ATPase have been suggested. One model for membrane fusion suggests that the $V_o$ sector forms a pore that creates a hemifusion intermediate between two vesicles during fusion (*61-63*). Point mutations in the $V_oC$ subunit inhibit vesicle fusion but do not disrupt proton translocation (*61*). Moreover, point mutations of the $V_oA$ subunit that retain acidification function disrupt fusion and exocytosis (*64*). Even though the role of $V_o$ in fusion has been demonstrated in various model organisms, it remains controversial.

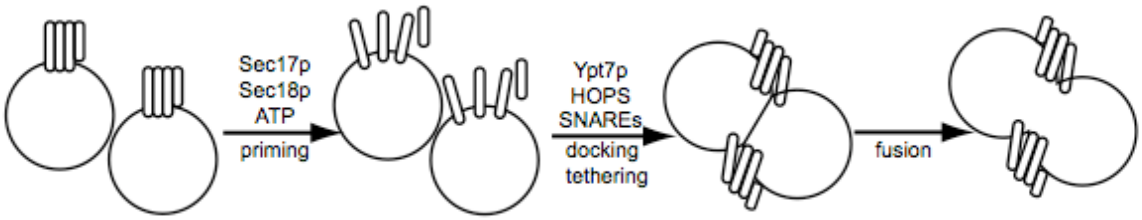


**Figure 7. Vesicle fusion occurs in three distinct steps that are regulated.** Sec17p (α-SNAP) and Sec18p (NSF) disassemble the cis-SNARE complexes during priming. Next, the Ypt7 GTPase and the HOPS complex aid in docking and tethering of the vacuoles. In the final step of fusion, the lipid and lumenal contents mix.

**VopQ**

Bacterial effectors serve as a powerful tool in elucidating novel eukaryotic signaling pathways. With the discovery of bacterial effectors that manipulate host membranes, many eukaryotic vesicle trafficking pathways have been unveiled, and new questions have arisen about the mechanisms of bacterial effectors. VopQ is a unique bacterial effector with no apparent homology to any protein of known function. Previous work from our laboratory has shown that VopQ is a cytotoxic effector that accelerates host cell death and is essential in protecting *V. parahaemolyticus* from phagocytic uptake during infection (**Figure 9A&B**) (*36*). Based on microbial genetic studies, VopQ was shown to be necessary for the formation of an extensive network of autophagic vesicles in host cells within an hour of *V. parahaemolyticus* infection (**Figure 9C**) (*36*). Strikingly, recombinant VopQ alone is sufficient to induce this massive accumulation of autophagic vesicles (GFP labeled autophagosomes), observed within minutes of microinjection of recombinant VopQ (pmol concentrations) into eukaryotic cells (**Figure 9D**) (*36*). Note that this occurs independent of other effectors and stimuli from the presence of bacteria.

Although canonical autophagy proceeds through the PI3-kinase pathway, VopQ-induced autophagy is PI3-kinase *independent*. Using the PI 3-kinase inhibitor wortmanin, Burdette et al (2009) demonstrated that VopQ-induced autophagy is independent of the PI 3-kinase pathway indicating that VopQ acts through a novel mechanism (*36*). The need to identify and target novel autophagy pathways is highlighted by compounds that target the

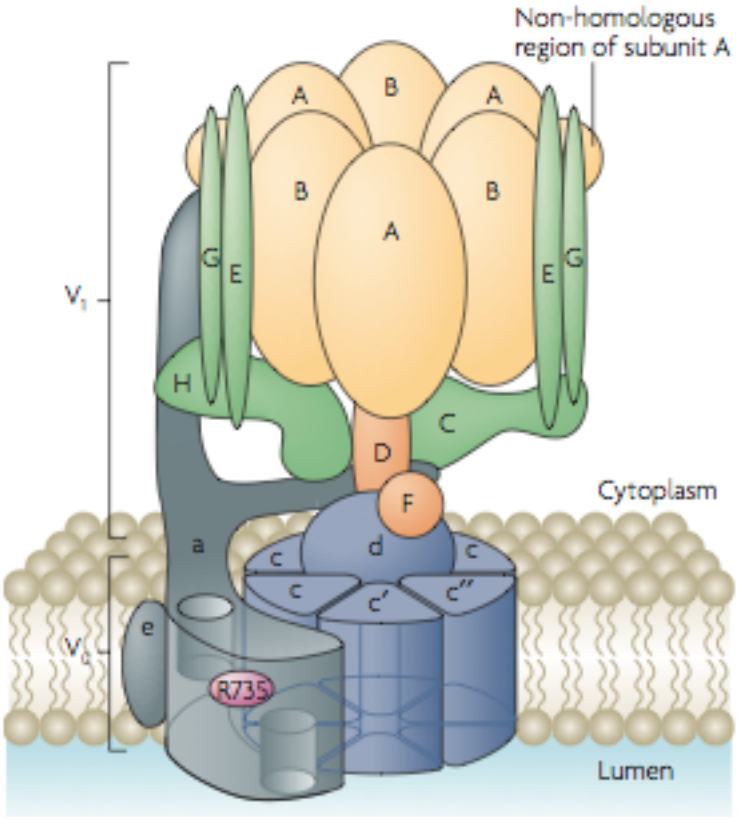


**Figure 8. The V-ATPase.** The V-ATPase is composed of two domains: The $V_1$ domain hydrolyzes ATP while the $V_o$ domain pumps protons into the lumen of acidic organelles. The V-ATPase is involved in many cellular processes such as neurotransmitter uptake, receptor mediated endocytosis and lysosomal degradation. Figure reproduced from (*55*)

canonical autophagy pathway, such as rapamycin, and have significant side effects. Much effort has been directed towards identifying pathways and inhibitors of autophagy for therapeutic use to treat many diseases such as cancer and neurological disorders.

Several pathogenic bacteria target the Mitogen-Activated Protein Kinases signaling pathway to alter host immune response (*65*). The MAPK are serine/threonine kinases that relay signaling from the cell surface to the nucleus where they control transcription of cytokines. *V. parahaemolyticus* T3SS2 effector, VopA inhibits the MAPK pathway to inhibit inflammatory response during an infection (*24*). In contrast, VopQ has been shown to activate the MAPK pathway and IL-8 secretion (*66, 67*). Inhibitors of the MAPK pathway diminish VopQ induced IL-8 secretion and pro-inflammatory cell death (*66*). The authors show that VopQ is the major cytotoxic effector from T3SS1; cytotoxicity of strains lacking VopQ is comparable to strains lacking T3SS1 (*67*). Therefore, elucidation of the molecular mechanism of VopQ will help us understand how *V. parahaemolyticus* tempers the host cell death and immune response.

A recent report shows that VopQ interacts with a $V_o$ subunit of the V-ATPase and induces lysosomal rupture in vitro and in vivo (*68*). The authors hypothesized that the V-ATPase acts as a scaffold for VopQ to bind to the lysosomes. VopQ then lyses the lysosomes or "suicide bags" which leads to the release of proteolytic enzymes that induces cell death. However, this hypothesis is mechanistically unfeasible and would not be predicted to occur within the timeframe that VopQ acts (minutes vs. hours) (*36, 69*). Therefore, the molecular mechanism of VopQ-mediated autophagy and cell death remains unclear.

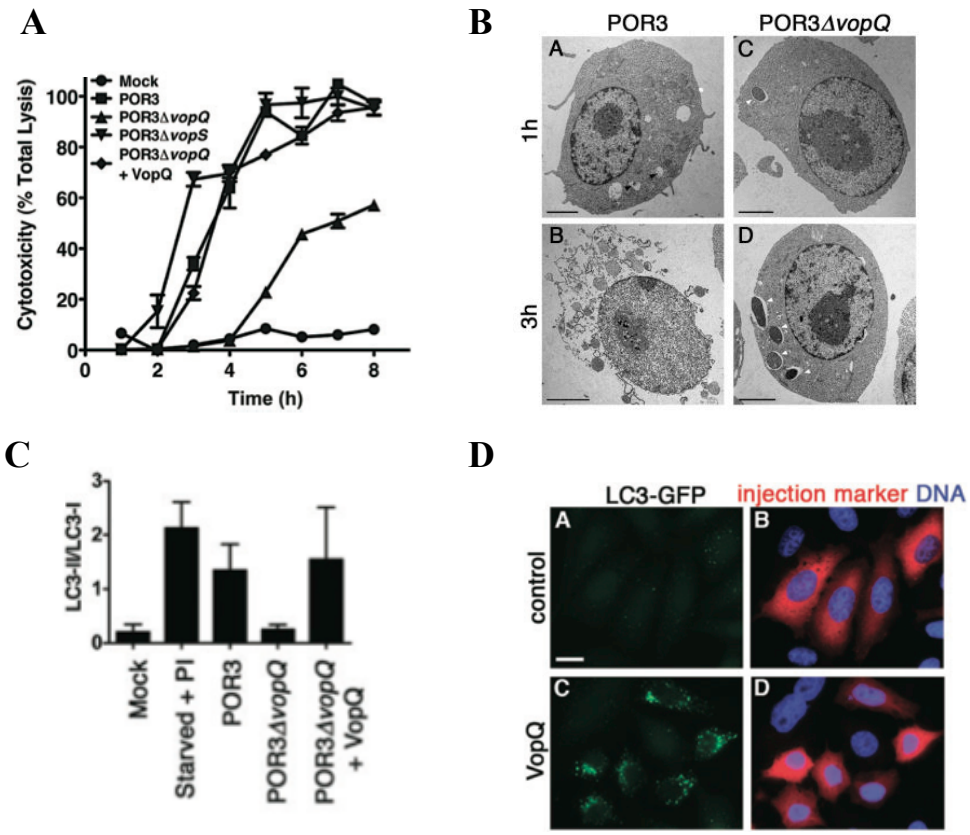


**Figure 9. VopQ is necessary and sufficient to induce autophagy.** GFP-LC3 cells were infected with *V. parahaemolyticus* harboring VopQ (POR3), strain lacking VopQ (POR3Δ*vopQ*), and strain lacking VopQ complemented with VopQ (POR3Δ*vopQ* + VopQ). **(A)** VopQ accelerates T3SS1 mediated cell death. (**B)** VopQ prevents phagocytosis of *V. parahaemolyticus* during POR3 infection of macrophages. Black arrows denote autophagic vesicles. White arrows denote bacteria that have been phagocytosed by the macrophage **(C)** T3SS1-induced autophagy is abolished upon deletion of VopQ, indicating that VopQ is necessary for T3SS1 -induced autophagy. (**D)** GFP-LC3 cells that are microinjected with VopQ accumulate GFP-labeled autophagosomes within 30 minutes indicating that VopQ is sufficient for autophagosome accumulation. Figure reproduced from (*36*)

**Aims of this study**

Defects in autophagic pathways are implicated in numerous human diseases such as neurodegenerative diseases and cancer, as well as defense against pathogen invasion. For example, the induction of autophagy is important in the degradation of intracellular pathogens such as *Mycobacterium tuberculosis*. However, other intracellular pathogens, such as *Legionella pneumophila* and *Coxiella burnetii,* have evolved strategies to harness autophagy to their own advantage by interrupting autophagosome maturation (*70*). Because of the extent to which pathogenic microorganisms must manipulate their host cells during infection, multiple studies have used bacterial virulence proteins as a powerful tool to uncover novel host signaling mechanisms and to further study host-pathogen interactions. The purpose of my study is to use VopQ as a tool to understand eukaryotic signaling and membrane trafficking.

VopQ is a unique bacterial effector that potently induces autophagosome accumulation and cell death. Firstly, I characterize the molecular mechanism by which VopQ alters autophagy. VopQ binds to the V-ATPase to target to the lysosomal membrane where it forms a voltage-gated channel to deacidify the lysosome. Lysosomal deacidification leads to inactivation of the lysosomal degradative proteases and consequent buildup of autophagosomes. These studies unravel a novel mechanism by which pathogens may alter autophagic flux. Next, I study a previously uncharacterized phenotype of VopQ: inhibition of membrane fusion. VopQ inhibits trans-SNARE complex formation and inhibits yeast vacuolar fusion independent of acidification. These studies support an acidification independent role of the V-ATPase in fusion. Finally, in order to gain structural insights into

this multifunctional protein, I used mutational and crystallographic studies to probe for domains. Various point and truncation mutants were used to determine the domain that binds to the V-ATPase and forms a channel. Finally, crystallography was used to study the structure of VopQ bound to its chaperone and VopQ membrane channel.

# CHAPTER TWO

# Materials and Methods

## Bacterial strains

*Vibrio parahaemolyticus* strains were passaged on minimal marine media (MMM) plates. Liquid cultures were grown overnight in marine LB (LB + 3% NaCl). POR3 was a generous gift from Takeshi Honda and Tetsuya Iida (**Table 1**). POR3ΔQ and POR3ΔQ + VopQ strains were described previously (*71*). Briefly, POR3ΔQ was constructed by replacing the VopQ sequence with a chloramphenicol-resistance cassette in POR3. POR3ΔQ + VopQ was constructed by reconstituting POR3ΔQ with the pLafR plasmid containing VopQ and 1000 bp of upstream sequence. POR3ΔQ + VopQ was maintained in marine LB + 20ug/mL tetracycline to maintain VopQ complementation plasmid.

## Yeast strains

Yeast strains BY4742 (*MAT* ‹ *his3Δ1 leu2Δ0 lys2Δ0 ura3Δ0*), BJ3505 (*MAT*a *ura3-52 trp1-Δ101 his3-Δ200 lys2-801 gal2 (gal3) can1 prb1-Δ1.6R pep4*::*HIS3*) (Jones, 2002), and DKY6281 (*MAT*a *ura3-52 leu2-3,112 trp1-Δ901 his3-Δ200 lys2-801 suc2-Δ9 pho8*::*TRP1*) (Haas et al., 1994) were used for vacuole production. Yeast strains were grown in YPD (1% yeast extract, 2% bacto-peptone, 2% glucose) without selection and in Yeast Complete Dropout media without selective amino acids (-W,H,U,L,K) for selection. 1% Raffinose and 2% galactose was used for induction and as the carbon source for yeast strains harboring the pRS413 plasmid.

**Cell culture**

HeLa cells (ATCC) were cultured in DMEM (Invitrogen) supplemented with 10% FBS. GFP-LC3 HeLa cells (a generous gift from Beth Levine) were cultured in DMEM (Invitrogen) supplemented with 10% FBS, NEAA (Invitrogen) and G418 (Hyclone). All mammalian cell lines were grown at 37°C with 5% CO2.

**Infection**

HeLa cells were plated at 10 x $10^4$ cell/well in a 6 well dish one day prior to infection. The following day, cells were infected at MOI of 10 with an overnight culture of *V. parahaemolyticus.* For western blot analysis, cells were washed with 1x PBS and harvested using cell scraper. Cell pellets were suspended in 100 µL of 2x SDS sample loading buffer and boiled for 10 minutes. For microscopy, cells plated on glass coverslips were washed with 1x PBS and fixed using 3.2 % paraformaldehyde in 1x PBS.

**Transfection**

HeLa cells were plated at 10 x $10^4$ cell/well in a 6 well dish one day prior to transfection. The following day, media was replaced with fresh media and cells were transfected using Fugene Xtreme HD transfection reagent. Transfection reaction mix was prepared using 200 µl OptiMEM media, 100 ng VopQ plasmid, 200 ng GFP, 1700 ng pCDNA3 and 2 µL Fugene Xtreme HD transfection reagent. Transfection mix was incubated at room temperature for 30 minutes and then added dropwise to the wells. 18 hours post transfection, cells were fixed for microscopy or harvested for western blot analysis.

**Microinjection**

HeLa or GFP LC3 cells were microinjected using a semi-automatic InjectMan NI2 micromanipulater (Eppendorf). Cell cytoplasm was microinjected with 10 μM protein and 10mg/mL cascade blue dextran in 25 mM HEPES-KOH pH 7.4, 50 mM KAc. Cells were placed back in incubator and then fixed using 3.2% paraformaldehyde in 1x PBS at indicated time points.

**Microscopy**

Cells plated on glass coverslips were fixed with 3.2 % paraformaldehyde. Fixed cells were washed with 1x PBS and mounted on glass coverslides using Invitrogen Prolong Antifade reagent. Samples were viewed using Zeiss LSM 510 or 710 scanning confocal microscope. Images were processed using ImageJ and Photoshop software.

**Reagent preparation**

Purified recombinant yeast proteins Pbi2p (*72*), Gyp1-46 (*73*), and Gdi1p (*74*) were isolated as previously described. Inhibitory antibodies against Vam3p were purified from serum, as previously described (*73*), and routinely used in fusion assays at 450 nM. Antisera against Nyv1p, Vam3p, and Vps33p were generous gifts from Dr. William Wickner (Dartmouth Medical School); antiserum against Vma6p was a gift from Dr. Christian Ungermann (University of Osnabrück). Nitrocefin was a generous gift from Dr. Shahriar Mobashery (University of Notre Dame). Monoclonal antisera against yeast Vph1p (clone 10D7A7B2) and Vma2p (clone 13D11B2) were purchased from Life Technologies. Rabbit anti-VoA,

anti-VoD, anti-LAMP1 were purchased from Abcam. Goat anti-cathepsin D and anti-aldolase was purchased from Santa-Cruz. Mouse anti-GFP was purchased from BD biosciences. Mouse anti-tubulin was purchased from Sigma. The following inhibitors were used: rapamycin (TSZ chem r1017), chloroquine (Sigma c6628) and bafilomycin (Sigma b1793). The following fluorophores were purchased from Invitrogen: LysoTracker Red DND-99 (L7528), Lysotracker Green DND-26 (L7526), Texas Red Dextran (d1863), FITC dextran 3 kD (D3305) and Cascade Blue Dextran (d1976). Carboxyfluorescein (21877) and FITC dextran 10 kD (FD10S) were purchased from Sigma.

**Plasmid construction**

Constructs used in this study are listed in **Table 3**. Primers used in this study are listed in **Table 4.** Genes were amplified by PCR using Vent polymerase. After amplification, genes were digested using Fast Digest enzymes and ligated into appropriate vectors using T4 DNA ligase. Ligated DNA was transformed into DH5α cells and grown overnight with antibiotics. Plasmid DNA was extracted from colonies using a miniprep kit. Constructs were screened using colony PCR or digestion and verified using DNA sequence analysis.

Point mutations were generated using Stratagene QuikChange$^{TM}$ Mutagenesis kit. Mutations were confirmed using DNA sequence analysis.

**Protein expression and purification**

VopQ protein expression plasmids were transformed into *E. Coli* BL21 cells. A single colony from a freshly transformed plate was used to inoculate the starter culture. The starter culture

was then used to inoculate 1.5 L culture grown in a 6 L flask at 37°C. Cultures were induced with 0.4 mM IPTG at log phase ~ 0.6-0.8 for protein expression up to 18 hours at room temperature. Following protein expression, cells were spun down and pellets were frozen and stored at -80°C.

His-tagged VopQ constructs were purified using standard nickel-affinity purification protocol. Briefly, frozen pellets were resuspended in ice cold 1x PBS with 14 mM BME, 1 mM PMSF. Cells were lysed the C3 Emulsiflex Cell disruptor. Cleared lysate was added to nickel beads and washed with 20 column volume (CV) and eluted with 5 CV. Protein was buffer exchanged into 25 mM Tris HCl pH 7.5, 0.15 M NaCl and stored at -80°C.

**Crystallography set-up**

In order to cleave the tag, affinity purified his and MBP-his tagged proteins were cleaved using 1 TEV: 50 MBP-his protein (w/w) overnight at 4°C. The following day, the protein of interest was separated from the tag using ion exchange or gel filtration chromatography. To improve homogeneity, proteins purified from the nickel affinity beads were run on a gel filtration column with 10 mM Tris-HCl pH 7.5, 50 mM NaCl. Proteins were then concentrated to >20 mg/mL and used to set up screening trays by hand or using the Rigaku Phoenix robot.

**Protein proteolysis**

20 µg VopQ was incubated with 100 ng/ml, 10 ng/mL, or 1 ng/mL protease in 20 µL reactions for 30 minutes at room temperature. After incubation, 1 mM PMSF and 5 µL of 5x

SDS sample buffer were added to the reaction. Samples were boiled and run on SDS-PAGE gel.

**Vacuolar pulldown**

200 µg vacuoles purified from BJ3505 were incubated with, or without, 5 µg $His_6$-VopQ (23°C, 30 minutes). Vacuoles were lysed using solubilization buffer (20 mM Tris-HCl pH 7.5, 0.15 M NaCl, 1 mM $MgCl_2$, 0.5% NP-40 alternative, 10% glycerol) on ice, and clarified via centrifugation (20,000xg, 5 minutes, 4°C). VopQ-associated proteins were isolated using nickel beads, and eluates were separated via SDS-PAGE, then visualized by Oriole™ fluorescent staining. The unique band seen in the VopQ-containing condition was excised, digested with trypsin, and run through reverse-phase high-performance liquid chromatography/ion trap. Tandem MS-MS files were searched against the NCBI non-redundant database, identifying Vma6p.

**HeLa lysate pulldown**

HeLa cells (~ 3 x $10^7$ cells) were harvested, lysed with solubilization buffer on ice, clarified via centrifugation (300xg, 5 minutes, 4°C), and applied to nickel beads previously bound by 5 µg $His_6$-VopQ. Eluents were separated by SDS-PAGE and immunoblotted for $V_oA$ and $V_oD$.

**VopQ:vacuole membrane interaction**

90 µl reactions contained 50 mM MES, 50 mM MOPS (adjusted to either pH 5.5 or 7.5), 125 mM KCl, 0.5 mM PMSF, 200 mM sorbitol. 18 µg vacuoles purified from the indicated strains (WT, BY4742; *vma6*Δ, BY4742 *vma6*Δ*::KANMX4*), and 25 nM $His_6$VopQ. After 30 minutes at 27°C, reactions were placed on ice 5 minutes, and one 30 µl aliquot was removed to a fresh tube on ice containing 30 µl pre-chilled PS buffer (20 mM PIPES-KOH pH 6.8, 200 mM sorbitol) with 125 mM KCl. This diluted sample was pelleted (5,300xg, 5 minutes, 4°C), and supernatants were withdrawn. Equal fractions of all samples were separated via SDS-PAGE, immunoblotted for Vma6p ($V_o$ subunit), Vam3p (transmembrane vacuolar SNARE marking the membrane fraction), and VopQ. T, total reaction (unseparated); P, vacuole pellet; S, supernatant.

**V-ATPase proton translocation**

Acidification of the vacuolar lumen was measured by the change in absorbance of acridine orange upon protonation, as previously described (*75*), with modifications. Vacuole reactions (6 x, 180 µl final volume) containing 6 µg vacuoles isolated from BJ3505, 20 mM PIPES-KOH, 200 mM sorbitol, 125 mM KCl, 5 mM $MgCl_2$, 15 µM acridine orange, and indicated reagents were preincubated for 5 minutes in a SynergyMX microplate reader (BioTek) pre-warmed to 27 °C, in a 96-well clear plate (Corning). Acridine orange absorbances (490 nm and 540 nm) were measured every minute, with path length correction enabled. Acidification was initiated with the addition of 2 mM ATP, and absorbance measurements were followed every 10 sec over 20 minutes. Absorbance is plotted as ($A_{490}$ - $A_{540}$); the loss

of absorbance indicates protonation of acridine orange and translocation of protons into the lumen of the vacuole.

**V-ATPase activity**

ATP hydrolysis activity of the V-ATPase was measured as in (*76*), with modifications. Reactions containing 6 µg BJ3505 vacuoles per 180 µl reaction, 20 mM PIPES-KOH, 200 mM sorbitol, 125 mM KCl, 5 mM $MgCl_2$, 3.2 U each pyruvate kinase/lactate dehydrogenase, 0.5 mM NADH, 2 mM phosphoenolpyruvate, 100 µM $Na_3VO_4$, and indicated reagents were preincubated for 5 minutes in a SynergyMX microplate reader (BioTek) prewarmed to 27 °C, in a 96-well clear plate (Corning). NADH absorbance (340 nm) was followed every minute, with path-length correction enabled. Assays were initiated with 2 mM ATP, and continued measuring absorbance every 10 sec over 20 minutes; loss of absorbance indicates oxidation of NADH, and correlates with the hydrolysis of ATP.

**Liposome leakage assay**

Carboxyfluorescein encapsulated liposomes were prepared as mentioned previously (*77, 78*). Briefly, dried lipid films of 85% POPC:15% DOPS (Avanti Polar Lipids) were hydrated using 100 mg/mL carboxyfluorescein dye solution to constitute a final concentration of 15mM lipid. Liposomes were disrupted by 5 freeze-thaw cycles in liquid nitrogen and then extruded using an Avanti mini-extruder and 80 nm polycarbonate membranes. Extruded liposomes were passed through a PD-10 desalting column to remove excess dye. For FD10 and FD3, a 24 mL Superdex200 column was used to remove excess dye. For the liposome

leakage assay, 100 μM of liposomes in 10 mM MES pH5.5 and 25 mM NaCl were added to a quartz cuvette, and fluorescence intensity ($l_{ex}$=480nm, $l_{em}$=514nm) was measured using PTI Felix 32Software. Carboxyfluorescein leakage is expressed as percentage of total lysis upon addition of 1% final n-octyl-β-D-glucopyranoside detergent. For floatation assays, liposomes were incubated with 10 μg of MBP-VopQ at room temperature for 5 minutes. Equal volume of 80% Histodenz was then added to the sample. The sample was overlaid with 35% Histodenz, followed by 30% Histodenz and buffer alone. Liposomes were collected from the 0%-30% interface.

**Lysosome preparation**

HeLa cells were harvested using a cell scraper and washed with 1x PBS. Cells were disrupted by a glass dounce homogenizer followed by differential centrifugation (*79*). Cell debris was cleared by centrifugation (500xg for 10 minutes), and the resultant supernatant was then clarified (3,000xg for 10 minutes). This supernatant was further centrifuged (17,000x*g* for 10 minutes) to pellet lysosomes. The resultant membrane pellet was resuspended in 1x PBS and used as the lysosomal fraction.

**VopQ activities in bilayer lipid membranes**

Electrical recordings from bilayer lipid membranes followed previously published procedures(*80*). Bilayer membranes were formed by painting across a 300 micron hole that was drilled in the side wall of a recording cup (Warner Instrument) with a capillary pestle carrying concentrated lipids in decane (20 mg/ml). After the stabilization of the membrane,

VopQ protein was introduced into the cis side at a final concentration of 25 or 100 nM. Electrical activities were recording in the voltage-clamp mode through an Axopatch 200B amplifier. Clampex10 was used to control the computer-interface with the amplifier and Clampfit 10 was used to analyze the data.

**Yeast Vacuole Staining**

BY4742 yeast strains harboring either the galactose-inducible control vector pRS413-Gal1 (WT) or pRS413-Gal1-*VOPQ* were subcultured from saturated CSM-his/2% glucose cultures to equal optical density in fresh CSM-his/2% glucose or CSM-uracil/2%galactose media. Cells in mid-logarithmic phase were resuspended in YPD with 8 μM FM4-64 and incubated at 30°C for 30 minutes. After incubation cells were harvested and resuspended in minimal media and shaken for 30 minutes. Cells were then harvested and visualized using a fluorescence microscope.

**Vacuole isolation and in vitro alkaline phosphatase fusion assay**

Vacuoles were freshly prepared from BJ3505 (pep4Δ) and DKY6281 (pho8Δ) yeast strains on discontinuous Ficoll gradients, as previously reported (*81*). Standard in vitro vacuole fusion assays (30 μl final volume, 27°C, 90 minutes) contained 3 μg each BJ3505 and DKY6281 vacuoles (6 μg total), fusion reaction buffer [20 mM piperizine-*N,N'*-bis(2-ethanesulfonic acid) (PIPES)-KOH (pH 6.8), 200 mM sorbitol, 10 μM coenzyme A, 125 mM KCl, 5 mM $MgCl_2$], 815 nM Pbi2p ($I_2^B$), and an ATP regenerating system [1 mM ATP, 1 mg/ml creatine kinase, and 29 mM creatine phosphate]. Reactions were assayed for Pho8p

alkaline phosphatase activity as a measure of vacuole fusion as described (*81*), except $CaCl_2$ was omitted from the development solution. Units of fusion are reported as nmol *p*-nitrophenylate formed $min^{-1}$ µg *pep4*Δ $vacuole^{-1}$.

**Trans-SNARE assay**

Fusion reactions were performed as described above. After 45 minutes, reactions were removed to ice for 5 minutes, vacuoles were precipitated (7600 x *g*, 5 minutes, 4 °C), solubilized, and calmodulin- affinity pulldowns were performed. Reactions contained either no inhibitor, left on ice, 1 µM Gdi1p and 1 µM Gyp1-46, or 100 nM rVopQ. Vps33p, Vam3p and Nyv1p detections were carried out via standard immunoblotting techniques. Fusion measured for each condition is as follows: standard-1.526U, ice- 0.084 U, GDI/Gyp - 0.062 U, VopQ- 0.062 U (*56*).

**β-lactamase vacuole fusion assay**

Assays of homotypic vacuole fusion via the fusion-dependent reconstitution of β-lactamase enzyme were performed as previously described (*82*). Briefly, vacuoles were prepared from BJ3505-Fos-ω and BJ3505-α-Jun strains, and 6 µg each vacuole type was incubated under standard fusion conditions (above) in a 60 µl volume, except that Pbi2p was replaced with 4.3 µM recombinant GST-Fos protein to quench fusion-independent reconstitution of β-lactamase (*82*). After 90 minutes at 27°C, tubes were removed to ice for 5 minutes, 140 µl developer solution (0.1 M sodium phosphate pH 7.0, 150 µM nitrocefin, and 0.2% Triton X-

100) was added to each tube, and 150 µl sample was removed to a clear 96-well plate. A blank well for reference consisted of 6 µg each vacuole type, 4.3 µM GST-Fos, and 140 µl developer solution in a final volume of 200 µl. β-lactamase-dependent hydrolysis of nitrocefin was measured via change in absorbance (λ = 492 nm) over 10 minutes (30 s intervals) in a Synergy MX plate-reading spectrophotometer (Bio-Tek). Rates of hydrolysis were calculated over the 10-minute interval, and "no inhibitor" fusion condition rates in each experimental set were set to 100 % fusion.

**Random mutagenesis of vopQ**

To identify VopQ mutant derivatives which are no longer toxic to yeast, pRS416-Gal1-VOPQ was transformed into the highly mutagenic *E. coli* strain XL1-Red (Stratagene), 100 µl of the transformation mixture was plated to LB + 100 µl/ml ampicillin and incubated at 37°C for 36 h. All colonies on this plate (>200) were scraped into 10 mL fresh LB + 100 µg / ml ampicillin and incubated at 37°C with shaking for 16 h. Plasmid was isolated from 4.5 ml of this culture (Round 1).

Round 1 mutagenized plasmid was transformed into *S. cerevisiae* BY4742, selecting for growth on CSM medium lacking uracil, and supplemented with 2% galactose. Colonies appearing under these conditions were likely defective in VopQ activity *in vivo*. Thirty independent colonies were isolated in this manner, and plasmid phenotypes were confirmed via introduction into a fresh BY4742 background. Of the original 30, eleven plasmids continued to display a defect in VopQ activity *in vivo*, and the *VOPQ* locus from these vectors was sequenced (University of Georgia).

**Yeast dilution plating**

Overnight cultures of yeast strains grown in YCD-H were washed and diluted to 1 $OD_{600}$/mL in water. Four 10-fold serial dilutions were made in water and 10 µL of each dilution was spotted on plates. Plates were incubated at 30°C for 2-3 days.

**Yeast protein extraction**

3 mL of yeast culture was spun down and resuspended in 100 µL ice cold lysis buffer (4% v/v 5N NaOH, 0.5% v/v BME). Cells were lysed on ice for 30 minutes. 4 µL of 6N HCl was added to adjust pH, then 30 µL of 3x SDS sample loading buffer was added. Samples were boiled for 10 minutes prior to separation on SDS-PAGE gel.

**Statistical analysis**

Where indicated, statistical analysis was performed within the Prism® software package (GraphPad Software, v. 6.0d). Statistics from experiments represented in column graphs were performed via a 1-way ANOVA Repeated Measures test and Tukey's Multiple Comparison post-test. Where noted in figures, ns = $P > 0.05$ (not significant); (*) = $P \leq 0.05$; (**) = $P \leq 0.01$; (***) = $P \leq 0.001$.

# TABLE 3. LIST OF CONSTRUCTS

| Constructs | Description | Reference |
|---|---|---|
| VopQ-pET15b | Protein expression; VopQ cloned into NdeI and BamHI sites | Cloned by Dara Burdette |
| VopQ-pET28b | Protein expression; VopQ cloned into BamHI and NotI sites | This study |
| vp1682-pET28a | Protein expression; vp1682 cloned into NcoI and XhoI sites | Cloned by Phi Luong |
| VopQ flag-pRS413 | Yeast protein expression; VopQ cloned into BamHI and EcoRI site | Cloned by Dara Burdette |
| VopQ-pRS413 | Yeast protein expression; VopQ cloned into BamHI and EcoRV site | This study |
| VopQ-pDGFP | Yeast protein expression; VopQ cloned into EcoRV and KpnI sites | This study |
| 1-100 VopQ-pET28b | Protein expression; VopQ cloned into BamHI and NotI sites | This study |
| 1-200 VopQ-pET28b | Protein expression; VopQ cloned into BamHI and NotI sites | This study |
| 1-300 VopQ-pET28b | Protein expression; VopQ cloned into BamHI and NotI sites | This study |
| 1-400 VopQ-pET28b | Protein expression; VopQ cloned into BamHI and NotI sites | This study |
| Δ 100 VopQ-pET28b | Protein expression; VopQ cloned into BamHI and NotI sites | This study |
| Δ 200 VopQ-pET28b | Protein expression; VopQ cloned into BamHI and NotI sites | This study |
| Δ 300 VopQ-pET28b | Protein expression; VopQ cloned into BamHI and NotI sites | This study |
| Δ 400 VopQ-pET28b | Protein expression; VopQ cloned into BamHI and NotI sites | This study |
| 1-100 VopQ-pET15b | Protein expression; VopQ cloned into NdeI and BamHI sites | This study |
| 1-200 VopQ-pET15b | Protein expression; VopQ cloned into NdeI and BamHI sites | This study |
| 1-300 VopQ-pET15b | Protein expression; VopQ cloned into NdeI and BamHI sites | This study |
| 1-400 VopQ-pET15b | Protein expression; VopQ cloned into NdeI and BamHI sites | This study |
| Δ 100 VopQ-pET15b | Protein expression; VopQ cloned into NdeI and BamHI sites | This study |
| Δ 200 VopQ-pET15b | Protein expression; VopQ cloned into | This study |

| | | |
|---|---|---|
| | NdeI and BamHI sites | |
| Δ 300 VopQ-pET15b | Protein expression; VopQ cloned into NdeI and BamHI sites | This study |
| Δ 400 VopQ-pET15b | Protein expression; VopQ cloned into NdeI and BamHI sites | This study |
| Δ100VopQ fusion Δc10vp1682 pProEx | Fusion protein expression construct; C-terminal Δ10 vp1682 cloned into NcoI and speI sites and N-terminal Δ100VopQ cloned into speI and XhoI sites | Cloned by Phi Luong |
| S200P pET28b | Protein expression; Serine to Proline point mutation at amino acid 200 VopQ | This study |
| F292I pET28b | Protein expression; Phenylalanine to isoleucine point mutation at amino acid 292 VopQ | This study |
| S200P F292I pET28b | Protein expression; Double point mutation VopQ | This study |
| S200P pET15b | Protein expression; Serine to Proline point mutation at amino acid 200 VopQ | This study |
| F292I pET15b | Protein expression; Phenylalanine to isoleucine point mutation at amino acid 292 VopQ | This study |
| S200P F292I pET15b | Protein expression; Double point mutation VopQ | This study |
| S200P flag pRS413 | Yeast protein expression; Serine to Proline point mutation at amino acid 200 VopQ | This study |
| F292I flag pRS413 | Yeast protein expression; Phenylalanine to isoleucine point mutation at amino acid 292 VopQ | This study |
| S200P F292I flag pRS413 | Yeast protein expression; Double point mutation VopQ | This study |

# TABLE 4. LIST OF PRIMERS

| Name | Sequence |
|---|---|
| R vopQ kpnI | GATC ggt acc gc AAT CCA GCC TTC GGC TAA GTA CAT |
| R VopQ 1-100aa | gatc gga tcc tta GTAGCCTGACGGACTGACTAA |
| R VopQ 1-200aa | gatc gga tcc tta GGACGCTTTATGAAGTTCACG |
| R VopQ 1-300aa | gatc gga tcc tta ATACGCCCCAGCTTGGCCAG |
| F VopQ delta100 | gatc cat atg atg CGAGGAGAACCATTAACC |
| F VopQ delta200 | gatc cat atg atg GTCAATGGCGATGCCGAA |
| F VopQ delta300 | gatc cat atg atg GGCTTAAATAACGAAGTG |
| F VopQ delta400 | gatc cat atg atg GACATGCCAAGTCAGACG |
| R VopQ 1-400aa | gatc gga tcc tta TTCATCGCTCAGTTTAAG |
| R VopQ 1-100aa | gatc gcg gcc gc tta GTAGCCTGACGGACTGACTAA |
| R VopQ 1-200aa | gatc gcg gcc gc tta GGACGCTTTATGAAGTTCACG |
| R VopQ 1-300aa | gatc gcg gcc gc tta ATACGCCCCAGCTTGGCCAG |
| R VopQ 1-400aa | gatc gcg gcc gc tta TTCATCGCTCAGTTTAAG |
| F VopQ delta100 | gatc gga tcc atg CGAGGAGAACCATTAACC |
| F VopQ delta200 | gatc gga tcc atg GTCAATGGCGATGCCGAA |
| F VopQ delta300 | gatc gga tcc atg GGCTTAAATAACGAAGTG |
| F VopQ delta400 | gatc gga tcc atg GACATGCCAAGTCAGACG |
| F VopQ NcoI | gatc cca tgg gc gtg aat aca acg caa aaa |
| R VopQ NotI | gatc gcg gcc gc tta aat cca gcc ttc ggc taa gta cat |
| G244A VopQ | tcacgcgatgttgtcggctgaggctgcagttggtgccacacttggta |
| G247A VopQ | ttgtcggctgagggtgcagttgctgccacacttggtatggcgaca |
| G251A VopQ | gtgcagttggtgccacacttgctatggcgacaggcggtttgggt |
| G255A VopQ | ccacacttggtatggcgacagccggtttgggtacgtttggtgtaa |
| G258A VopQ | ggtatggcgacaggcggtttggctacgtttggtgtaagctctgtg |
| S200P VopQ fwd | cttcataaagcgcccgtcaatggcgatgcc |
| S200P VopQ rev | ggcatcgccattgacgggcgctttatgaag |
| F292I VopQ fwd | ataatcagcggcgggggcattgttgctggccaagctggg |
| F292I VopQ rev | cccagcttggccagcaacaatgcccccgccgctgattat |

# CHAPTER THREE

## VopQ forms a gated channel on lysosomes

### Introduction

Macroautophagy is a cellular process by which cells degrade and recycle cytoplasmic contents by encapsulating them within a distinctive double bilayer membrane vesicle for delivery to the degradative lysosome (*41*). Disruption of normal autophagic pathways is implicated in numerous human diseases, stressing the importance of autophagy and its proper regulation (*40*). *V. parahaemolyticus* T3SS1 effector VopQ, also known as VepA (*vp1680),* is both necessary and sufficient for the rapid induction of autophagy, even in the presence of known chemical inhibitors of autophagy (*36*).

The following studies show that VopQ formed small pores on lysosomal and synthetic membranes, allowing particles of ~350 Da, but not particles greater than 3 kDa, to pass through the lipid bilayer. Further analysis of VopQ in lipid bilayers revealed that it forms a ~18 Å gated, outward rectifying channel upon the electrostatic association of VopQ with phospholipids. The presence of the $V_o$ domain of the V-ATPase allowed the targeting of VopQ to the appropriate acidic compartments during an infection. The molecular mechanism hijacked by VopQ for disrupting host lysosomal homeostasis during *V. parahaemolyticus* infection provides insight into the signals that regulate autophagy in host cells.

**Results**

*VopQ interacts with $V_o$ subunits of the V-ATPase proton pump*.

The V-ATPase is the main electrogenic proton pump involved in the acidification of many intracellular organelles within the endomembrane system, such as yeast vacuoles and mammalian lysosomes (*83*). It is made up of two heterologous subunits: the cytoplasmic $V_1$ domain hydrolyzes ATP, which energizes the translocation of protons through the membrane-bound $V_o$ proton channel, and into the lumen of the acidic organelle (**Figure 8**). A recent study indicated that the *Vibrio* effector, VopQ (*vp1680,* VepA) interacts with Vma3p (subunit c) of the highly conserved V-ATPase $V_o$ proton translocation domain (*68*). Our analyses revealed that His-VopQ interacts with Vma6 (subunit d) of the $V_o$ domain when incubated with highly enriched preparations of yeast vacuoles (**Figure 10A**). Using immunoblot analysis, we noted that VopQ interacts with Vma6 and Vph1p $V_o$ domain subunits *in vitro* suggesting that VopQ has an affinity for the assembled $V_o$ domain (**Figure 10B).** This interaction does not appear to involve the entire V-ATPase, however, as Vma2p, subunit B of the ATP-hydrolyzing $V_1$ domain, was not detected in this interaction (**Figure 10B**). The VopQ:Vma6p interaction was conserved in higher eukaryotes, as the human orthologue, $V_o$ d subunit, co-precipitated from HeLa extracts in a VopQ-dependent manner (**Figure 10C**) (*83*). Therefore, consistent with previous observations, we propose that VopQ has an affinity for the V-ATPase $V_o$ domain, but does not appear to interact with the $V_1$ domain of the V-ATPase.

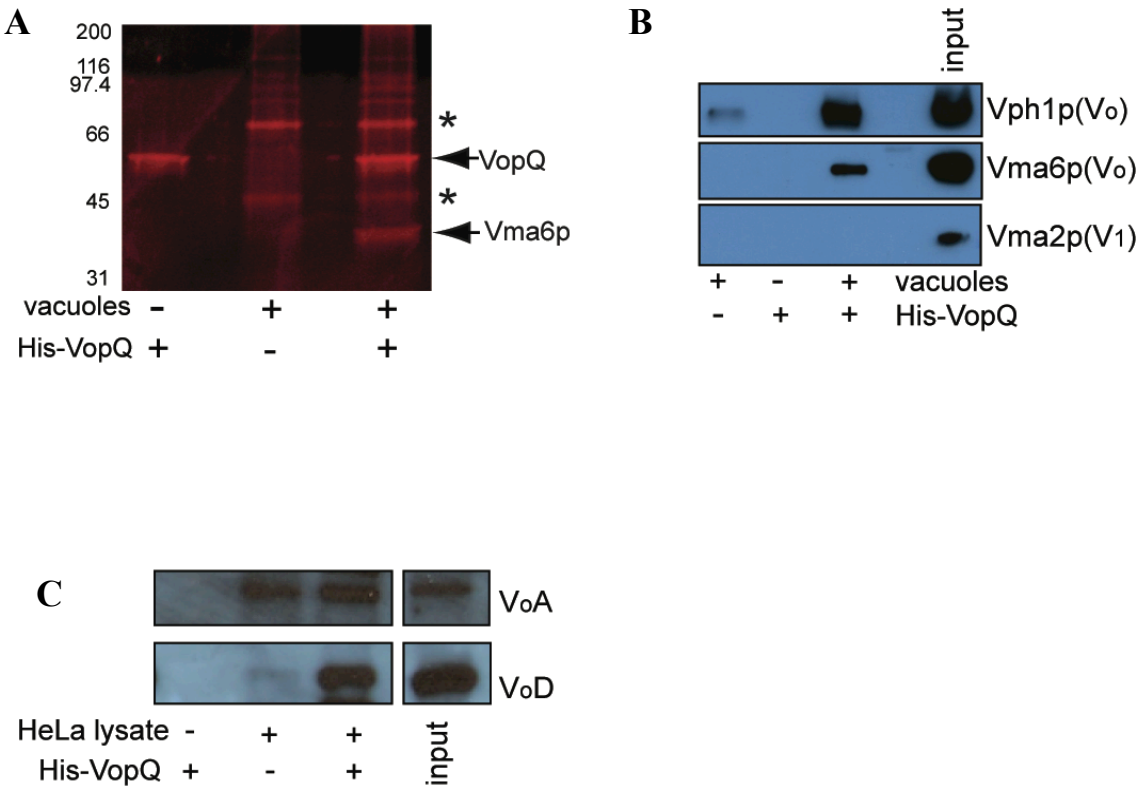


**Figure 10. VopQ interacts with V-ATPase $V_o$ domain.** (**A**) $His_6$-VopQ associated proteins were isolated using nickel beads and eluents were separated via SDS-PAGE and visualized by Oriole stain. Vma6p band was excised and identified using mass spectrometry. *denotes non-specific bands. (**B**) Immunoblot analysis of VopQ-associated proteins from a; Vph1p ($V_o$), Vma6p ($V_o$), and Vma2p ($V_1$). (**C**) Immunoblot analysis of VopQ-associated proteins from HeLa cell lysates.

*VopQ disrupts proton translocation but not ATPase activity of V-ATPase.*

Based on these interactions with the V-ATPase, we next investigated the effect of VopQ on the ATPase activity and ATP-dependent proton translocation of the V-ATPase in yeast vacuoles. Because of the modular nature of this enzyme, each of these activities can be measured separately. By using a standard assay which measures the protonation of acridine orange in acidic environments (via loss of absorbance), we find that recombinant VopQ (rVopQ) completely abrogated the V-ATPase proton translocation activity in a concentration dependent manner, to levels seen with an inhibitor of the V-ATPase, bafilomycin (**Figure 11A**). In contrast to bafilomycin, however, rVopQ did not affect the vacuolar ATPase activity (**Table 5**). Furthermore, 25 nM rVopQ (tagged with either 6xHistidine or maltose binding protein, MBP) was sufficient to prevent acidification of vacuoles (**Figure 11B**) and deacidify previously-acidified vacuoles, as VopQ caused near-immediate proton equilibration when added to vacuoles 20 minutes after ATP addition (**Figure 11C**). These studies support the hypothesis that VopQ has the ability to disrupt the proton gradient across acidic organellar membranes.

| Reaction condition | $H^+$ pumping rate[a] | ATP hydrolysis rate[b] |
|---|---|---|
| 1. no addition | 0.094 ± 0.019 | 0.29 ± 0.02 |
| 2. -ATP | -0.005 ± 0.002 | 0.06 ± 0.03 |
| 3. 50 nM bafilomycin | 0.007 ± 0.004 | 0.17 ± 0.04 |
| 4. 100 nM VopQ | -0.012 ± 0.017 | 0.32 ± 0.04 |

**Table 5. VopQ inhibits yeast vacuolar proton pumping**

[a] defined as 10x $\Delta A_{490\text{-}540}$ $min^{-1}$ μg $vacuole^{-1}$.

[b] defined as nmol NADH oxidized $min^{-1}$ μg vacuolar $protein^{-1}$.

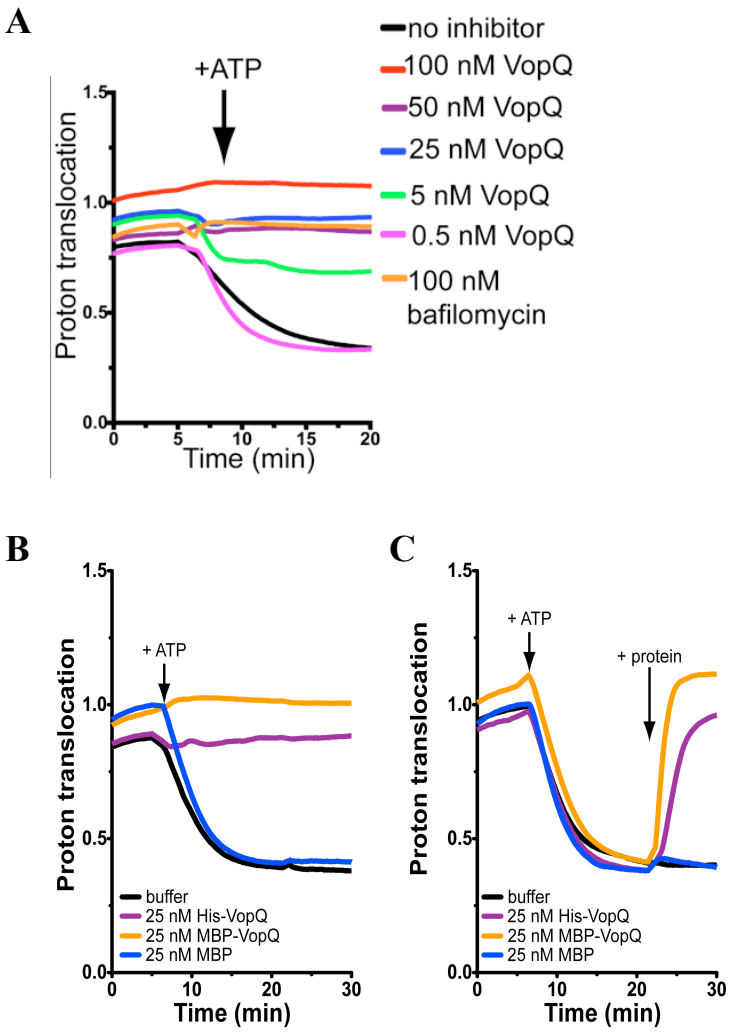


**Figure 11. VopQ disrupts acidification in yeast vacuoles (A)** Proton translocation activity of vacuoles was measured in the presence of 100 nM bafilomycin or increasing concentrations of $His_6$VopQ. **(B)** Proton translocation activity of yeast vacuoles was measured in the presence of 25 nM $His_6$-VopQ, MBP-VopQ or MBP **(C)** Proton translocation activity of yeast vacuoles was measured upon addition of 25 nM $His_6$-VopQ, MBP-VopQ or MBP, 15 minutes after addition of ATP**.**

*VopQ disrupts lysosomal acidification and autophagic flux.*

To confirm the ability of VopQ to disrupt the acidification of lysosomes in host cells during an infection, we performed *V. parahaemolyticus* POR3 infections followed by staining with LysoTracker, a pH-sensitive indicator, which accumulates within acidic organelles. POR3 is a derivative of the pathogenic RIMD2210633 strain where only the first T3SS remains active, and thus we can focus on the activity of only T3SS1 effector proteins. During POR3 infection, we see a loss of acidic punctae by 3 hours; this observation is VopQ-dependent, as strains lacking VopQ (Δ*vopQ*) maintain acidic organelles over this timeframe (**Figure 12A**). Therefore, VopQ activity is necessary to cause de-acidification of these organelles during an infection. To confirm that VopQ alone is sufficient to induce deacidification of these compartments, we microinjected purified rVopQ or a control protein, glutathione–S-transferase (GST) into HeLa cells expressing GFP-LC3 and assessed for the presence of acidic vesicles using LysoTracker. Concomitantly, we assayed for the induction of autophagy, the previously-identified activity of VopQ (*36*).

Upon induction of autophagy, cytosolic GFP-LC3-I in these cells is cleaved and lipidated to form GFP-LC3-II, which then becomes localized to autophagosomal membranes, allowing visualization of autophagosomes (*84*). As expected, microinjection of rVopQ, but not the control protein GST (**Figure 12B**), was sufficient to induce autophagosome formation, as measured by the accumulation of GFP-LC3-II-positive vesicles. Furthermore, injection of VopQ, but not GST, completely blocked lysosomal acidification in the same cells within 20 minutes, as measured by the loss of LysoTracker within acidic compartments (**Figure 12B**). Interestingly, the kinetics of lysosome deacidification by VopQ was nearly

identical to the observed accumulation of autophagosomes as measured by the membrane targeting of GFP-LC3-II, all occurring within 20 min of injection (*36, 84*). Thus, VopQ is necessary and sufficient to directly and rapidly induce not only autophagosome accumulation but also inhibit the acidification of endolysosomal compartments in host cells (*36*).

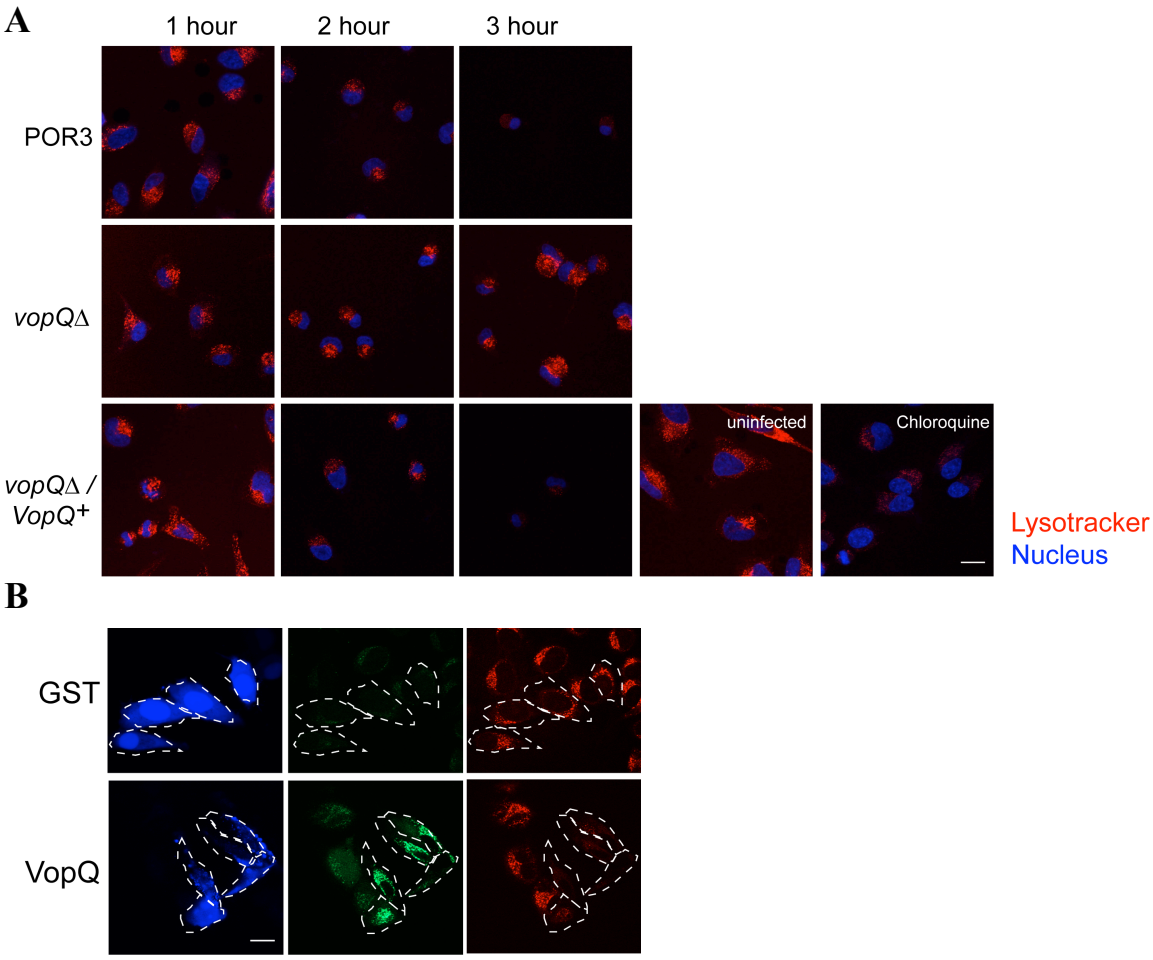


**Figure 12. VopQ is necessary and sufficient to deacidify host lysosomes (A)** HeLa cells were left either untreated, or treated for 3 hours with 25 μM chloroquine, or infected with noted *V. parahaemolyticus* strains at an MOI of 10. Cells were stained with 75 nM Lysotracker Red (10 minutes), and visualized by microscopy. Bar = 20 μ. **(B)** HeLa cells expressing GFP-LC3 were microinjected with 10 μM GST or $His_6$VopQ, incubated 10 min (37 °C, 5% $CO_2$), then incubated with 75 nM LysoTracker Red for 10 minutes and visualized. Bar = 20 μ

*VopQ, similar to chloroquine, inhibits turnover of autophagosomes.*

Autophagosomes are transient vesicles that are constantly turned over through fusion with the acidic, degradative lysosome. Chloroquine, a lysosomotropic agent, neutralizes acidic compartments, thereby inhibiting the activity of lumenal lysosomal proteases and preventing the lysosome-dependent turnover of autophagosomes (*85*). We hypothesized that VopQ might be disrupting autophagic flux in a similar manner by deacidifying the lysosomes. Therefore, we tested whether VopQ-mediated accumulation of autophagic vesicles was due to increased formation of autophagosomes or decreased turnover of autophagosome concomitant with GFP-LC3-II degradation. In order to investigate these possibilities, HeLa cells stably expressing GFP-LC3 (HeLa-GFP-LC3) were pretreated with chloroquine, a drug that inhibits autophagosome turnover, followed by infection with *V. parahaemolyticus* POR3 strains or treatment with rapamycin. Rapamycin is a potent inhibitor of mTORC1 activity, which induces the formation of autophagic vesicles through the derepression of ULK1/Atg13/FIP200 activities (*86*). We hypothesized that if VopQ did not inhibit autophagosome turnover, but rather directly induced an increase in autophagosome formation, similar to rapamycin, an increase in GFP-LC3-II would be observed upon treatment with chloroquine. Alternatively, if VopQ inhibited turnover of autophagosomes, no increase in GFP-LC3-II would be observed upon treatment with chloroquine because these two activities would be redundant.

Using an immunoblot analysis of cell lysates, we analyzed the conversion of GFP-LC3-I to GFP-LC3-II under these treatments. As expected, treatment of cells with rapamycin caused an increase in the appearance of GFP-LC3-II (**Figure 13A, lane 2**).

Furthermore, complete LC3-I conversion was observed with cells co-treated with chloroquine and rapamycin (**Figure 13A, lane 7**), consistent with an enhanced accumulation of autophagosomes due to both the blocked turnover of these vesicles by chloroquine treatment, and the additional induction of autophagosome formation via mTOR inhibition. When comparing these results to those observed in cells infected with *V. parahaemolyticus*, we see that conversion of LC3-I to LC3-II appeared essentially complete in cells infected with strains expressing VopQ, but not in the Δ*vopQ* strain (**Figure 13A, lanes 3-5**). The effect on LC3 conversion increased upon treatment with chloroquine of the D*vopQ* infected cells (**Figure 13A, lane 9**), but not cells infected with the strains expressing VopQ (**Figure 13A, lanes 8 and 10).** Further cell biology studies demonstrated that the formation of green punctae representative of autophagosomes is consistent with this biochemical analysis of LC3-I conversion (**Figure 13B**), and therefore these observations strongly support the hypothesis that VopQ mimics chloroquine treatments, which disrupts autophagosome:lysosome turnover by disrupting lysosomal acidification. Therefore autophagosomal accumulation is a result of the pore formation activity of VopQ rather than the mechanism of VopQ.

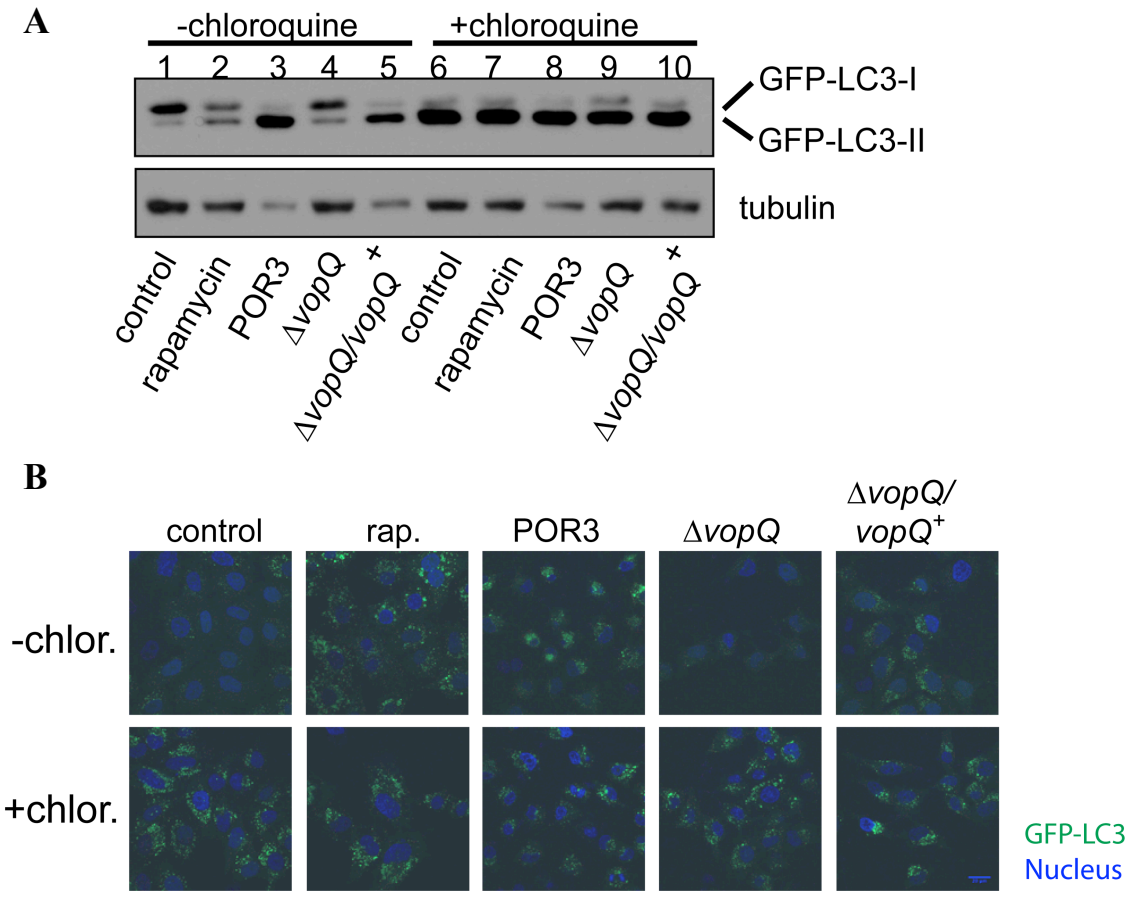


**Figure 13. VopQ disrupts autophagic flux.** HeLa cells expressing GFP-LC3 were incubated without (top row) or with (bottom row) 25 μM chloroquine for 30 minutes, then either treated with 100 μM rapamycin, or infected with noted *V. parahaemolyticus* strains at an MOI of 10 for 3 hours **(A)** Cell lysates were separated via SDS-PAGE and immunoblotted for GFP and tubulin. **(B)** Cells were fixed with paraformaldehyde, stained with Hoeschst 33342, and visualized. Bar = 20 μ.

*VopQ allows release of molecules <350 daltons, but does not rupture lysosomes.*

The observation that VopQ induces deacidification, coupled with the previous observation that indicates that VopQ has a membrane-disrupting activity (*68*), led us to further investigate the molecular mechanism of VopQ on membranes. Limited bioinformatics on VopQ indicates the presence of two or three transmembrane helices, suggesting that VopQ could have a pore-forming activity in host membranes. To test this hypothesis, POPC:DOPS (85:15 molar ratio) liposomes were made to encapsulate quenching concentrations of carboxyfluorescein (376 Da). Pore formation was measured as a result of fluorescence increase upon dye release and dequenching (*87*). Similar to the results seen with yeast vacuole deacidification, we notice that VopQ induced dye release in a concentration-dependent manner. MBP-VopQ, but not MBP, induced leakage of dye within seconds as measured by fluorescence dequenching (**Figure 11A**); heat inactivation of VopQ completely abrogated this activity (**Figure 14A**, light blue line). To examine whether VopQ is causing the release of only small molecules, rather than the complete liposomal rupture, we assessed the size of the potential VopQ pores using quenching concentrations of fluorescein dextrans of differing sizes encapsulated within liposomes. Neither a 3 kD, nor 10 kD fluorescein dextran was released from liposomes treated with VopQ, indicating that VopQ likely forms a pore of a defined size (<28Å diameter), allowing only molecules smaller than 3 kD to escape the lumen (**Figure 14 B-D**).

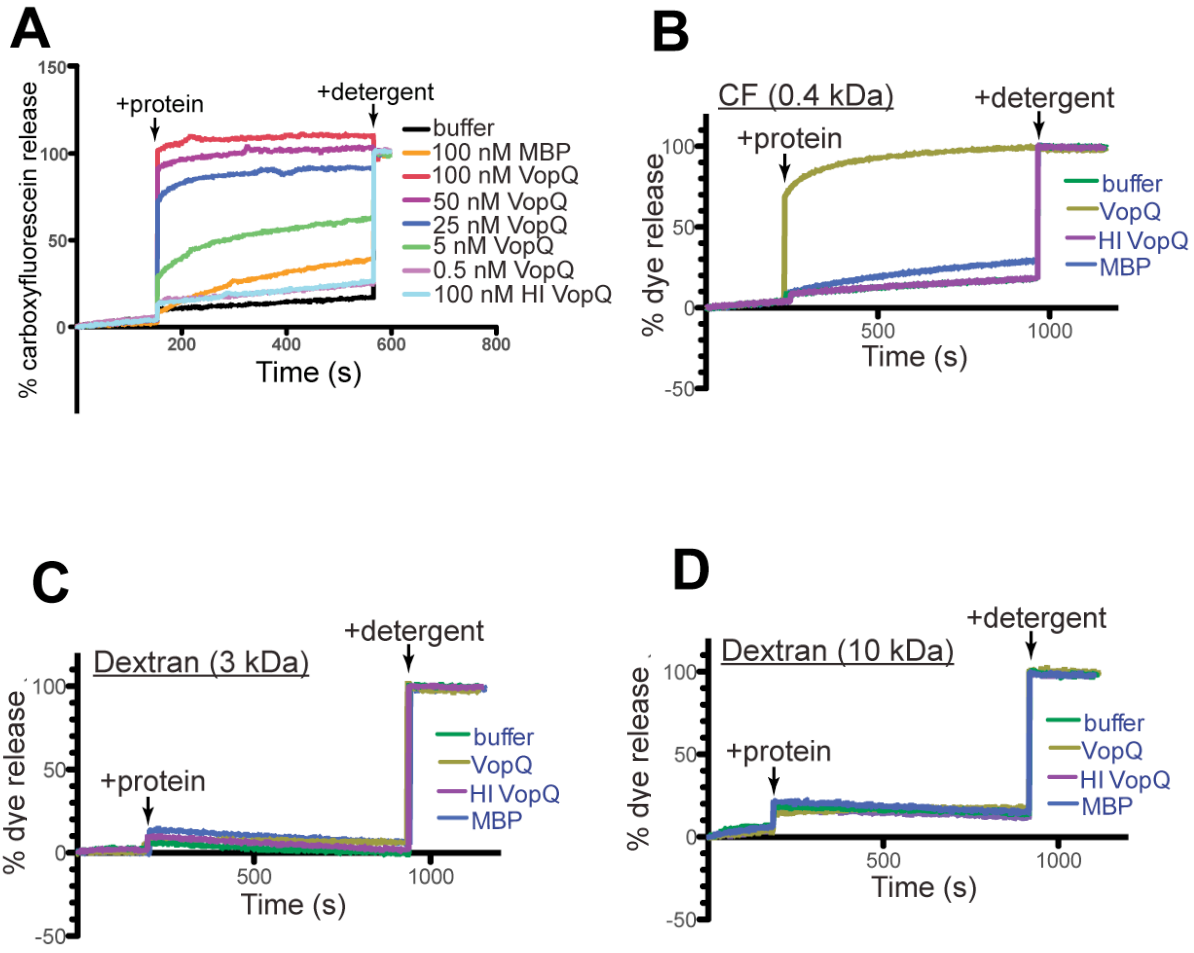


**Figure 14. VopQ does not rupture lysosomes, but allows for release of molecules <3 kD.** **(A)** Carboxyfluorescein dye release was measured upon addition of increasing concentrations of MBP-VopQ, 100 nM heat-inactivated MBP-VopQ, or 100 nM MBP to carboxyfluorescein-containing liposomes **(B-D)** Carboxyfluorescein or FITC dextran release was measured upon addition of 25nM MBP-VopQ, 25 nM heat-inactivated MBP-VopQ, or 25 nM MBP to quenched liposomes.

A report by Matsuda et al. suggested that VopQ causes rupture of lysosomes *in vivo* and *in vitro*, resulting in the release of lumenal enzymes (*68*). Because our findings are in direct contrast to this previously-published work, we revisited these studies. During a 3 hour *V. parahaemolyticus* infection, we did not observe the release of the ~33 kD lumenal cathepsin D from lysosomes (**Figure 15A**), yet cells treated with the nonionic detergent Triton X-100 showed the complete release of cathepsin D into the cytosolic fraction. Importantly, we see both VopQ-dependent lysosomal deacidification and disruption of autophagic flux within this infection timeframe (**Figure 12A and 13B**), supporting previous results that VopQ is highly active during these conditions. Furthermore, an isolated membrane fraction highly enriched in lysosomes incubated with either recombinant MBP or MBP-VopQ for 30 minutes at 23°C did not result in a VopQ-dependent release of cathepsin D (**Figure 15B**). Treatment of these lysosomes at 37°C for 2 hours with either recombinant MBP or MBP-VopQ did induce small amounts of cathepsin D release.

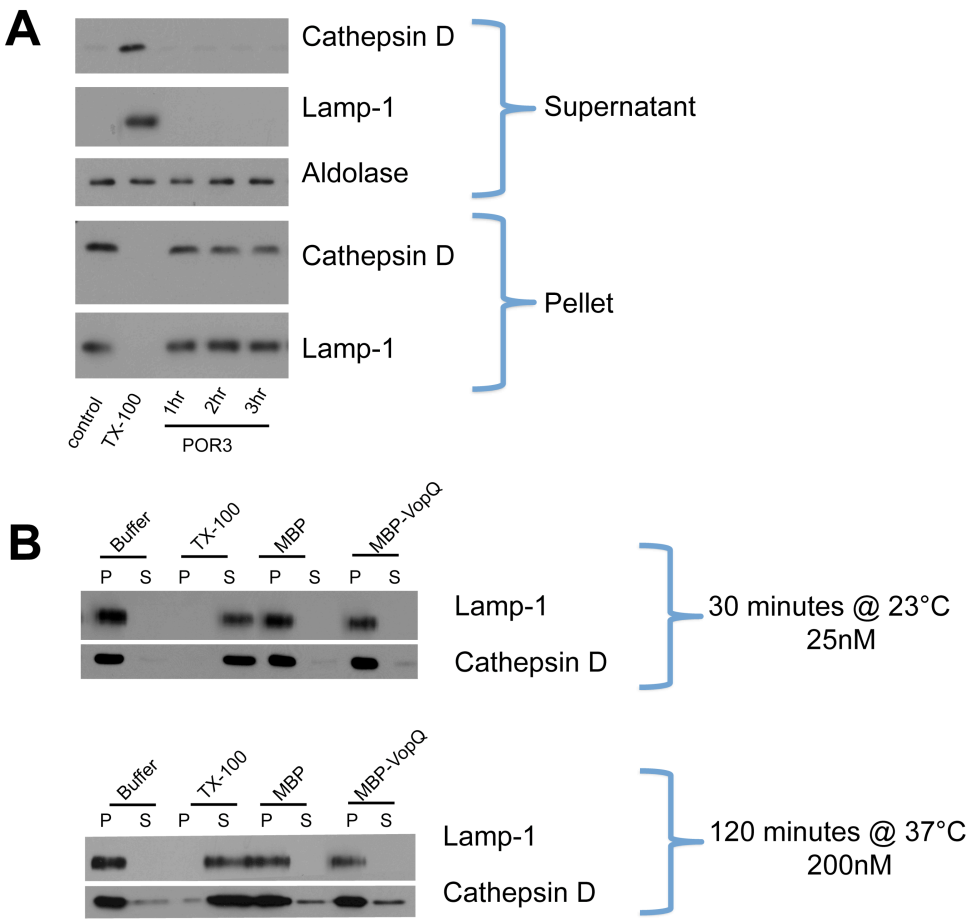


**Figure 15. VopQ does not rupture lysosomes (A)** HeLa cells, uninfected or infected with *V.parahaemolyticus* POR3, were harvested and treated with 0.1% saponin for 10 minutes on ice to solubilize the plasma membrane. Uninfected cells were treated with 1% Triton X-100 for 10 minutes on ice to completely solubilize all cell membranes. Cells were then spun down 15,000xg 10 minutes to yield lysosomal pellet fraction and cytosolic supernatant fraction. **(B)** 50 µg of lysosomes were incubated with buffer, MBP, MBP-VopQ, or 1% (v/v) Triton X-100 (23°C, 30 min or 37°C, 120 minutes). Lysosomes were pelleted (17000xg for 10 min.), and supernatant and pellet fractions were immunoblotted for Cathepsin D and Lamp-1.

Our previous observations suggested that VopQ does not allow release of large dextrans from liposomal membranes. To test this observation *in vivo*, we loaded HeLa lysosomes with 10 kD Texas Red Dextran (TRD). When purified VopQ, but not GST, is injected into these cells, lysosomes released protons, as measured by the loss of LysoTracker accumulation, but not the 10 kD Texas Red Dextran (**Figure 16A**). Similarly, in uninfected cells and cells infected with *V. parahaemolyticus* strains, we observed retention of TRD in intact lysosomes, regardless of the presence of VopQ (**Figure 16B**). We also observed that TRD is localized to the lysosomes in cells treated with chloroquine, indicating that retention of TRD in lysosomes is independent of acidification. Therefore, we found no evidence for VopQ-mediated lysosomal rupture *in vitro* or *in vivo*, but consistently observed VopQ-mediated deacidification of the lysosome coupled with the induction of autophagy.

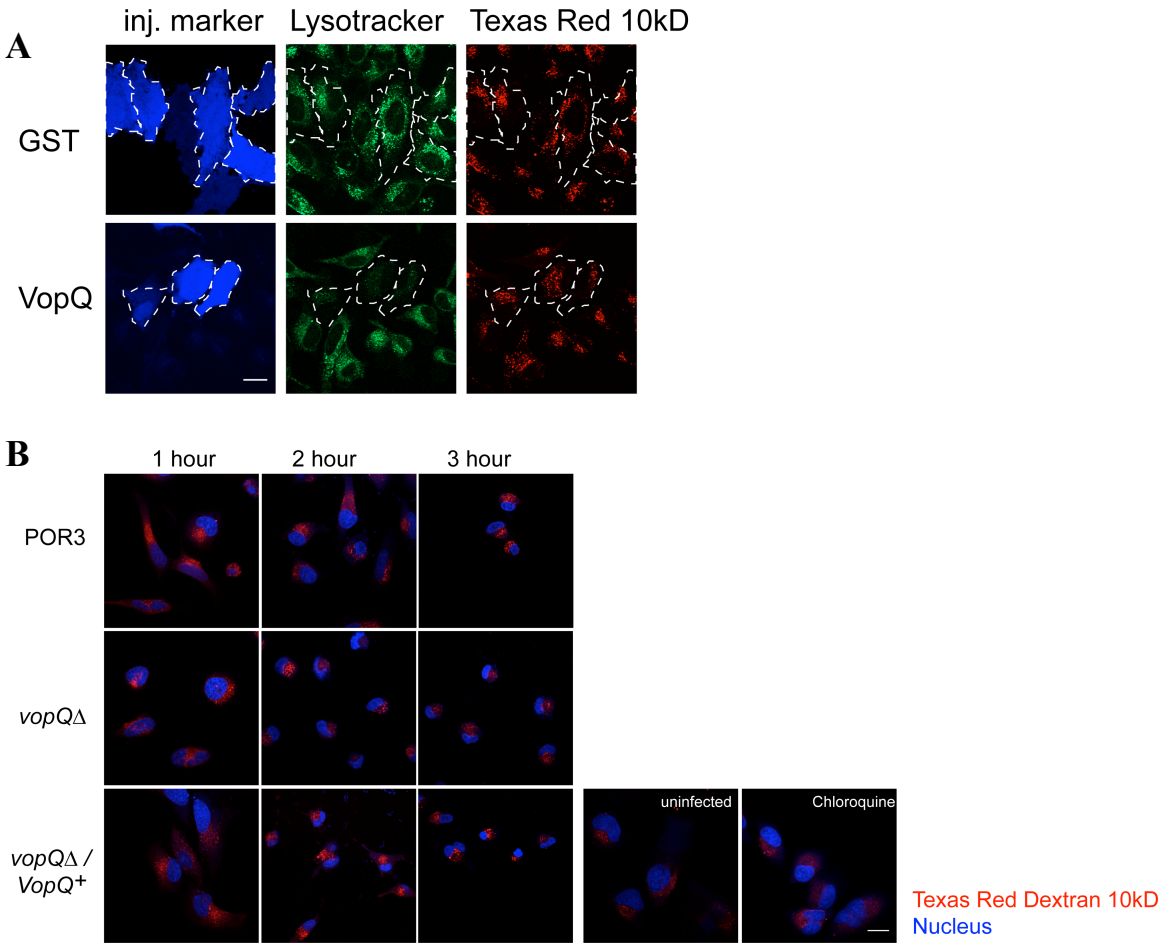


**Figure 16. VopQ does not induce lysosomal rupture.** HeLa cells were loaded with 1mg/mL Texas Red Dextran for 6 hours and chased overnight. **(A)** The following day, cells were microinjected with 10 µM GST or $His_6$VopQ, incubated 10 min (37 °C, 5% $CO_2$), then incubated with 75 nM LysoTracker Green for 10 min and visualized. Bar = 20 µ. **(B)** The following day, cells were left untreated, treated with 25 µM chloroquine or infected with noted *V. parahaemolyticus* strains at an MOI of 10. Cells were fixed with paraformaldehyde, stained with Hoeschst 33342, and visualized. Bar = 20 µ.

*VopQ forms a gated outward rectifying channel in lipid bilayers.*

To determine the physical parameters for the potential VopQ channels in membranes, we measured the electrical activities of VopQ inserted in reconstituted lipid bilayers made of POPC:DOPS (85:15 molar ratio) (*88*). When 25 nM VopQ was introduced to one side of the bilayer, we observed spontaneous channel activities within minutes (**Figure 17A**). A voltage ramp elicited an outward rectifying current between -20 mV and +40 mV, and, beyond this voltage range, the channels became inactivated, suggesting an inactivation gate in the pore (**Figure 17B**). Similar observations were obtained in the presence of a 10-fold gradient of NaCl across the bilayer. The near 0 mV reversal potentials in both cases suggest that the VopQ channel is only slightly selective for $Na^+$ over $Cl^-$ with a permeation ratio $P_{Na} / P_{Cl} =$ 1.4. When single channel currents were recorded and analyzed at different holding potentials (**Figure 17 C and D**), the single channel conductance of VopQ with equal 100 mM NaCl on both sides of the bilayer was calculated to be 129 pS (**Figure 17E**). Using the Nernst-Planck equation, we estimated its pore diameter of ~18 Å (*89*), which falls under our previous rough estimate based on the permeability of different dye molecules (**Figure 14**). Under the same conditions, VopQ was not able to form active channels in the POPC membranes, suggesting the requirement of negatively charged lipids for VopQ membrane insertion or channel formation (**Figure 17F**). We envision that electrostatic interactions between VopQ and the negatively-charged lipids may contribute significantly to the free energy change that favors the stable VopQ channel in membrane.

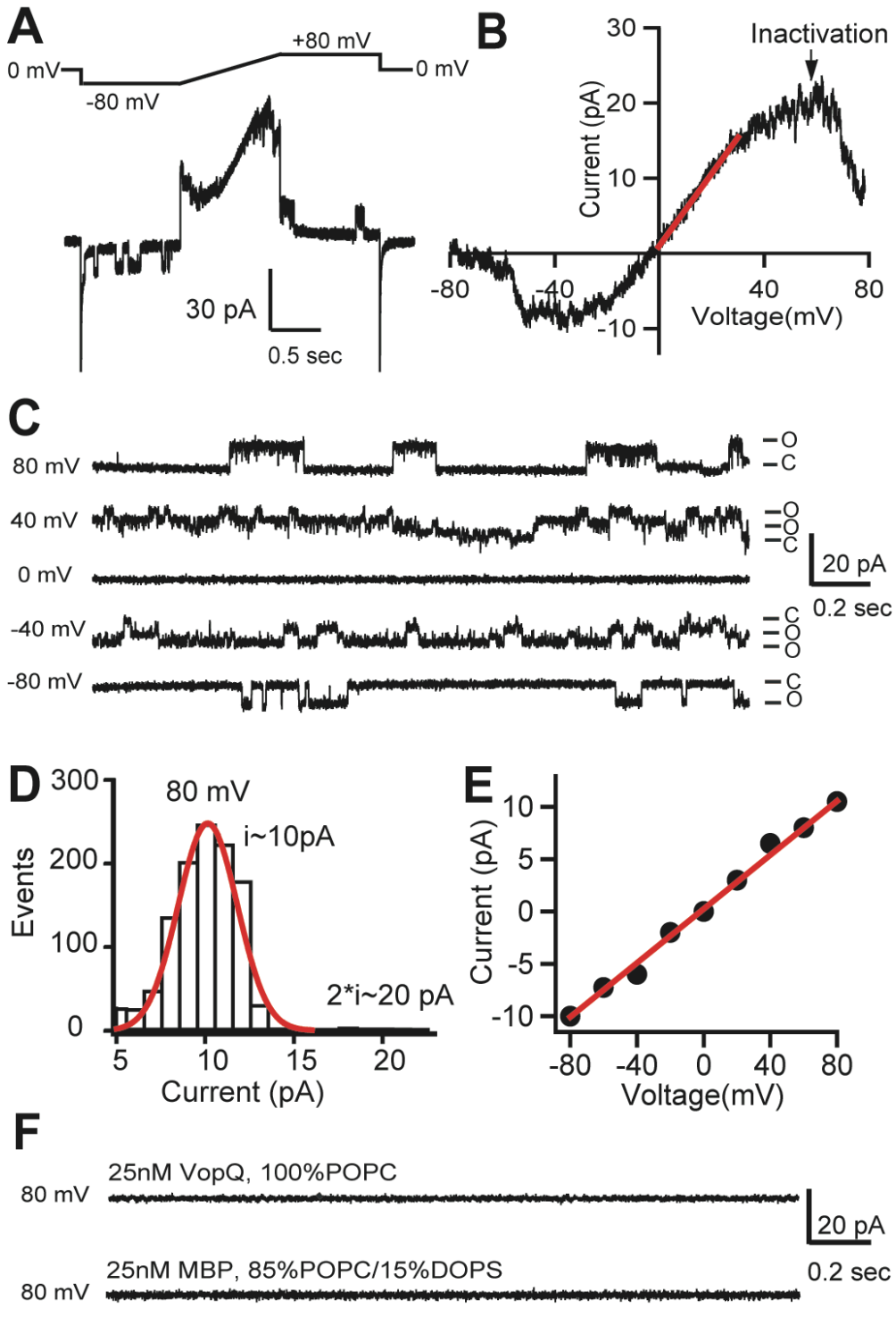
A
0 mV
+80 mV
0 mV
-80 mV
30 pA
0.5 sec
B
Inactivation
Current (pA)
30
20
10
-10
-80
-40
40
80
Voltage(mV)
C
80 mV
40 mV
0 mV
-40 mV
-80 mV
O
C
20 pA
0.2 sec
D
80 mV
i~10pA
2*i~20 pA
Events
300
200
100
0
5
10
15
20
Current (pA)
E
Current (pA)
10
5
0
-5
-10
-80
-40
0
40
80
Voltage(mV)
F
25nM VopQ, 100%POPC
80 mV
20 pA
0.2 sec
25nM MBP, 85%POPC/15%DOPS
80 mV

**Figure 17. VopQ forms a gated channel in membranes. (A)** Current recorded after 25nM MBP-VopQ was incubated with a POPC/DOPS (85:15 molar ratio) bilayer. The voltage pulse stimulation is on the top. **(B)** The averaged ramp current after the capacitance components were subtracted. The red trace was a linear fit from 0 mV to +30mV with a chord conductance of 448.11±1.67 pS. The inactivation of the channel becomes obvious when the voltage is higher than 40 mV or lower than -20 mV. **(C)** The VopQ single channel activity at different transmembrane voltages. 'O': open state; 'C': close state. (**D)** Histogram of single channel events at +80mV. We estimated the pore diameters by applying the Nernst-Planck equation, $J_k = -D_k z_k F \left(\nabla c_k + \frac{c_k z_k F}{RT} \nabla \Phi\right)$ for specific ion *k*. The measured current in our recordings was expressed as the sum of sodium and chloride flows, and the estimated pore diameter is ~18Å. **(E)** The measured single channel current-voltage relation. The linear fitting (red line) yields a single channel conductance of 128.9 ± 3.4 pS. **(F)** 25 nM VopQ incubated with 100%POPC membranes did not produce any channel activity (80mV, n=4). 25 nM MBP incubated with the POPC/DOPS membranes did not produce any channel activity (80 mV, n=6).

*VopQ forms channels in V-ATPase containing membranes.*

Having determined that VopQ can form a channel in a lipid bilayer, we wondered how this effector specifically recognizes host lysosomal membranes while avoiding *V. parahaemolyticus* bacterial membranes. Our first clue came from our in vitro liposome dequenching experiments, where we observed pore formation at pH 5.5 but not at the near-physiological pH 7.5 (**Figure 18A**). The estimated pI of VopQ is 6, and therefore VopQ would be positively charged at pH 5.5 and attracted to the negatively charged, PS-containing liposomes. However at pH 7.5, negatively charged VopQ would not bind to these negatively charged liposomes. To further investigate the interaction of VopQ with liposomes, we altered the charge of CF encapsulated liposomes by changing the PC:PS molar ratio, and hence the negative charge, of these membranes. At pH 5.5, positively charged VopQ bound and induced dye leakage in 10% and above PS-containing liposomes, but at not lower PS concentrations (**Figure 18B and C**). As seen before, the presence of V-ATPase subunits was not required for VopQ pore-forming activity in these artificial liposomes. However, we hypothesize that at physiological pH, the presence of the $V_o$ domain of the V-ATPase allows the targeting of VopQ to the appropriate acidic compartments.

In confirmation of this hypothesis, we observed that VopQ associates with yeast vacuolar membrane at pH 5.5, and this association was independent of the presence of the $V_o$ domain of the V-ATPase, which is lacking in *vma6*Δ vacuoles (**Figure 18D**). Strikingly, VopQ only bound to yeast vacuoles at pH 7.5 when the $V_o$ domain of the V-ATPase is present (**Figure 18D**). Therefore, we propose that the association of VopQ with a membrane at physiological pH is restricted to membranes containing the $V_o$ domain of the V-ATPase,

thereby acting as a protective mechanism against promiscuous pore-forming activity in the bacterium and the host (**Figure 18E**).

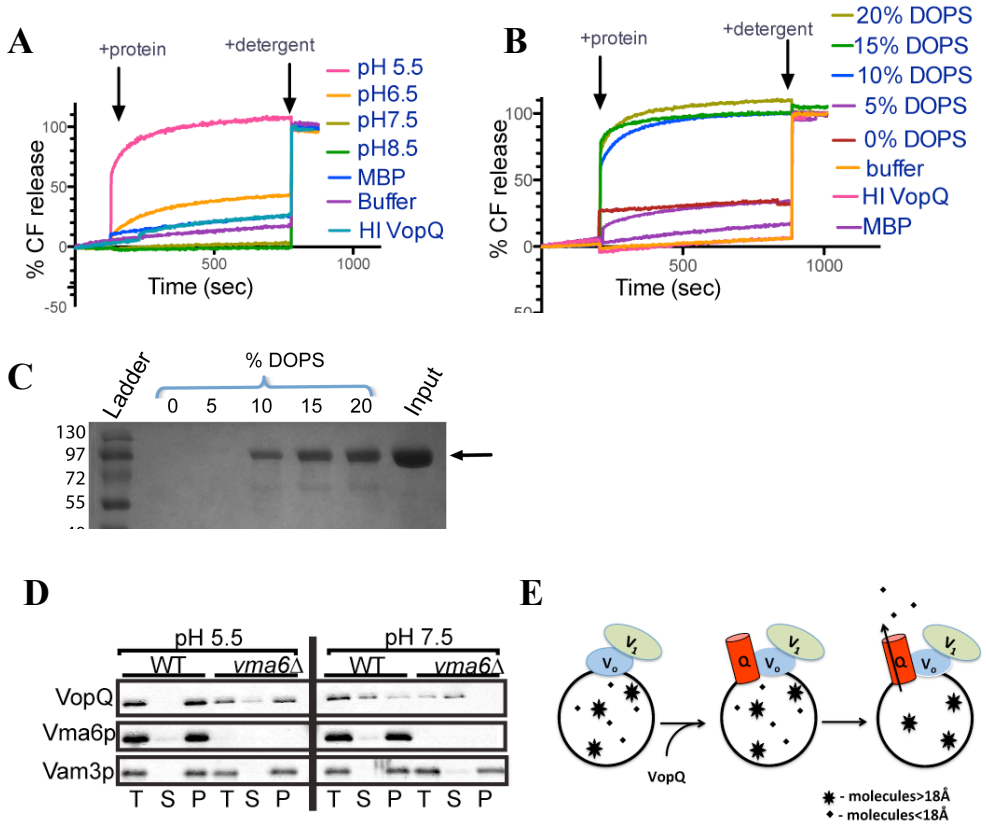


**Figure 18. VopQ is a targeted pore forming bacterial effector**. Carboxyfluorescein release was measured upon addition of 25 nM MBP-VopQ, 25 nM heat-inactivated MBP-VopQ, or 25 nM MBP to **(A)** liposomes in buffer with varying pH. **(B)** liposomes made of increasing concentrations of phosphatidylserine (0%-20% DOPS). **(C)** Binding of VopQ to liposomes (0%-20% DOPS) was analyzed using a floatation gradient and SDS-PAGE **(D)** Immunoblot analysis of VopQ association with vacuoles isolated from wild type or V-ATPase mutant yeast strains at pH 5.5 or pH 7.5. T, total reaction; P, vacuole pellet; S, supernatant. **(E)** Model for VopQ localization and pore forming activity. VopQ docks onto the $V_o$ domain of the V-ATPase and forms an 18Å channel in the membrane.

**Discussion**

Bacterial pathogens have evolved a number of unique mechanisms to target and manipulate host cell signaling (*90*). *V. parahaemolyticus* appears to secrete approximately half a dozen T3SS1 effectors to sequentially induce rapid autophagosome accumulation, followed by cell rounding and lysis. The efficiency of these activities can be attributed in many cases to the directed localization of an effector activity. We observed that VopQ targets the endolysosomal membranes by binding to the $V_o$ complex of the V-ATPase (*68, 83*). This ensures specificity for VopQ-mediated pore formation in the membranes of acidic compartments where at least protons are released within a rapid timeframe (minutes). VopQ antagonized the activity of the V-ATPase and formed a gated, outward rectifying channel that disrupts ion homeostasis, resulting in rapid accumulation of autophagosomes. These observations are consistent with rapid autophagosome accumulation resulting from the neutralization of the lysosome, similar to what is observed with the buffering activity of lysosomotropic agents, such as chloroquine (*36*).

Autophagy is used as a mechanism by which host cells recycle nutrients as well as defend themselves against invasion by bacteria. Because of the extent to which pathogenic microorganisms must manipulate their host cells during infection, multiple studies have used bacterial effectors as a powerful tool to study the regulation of autophagic pathways. Herein, we show that disruption of the autophagic flux by VopQ can result in rapid accumulation of these vesicles. As many effectors mimic the activity of host factors, it is reasonable to hypothesize that rapid autophagosomal accumulation could be mediated by a regulated outward rectifying channel. This channel could open resulting in lysosomal deacidification

and accumulation of autophagosomes. The channel could then close to allow the lysosome to reacidify by proton translocation by the V-ATPase. The accumulated autophagosomes could then be degraded by the lysosome. In support of this hypothesis, Cang et al. recently identified a eukaryotic endolysosomal ATP sensitive $Na^+$ channel that couples endolysosomal function to the cell's energy state (*91*). Upon nutrient starvation, mTOR is recruited away from the lysosome and the $Na^+$ channel controls lysosomal membrane potential and pH stability. Upon nutrient repletion, the channel is responsive to cellular ATP levels and opens and closes to control lysosomal ion and amino acid homeostasis. It is interesting to note that VopQ forms a pore large enough to disrupt amino acid homeostasis and thereby induce autophagy (*92*).

In a recent study by Matsuda and colleagues, VopQ (VepA) was implicated in the complete rupture of lysosomes. However, this VopQ-mediated effect was only observed after extensive (hours) incubations and infections (*68*). While VopQ may indeed contribute to the eventual lysis of this organelle after extended time, we find that the molecular activity of VopQ is more refined. We show that VopQ directly formed small pores within minutes, allowing the release of small molecules from acidic compartments causing a collapse of ion homeostasis inside eukaryotic cells. Previously, the activity of VopQ was implicated in modulating MAPK signaling and inducing IL-8 secretion during *V. parahaemolyticus* infection (*93, 94*); researchers have shown that pore forming toxins can directly regulate these same pathways (*95*). Therefore, we hypothesize that VopQ could induce IL-8 secretion by forming pores on lysosomes and rapidly disturbing cytosolic ion concentrations. Whereas many toxins use pore-forming mechanisms, this is the first example of a T3SS effector that

creates a gated, outward rectifying ion channel on the lysosome. It is reasonable to speculate that other pathogens may alter cellular homeostasis by using targeted effectors that act as channels to disrupt organelles, such as the mitochondria (*96*).

Bioinformatics analysis indicates that VopQ may encode multiple domains. Further studies using X-ray crystallography and mutational studies are being performed to not only elucidate the interactions between VopQ and the eukaryotic V-ATPase, but to better understand the mechanism by which VopQ may induce membrane pore formation and ion mobilization during a *V. parahaemolyticus* infection. The delivery of the bacterial effector VopQ into cells immediately created a gated outward rectifying channel within acidic compartment's membrane in the infected cell, disrupting membrane and vacuolar trafficking, ion potentials, and second messenger signaling. Future studies will involve understanding the biophysics and biochemistry of this soluble 53 kD protein that efficiently embeds into the host lysosomal membrane to form a gated channel.

# CHAPTER FOUR

## VopQ inhibits vacuole fusion

### Introduction

Vesicle fusion governs many important physiological processes including protein trafficking, neurotransmitter release, and exocytosis. As such, many studies have focused on understanding the process and proteins involved in fusion using various models such as *Drosophila* synaptic vesicles and yeast vacuoles (*97, 98*). The conserved eukaryotic V-ATPase is the main electrogenic proton pump involved in the acidification of many intracellular organelles within the endomembrane system such as the yeast vacuoles (*99*). An extensive body of research has shown the contribution of V-ATPases in a broad range of biological processes, including the proper trafficking of secreted and endocytosed cargos, viral fusion (*100*), and the SNARE-dependent membrane fusion of yeast vacuoles and *Drosophila* synaptic vesicles (*97*). The V-ATPase consists of two domains: the membrane bound $V_o$ domain and the cytoplasmic $V_1$ domain. The $V_1$ domain hydrolyses ATP while the $V_o$ domain acts as the proton pore to acidify the lumen of the vesicle. The $V_o$ domain has been shown to play a role in membrane fusion (*61, 62, 64, 101*). In particular, the $V_oC$ subunit interacts with the v-SNARE, synaptobrevin to promote exocytosis (*102*). The $V_oA$ subunit serves an acidification independent role and interacts with syntaxins to promote exocytosis (*97*). However, the role of the V-ATPase in fusion has been controversial due its dual function in acidification and fusion. Therefore, more studies are necessary to differentiate the role of V-ATPase in fusion.

The *Vibrio* effector protein, VopQ strongly associates with the conserved eukaryotic V-ATPase found on acidic organelles such as the lysosome (*31, 68*). VopQ thereby localizes to the lysosome where it inhibits autophagic flux by deacidifying the lysosome (*10*). Studies have shown that deacidification of the lysosome inhibits autophagosome-lysosome fusion (*103*). In light of this finding, we sought to measure the effect of VopQ on fusion using the well-defined biochemical model system of eukaryotic membrane fusion from the budding yeast *S. cerevisiae*. In this study, we demonstrate that expression of VopQ causes extensive yeast vacuolar fragmentation, indicative of a defect in vacuole fusion. *In vitro* homotypic vacuole fusion assays confirmed VopQ is a potent inhibitor of a conserved Rab GTPase- and SNARE-dependent membrane fusion pathway.

**Results**

*VopQ alters autophagosome-lysosome fusion in vivo*

VopQ is both necessary and sufficient to rapidly induce autophagosomal accumulation during *V.parahaemolyticus* infection (*36*). VopQ mediated autophagosomal accumulation is a result of decreased degradation of autophagosomes (*31*). This can be caused by deacidification of the lysosome or due to the lack of autophagosome-lysosome fusion (**Figure 19A**), or both. VopQ deacidifies the lysosome and blocks the degradation of autophagosomes leading to its accumulation. However, recent studies have shown that deacidification of the lysosome may inhibit autophagosome-lysosome fusion (*103, 104*).

To observe the effect of VopQ on autophagosome-lysosome fusion *in vivo* without a dependence on acidification of autophagosomes, we analyzed the localization of a mRFP-LC3 protein, with respect to LAMP-eGFP (Kimura et al., 2007). In uninfected conditions, we observed few autophagosomes (red), most of which were surrounded by lysosomal compartments (green), indicating a low level of autophagy (**Figure 19B**). Adding rapamycin to the cells induced the formation autophagosomes and more vacuoles with both mRFP-LC3-II and GFP-LAMP were observed (**Figure 19C**). Bafilomycin-treated cells showed extensive co-localization of mRFP-LC3-II and GFP-LAMP (**Figure 19D**), indicating that bafilomycin did not block autophagosome-lysosome fusion. The $Ca^{2+}$-ATPase inhibitor, thapsigargin, blocks autophagosome-lysosome fusion by inhibiting the recruitment of Rab7 to the autophagosomes (*105, 106*). Cells treated with thapsigargin showed a distinct delocalization of markers, confirming a block in autophagosome-lysosome fusion (**Figure 19E**). Cells infected with *V.parahaemolyticus* POR3 showed similar delocalization of LC3-II and LAMP

(**Figure 19F**), and this activity was completely dependent upon the presence of *VopQ* (**Figure 19G**). Cells infected with the complemented Δ*vopQ*+*VopQ* strain, but not the Δ*vopQ* strain, had low levels of LC3-II and LAMP co-localization (**Figure 19H**). These in vivo assays support our hypothesis that VopQ is an inhibitor of membrane fusion.

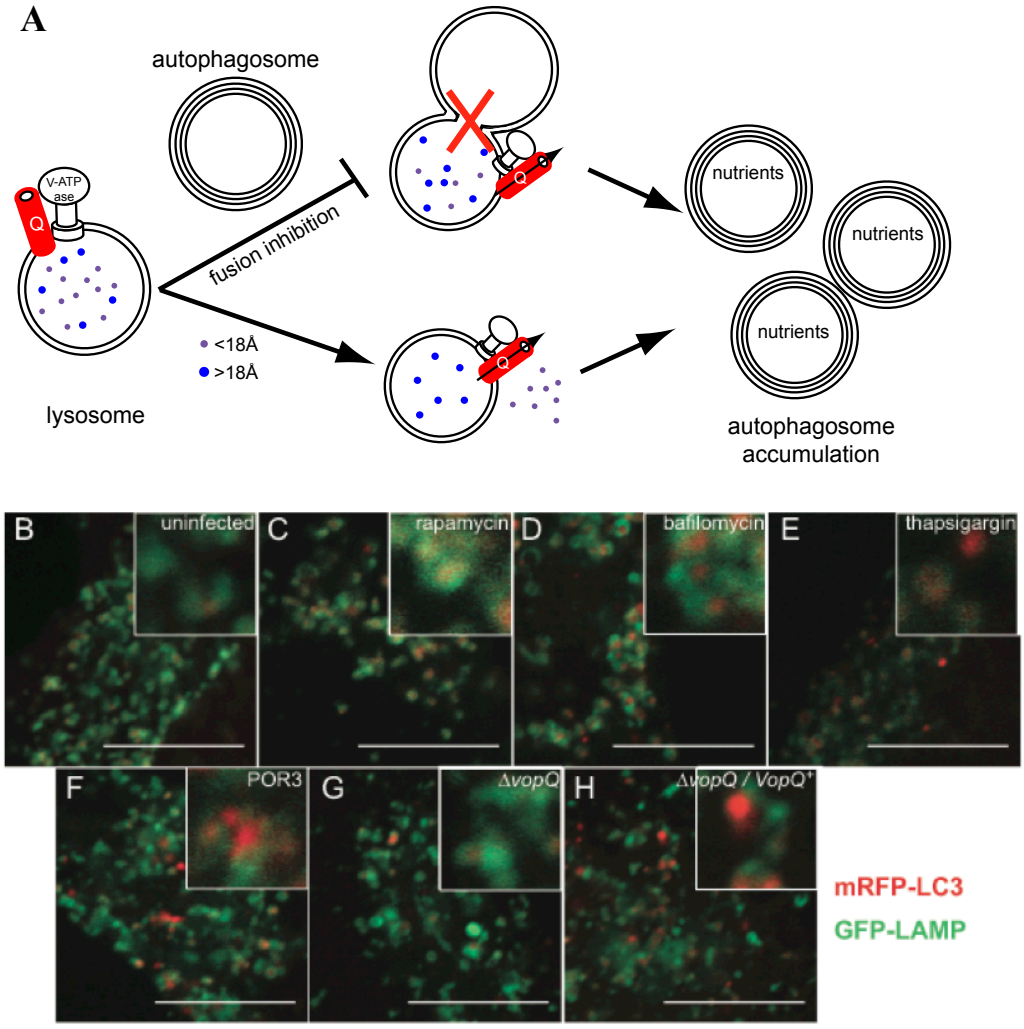


**Figure 19. VopQ inhibits autophagosome-lysosome fusion.** (**A**) The model shows VopQ (red cylinder) binds to the V-ATPase $V_o$ domain and forms a channel, resulting in deacidification of lysosomes. Deacidification of the lysosome or binding to the $V_o$ domain may also lead to inhibition of autophagosome-lysosome fusion (*107*) (**B**) HeLa cells transfected with mRFP-LC3 and GFP-LAMP were left untreated, or treated with: (**C**) 1 μM thapsigargin, (**D**) 100 nM bafilomycin, (**E**) 100 μM rapamycin, or (**F-H**) the infected with the indicated *V. parahaemolyticus* strains for 2 hours. bar=20 μ.

*VopQ inhibits yeast homotypic vacuole fusion*

As VopQ is already known to interact directly with the $V_o$ domain of the V-ATPase on the yeast vacuole, we measured the effects of VopQ on yeast vacuole dynamics *in vivo* by visualizing the vacuolar structure in the presence of VopQ. The yeast vacuole can be stained by FM4-64, which intercalates into the vacuolar membrane upon endocytic delivery (*108*). Normally, yeast cells contain 1-3 large vacuoles (**Figure 20**). The Vps33p protein, a component of the endosomal/vacuolar membrane tethering complexes, CORVET and HOPS, is required for normal vacuolar morphology, vacuolar protein sorting, and homotypic vacuole fusion [5,59], and yeast strains lacking that protein display highly fragmented vacuoles (**Figure 20**). When VopQ was expressed in yeast under a galactose-inducible promoter, we observed the striking fragmentation of the vacuolar compartment, similar to that seen in *vps33*Δ strains (**Figure 20**). Therefore, VopQ appears to have the ability to modulate vacuolar membrane dynamics *in vivo*.

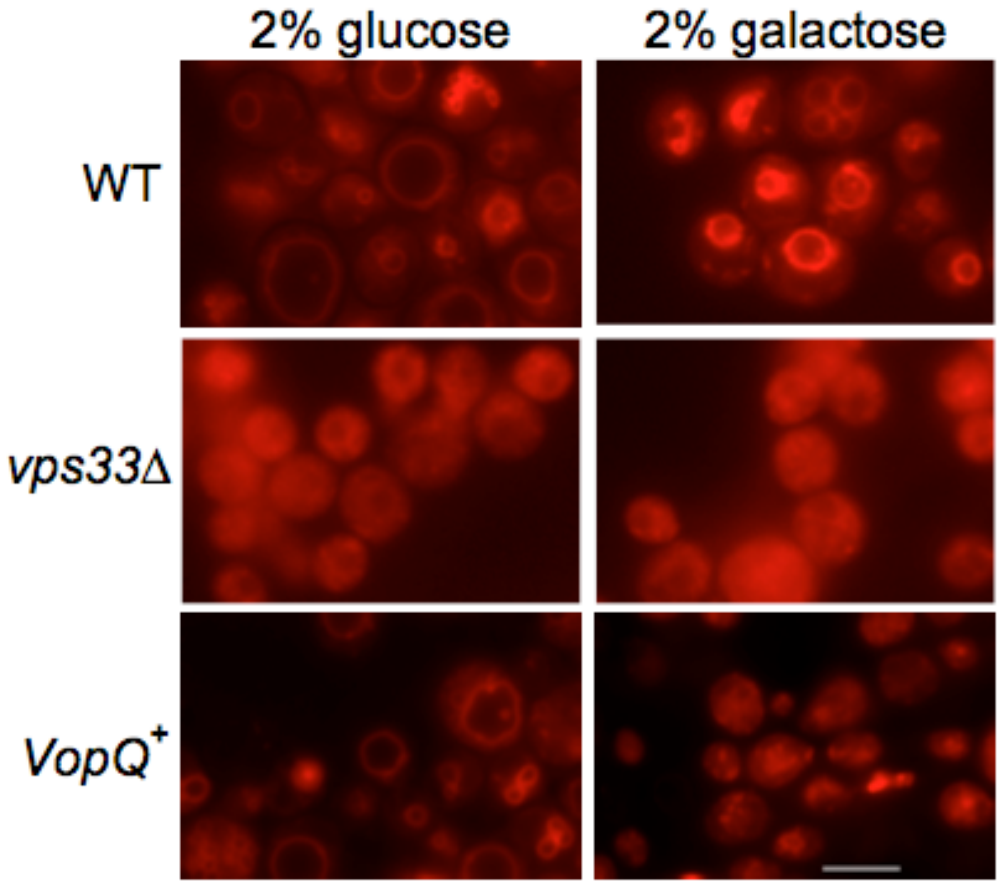


**Figure 20. VopQ induces yeast vacuole fragmentation.** BY4742 yeast strains harboring the galactose-inducible vector pRS413-Gal1 (WT), pRS413-Gal1-*VOPQ* (*VopQ*$^{+}$), or with deletions in *VPS33* (*vps33*Δ) were visualized via FM4-64 staining (*108*). bar = 5 μ.

To assay whether this effect is through the direct inhibition of the yeast vacuole fusion machinery, we measured the effect of VopQ on a highly-purified, well-studied homotypic vacuole fusion system (**Figure 21A**). As this system is known to be sensitive to a full complement of Rab-GTPase, SNARE-, and lipid-directed reagents, observations made in the context of this system are often found to be conserved in endolysosomal fusion events in higher organisms (*98*). Yeast vacuoles were isolated from two strains of yeast: one lacking Pho8p, the normal vacuolar alkaline phosphatase, and one lacking Pep4p, the lumenal vacuolar protease responsible for activating Pho8p in vivo. While neither of these purified vacuoles has alkaline phosphatase activity alone, upon successful fusion Pep4p gains access to the catalytically inactive Pho8p, thereby activating Pho8p by proteolyisis and enabling the phosphatase activity to be measured colorimetrically (*109*). In this assay, treatment of vacuoles with a buffer control exhibits efficient homotypic vacuole fusion and lumenal content mixing (**Figure 21B, closed circles**). Strikingly, recombinant VopQ protein was a powerful inhibitor of the vacuole fusion reaction in a dose-dependent manner (**Figure 21B**, **closed squares**). This inhibition was on par with standard inhibitors of the fusion reaction including antisera against the Sec17p (α -SNAP) SNARE chaperone and the Vam3p syntaxin (*56*). Therefore, VopQ appears to be capable of directly inhibiting homotypic vacuole fusion *in vitro*.

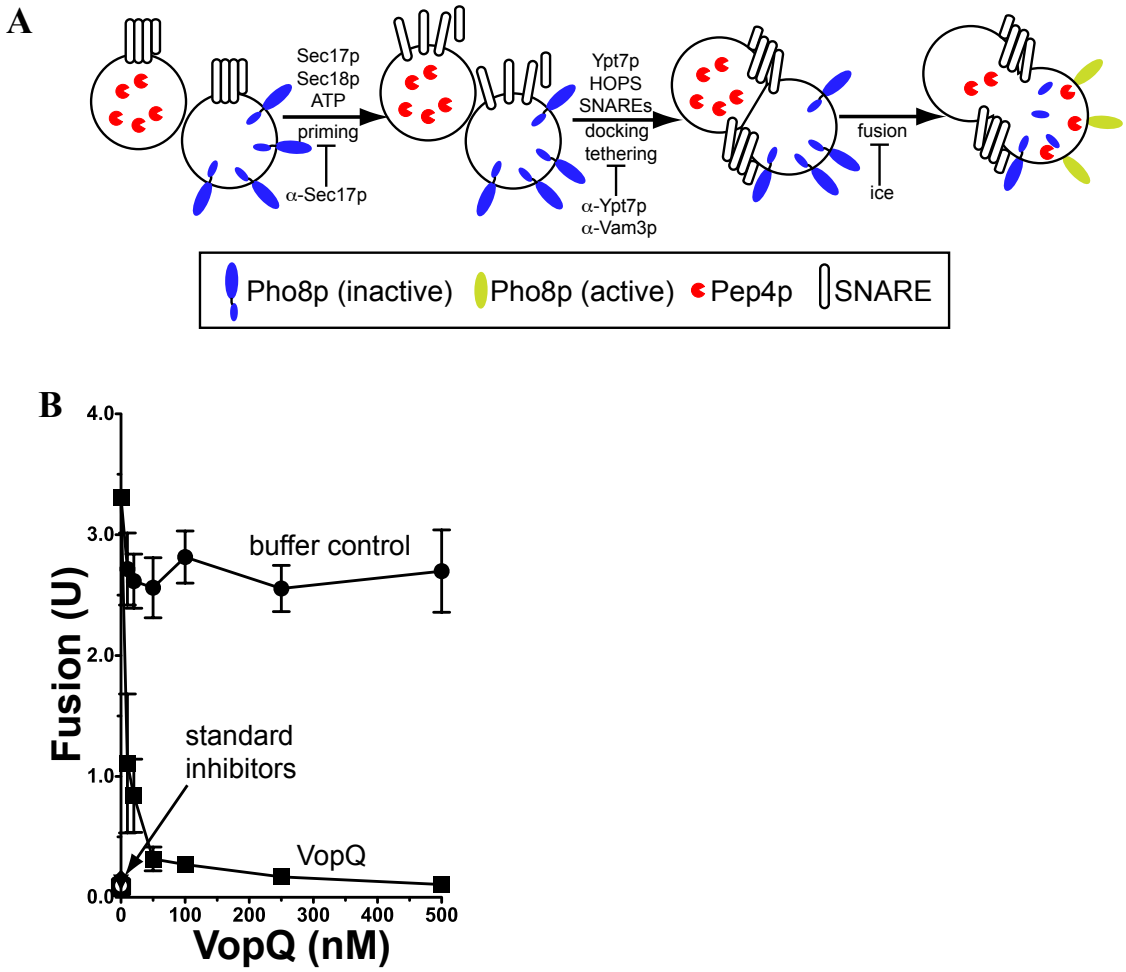


**Figure 21. VopQ inhibits vacuole fusion**. (**A**) Cartoon summarizing the kinetic progression of vacuole fusion (**B**) Standard vacuole fusion reactions were performed with vacuoles harvested from BJ3505 and DKY6281, in the absence (closed circles), or presence of $His_6$VopQ protein (squares) or standard inhibitors (0°C, α-Vam3, and GDI/Gyp1-46 (1 μM each)). Fusion activity was normalized to the mean of a "no addition" reaction (3.31 U ± 0.38); error is mean ± SD, *n* =3.

To better characterize the inhibitory nature of VopQ on yeast vacuole fusion, we took advantage of the fact that fusion occurs in three biochemically-distinct stages: first, the Sec17/18p (α-SNAP/NSF)-dependent priming of *cis*-SNARE complexes to free SNAREs (*54, 110*); second, the RabGTPase- and HOPS tethering factor-dependent docking of vacuoles resulting in the formation of the essential fusion-competent *trans*-SNARE complexes (*57, 111-113*), and third the mixing of lipid bilayers and lumenal contents which define the terminal stages of fusion (*114, 115*) (**Figure 21A**). Fusion can be analyzed using a kinetic assay designed to determine the step at which the vacuole fusion reaction becomes resistant to particular sub-reaction inhibitors (*116*). The kinetic profiles for blocking the priming, docking, and fusion steps in vacuole fusion were exemplified by the addition of antibodies to Sec17p, Ypt7p or Vam3p, or ice respectively, over the course of the fusion reaction. Addition of the priming inhibitor, α-Sec17p, to the reaction after 20 minutes did not inhibit fusion, indicating that the priming step has been surpassed at 20 minutes (**Figure 22A**). Similarly, the addition of the docking inhibitors, α-Ypt7p and α-Vam3p, after 45 minutes did not inhibit fusion indicating the completion of docking by this time (**Figure 22A**). Addition of the fusion inhibitor, ice, after 20 minutes inhibits the reaction indicating that the final step of fusion has not been surpassed. Accordingly, vacuoles become resistant to VopQ inhibition after resistance to the priming inhibitor α-Sec17p (**Figure 22A, closed squared vs. closed circles**), but before the final stage of lipid and content exchange, as measured by resistance to ice incubation (**Figure 22A**, **open squares**). Vacuoles display kinetic resistance to VopQ most similar to the docking/tethering inhibitors α-Ypt7p (**Figure 22A, open diamonds**) and α-Vam3p (**Figure 22A, closed triangles**), suggesting VopQ

inhibits the formation of *trans*-SNARE complexes.

To test the effect of VopQ on trans-SNARE complex formation during fusion, we employed an assay that measures the extent of trans-SNARE complex formation during fusion via visualization of an epitope-tagged Vam3p SNARE (CBP-Vam3p) with its cognate vacuolar R-SNARE, Nyv1p (**Figure 22B**) (*56*). Under normal fusion conditions, CBP-Vam3p and Nyv1p interact (**Figure 22C, lane 5**). This SNARE interaction was strongly disrupted by ice incubation (**Figure 22C, lane 6**), and with the extraction of Ypt7p with GDI/Gyp1-46 (**Figure 22C, lane 7**), corresponding with low levels of fusion. Addition of VopQ strongly inhibited fusion and prevented the formation of trans-SNARE complexes (**Figure 22C, lane 8**), consistent with its distinct mechanism for inhibition of vacuole fusion observed in the kinetic fusion assay.

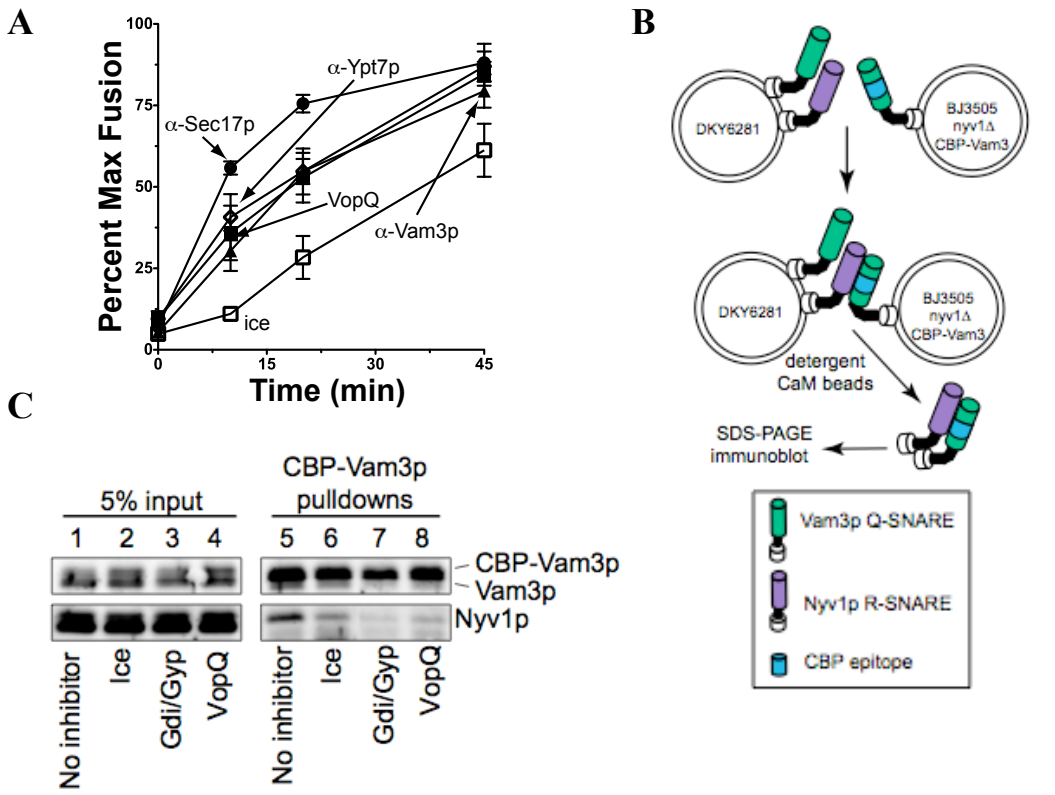


**Figure 22. VopQ inhibits the docking step of fusion and trans-SNARE pair formation.** (**A**) Fusion inhibitors α-Sec17p (closed circles), α-Ypt7p (open diamonds), $His_6$VopQ (100 nM; closed squares), α-Vam3p (closed triangles), or removal to ice (open squares) was added at 0-, 10-, 20-, 45-, 60-, and 90-min intervals. After 90 min, fusion was measured and compared with the fusion of an uninhibited fusion reaction after 90 min. Results are the mean ± SD, *n* = 3. (**B**) Schematic of trans SNARE complex formation assay. (**C**) Vacuoles from BJ3505 *nyv1Δ CBP-VAM3* and DKY6281 were used to detect formation of trans-SNARE complexes during fusion. Interactions between CBP-Vam3p Q-SNARE and Nyv1p R-SNARE are indicative of a proper trans-SNARE complex assembly.

*In vitro inhibition of vacuole fusion by VopQ*

Previous work with the purified homotypic vacuole fusion system had identified the V-ATPase as being an essential regulator of vacuole fusion, and V-ATPase inhibitors, such as bafilomycin, were shown to inhibit this reaction in vitro (*117*). The proteolytic processing and activation of the alkaline phosphatase can be used as a measure for successful yeast vacuolar fusion. However, lumenal proteases that cleave the phosphatase require an acidic environment not only for proper trafficking in vivo, but also for optimal activity in vitro (*118*). Armed with the knowledge that VopQ de-acidifies yeast vacuoles and that our readout for fusion is sensitive to pH, we chose to revisit VopQ's ability to inhibit membrane fusion with assays that do not depend upon proteolysis.

An assay to measure yeast homotypic vacuole fusion that does not depend on the proteolytic processing of Pho8p was developed previously (*82*). This assay reconstitutes the activity of a soluble, vacuole lumen-directed bifurcated enzyme, β-lactamase. When vacuolar contents are mixed as a result of fusion, the halves of β-lactamase are brought together by interacting leucine zipper domains of the c-Jun and c-Fos proteins resulting in an active β-lactamase enzyme; this β-lactamase activity can be measured colorimetrically via the hydrolysis of nitrocefin (**Figure 23A**). To confirm that VopQ is an authentic inhibitor of vacuolar fusion, vacuoles containing the split, chimeric β-lactamase subunits were assayed for fusion via the reconstitution of functional β-lactamase activity in the presence and absence of VopQ. Normal fusion is observed in the absence of inhibitors and this is used to indicate complete fusion for each assay. In the presence of fusion inhibitors (no ATP, α -Vam3p), vacuolar fusion was strongly inhibited (**Figure 23B**), as expected. Addition of

MBP-VopQ protein, but not MBP protein alone, inhibited vacuolar fusion (**Figure 23B**).

Another acidification-independent fusion assay measures lipid mixing during vacuole fusion. Purified vacuolar membranes can be labeled with Rhodamine-PE and fused to unlabeled vacuoles to measure lipid bilayer mixing via fluorescence dequenching (*119*). Standard fusion shows concurrent lipid and content mixing when used with modified vacuoles containing the components for the β-lactamase reconstitution fusion assay (**Figure 23B, C**). Standard fusion inhibitors (no ATP, α-Vam3p) inhibit both lipid and content mixing (**Figure 23C, red and blue curves**). Consistent with the context mixing experiments, MBP-VopQ, but not MBP alone, inhibited lipid mixing (**Figure 23C purple vs. green curves**). Coupled with its ability to inhibit vacuolar trans-SNARE pairing, Pho8p activation, the β-lactamase activity, and the vacuolar lipid mixing, VopQ was validated as an authentic inhibitor of yeast vacuole fusion in vitro (**Figure 22 and 23**).

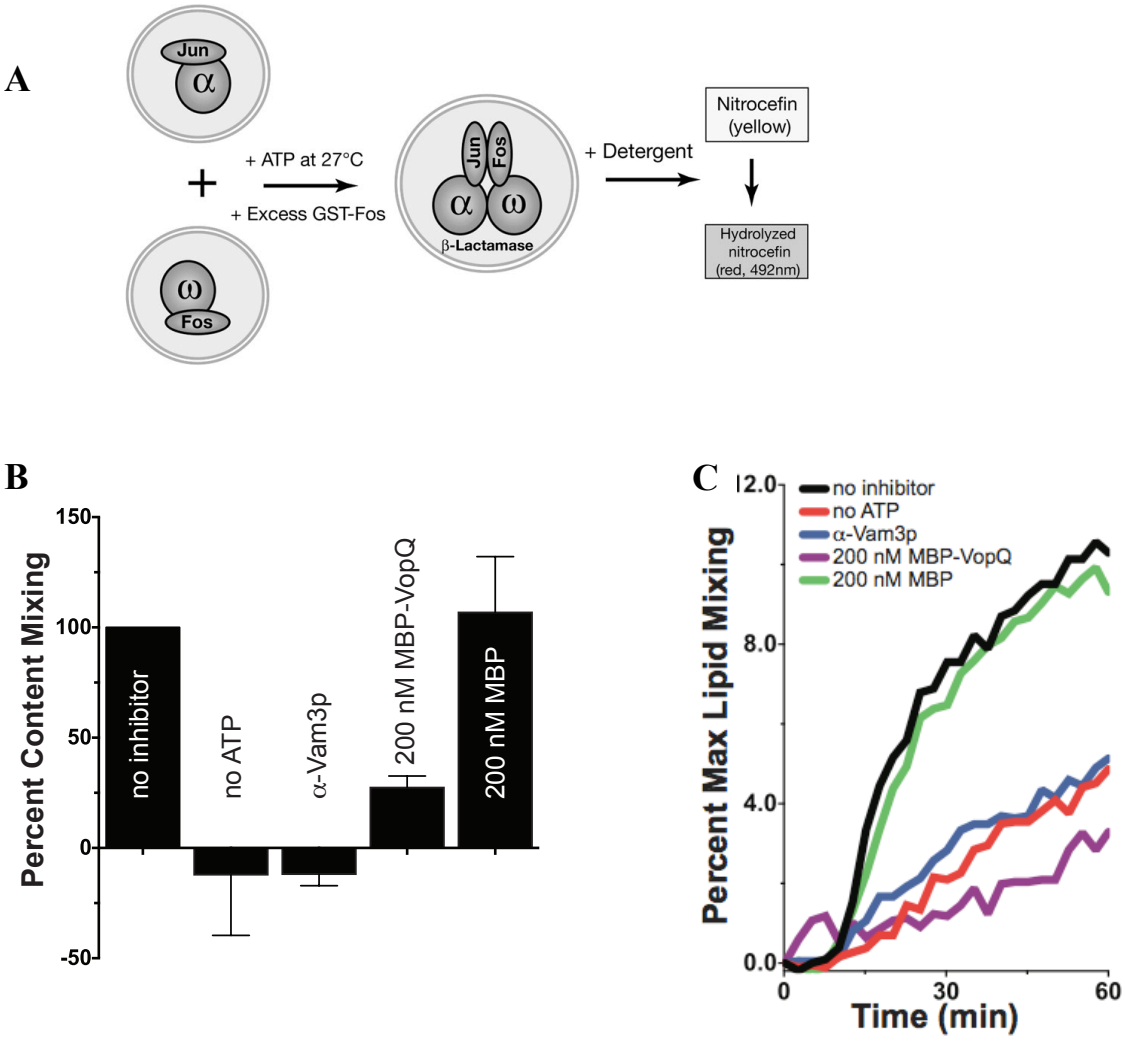


**Figure 23. VopQ inhibits vacuolar content and lipid mixing**. (**A**) Schematic of β-lactamase assay. Figure reproduced from (*82*) Copyright (2007) National Academy of Sciences, U.S.A (**B**) β-lactamase content mixing assay was performed in tandem with (**C**) a lipid mixing assay to test whether VopQ inhibits fusion.

*Vacuolar acidification is not required for vacuolar fusion*

VopQ de-acidifies the lumen of vacuoles through the rapid formation of an 18Å channel in the membrane (*31*). This process is initiated through the interaction of VopQ with the $V_o$ subunits of the V-ATPase, although the presence of the V-ATPase is not explicitly required for VopQ activity in vitro (*31*). Many reports have implied that V-ATPase subunits, particularly those which comprise the $V_o$ subdomain, are absolutely essential for the fusion of some intracellular membranes including yeast vacuoles (*61, 62*) and synaptic vesicles in Drospophila (*64*), although it remains difficult to separate the acidification activity of the V-ATPase from any potential role in a membrane fusion event. A recent publication by Coonrod, et al (2013) shows that acidification of the yeast vacuole by the V-ATPase is absolutely required for vacuole:vacuole fusion in vivo (*120*), and therefore VopQ may inhibit fusion simply through the collapse of the vacuole pH gradient.

To determine whether VopQ inhibits vacuole fusion via its deacidification activity, we compared VopQ's inhibitory activity to that of a specific inhibitor of the V-ATPase, bafilomycin A1. Previously, using the alkaline phosphatase assay, bafilomycin A1 was shown to be an inhibitor of yeast vacuole fusion in vitro (*117*). We therefore tested VopQ and bafilomycin in acidification-dependent and -independent fusion assays. When assayed for inhibition of vacuole fusion, 200 nM MBP-VopQ inhibited both the alkaline phosphatase (**Figure 24, black bars**) and β-lactamase fusion assays (**Figure 24, white bars**). Addition of equimolar MBP had no effect on either assay (**Figure 24**). When these assays are performed in the presence of 500 nM bafilomycin A1, the alkaline phosphatase activation was inhibited to approximately 60% of the maximal fusion level (**Figure 24, black bars**), yet is there is no

inhibitory activity for the activation of β-lactamase (**Figure 24, white bars**). These results show that, in contrast to VopQ, bafilomycin is not an inhibitor of yeast vacuole fusion based on the β-lactamase, but does inhibit vacuolar fusion based on the acidification-dependent alkaline phosphatase assay.

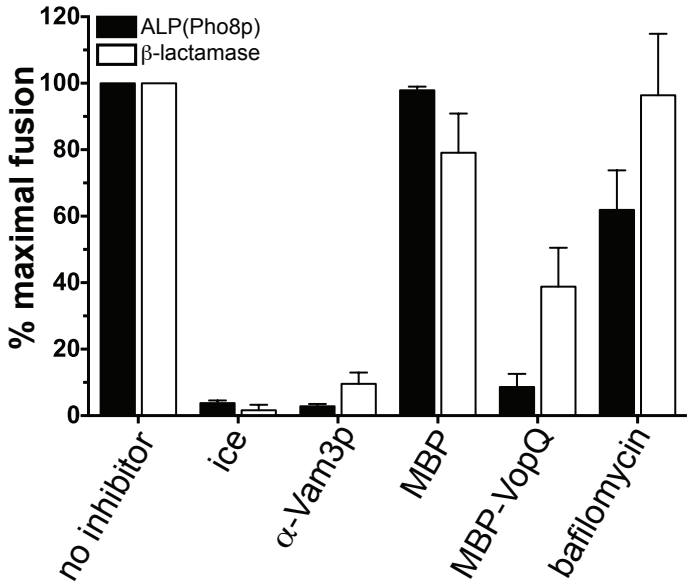


**Figure 24. VopQ inhibits vacuole fusion independent of acidification.** Standard Pho8p-dependent vacuole fusion reactions (black bars), or reactions following the reconstitution of β-lactamase (white bars, Experimental Procedures) were performed in parallel, using standard inhibitors or MBP-His protein control (100 nM), MBP-His-VopQ (100 nM), or bafilomycin (200 nM). Each reaction was compared to the extent of fusion of the "no inhibitor" reaction (Maximal Fusion); error is SD from mean, $n = 3$.

**Discussion**

Yeast vacuole fusion has been a long-studied model for the biochemical regulation of intracellular membrane fusion pathways (*121*). Herein, we demonstrate that VopQ inhibits homotypic fusion of yeast vacuoles using a purified biochemical model of a RabGTPase- and SNARE-dependent membrane fusion. VopQ binds to the $V_o$ domain of the yeast V-ATPase and inhibits trans-SNARE complex formation. Multiple studies have indicated that the $V_o$ domain subunits are required for the proper fusion of yeast vacuoles (*61, 62*). Furthermore, the $V_o$ subunit a1 (Vph1p) has been shown to be critical for other membrane fusion-mediated events, such as synaptic vesicle exocytosis in *Drosophila (97)*, as well as neuronal turnover by phagocytic uptake by microglia in zebrafish (*122*).

To date, it is still unclear how the membrane sector of the V-ATPase mediates these fusion events. As the $V_o$ domain proteins can interact directly with SNARE proteins, a mechanism for $V_o$ directly regulating trans-SNARE complexes during fusion has been proposed (*62*). Interestingly, Strasser et al. (2011) found that specific mutations in the $V_o$ subunits Vma3p and Vma11p, which physically form the proteolipid proton channel in yeast vacuole membranes (*61*), inhibits the mixing of lipid bilayers during homotypic vacuole fusion, while allowing the formation of proper trans-SNARE pairs during fusion (*61*). This provides enticing evidence that the $V_o$ proteolipid channel may form a so-called “fusion pore” during some physiological membrane fusion events. However, other biochemical studies with vacuole SNARE-containing proteoliposomes have shown that V-ATPase $V_o$ subunits are not absolutely required for bilayer mixing (*123-125*). Since we detect reduced

trans-SNARE pairing during vacuole fusion with treatment of VopQ (Figure 18C), we propose that the physical interaction of VopQ with the $V_o$ domain is responsible for disrupting membrane fusion, but based on the bafilomycin experiments, the de-acidification activity of VopQ is not directly contributing to its ability to hinder membrane fusion. This inhibition of fusion could either take place through steric hindrance of vacuolar docking introduced by VopQ:$V_o$ binding, or through VopQ-dependent uncoupling of the known Vam3p SNARE:$V_o$ interaction during fusion. Studies to address these possibilities are currently underway, and will provide important new insights into the mechanisms by which $V_o$ domains may catalyze intracellular membrane fusion events. Further studies using X-ray crystallography and mutational studies are being performed to elucidate the interactions between VopQ and the V-ATPase, and to better understand the mechanism by which VopQ inhibits fusion independent of deacidification. To the best of our knowledge, VopQ is the first bacterial effector shown to inhibit membrane fusion by a direct interaction with the $V_o$ domain.

# CHAPTER FIVE

## Structural studies of VopQ

### Introduction

VopQ is a 53 kD bacterial effector protein that binds to the conserved eukaryotic V-ATPase (*31*). The membrane associated VopQ then forms a voltage-gated channel in the vacuolar membrane and inhibits vacuole fusion (*31*). The purpose of this chapter is to use structural studies to dissect the two activities of VopQ: channel formation and inhibition of vacuolar fusion. VopQ can be divided into three parts based on primary structure: 1-30 aa, 31-100 aa and 101-492 aa (**Figure 25A**). The first 30 amino acids of VopQ consist of a disordered and unstable region that aids in secretion of VopQ through the T3SS (*126*). Amino acids 31-100 bind to the chaperone, vp1682 (*126*). Amino acids 101-492 have three transmembrane helices that may form a hydrophobic pore based on hydrophobicity predictions (*127*). The secondary structure of VopQ consists predominantly of α-helices as predicted by bioinformatics and confirmed by CD (**Figure 25B and C**). The tertiary structure of VopQ has been elusive since it shares no homology to known toxins or membrane proteins. In order to gain structural insight into the mechanism of the VopQ, we decided to take two approaches. First, we used truncation and point mutations to study putative functional domains of VopQ. Second, we attempted to crystallize VopQ in its soluble chaperone-bound form as well as in its membrane-bound channel form.

**A**

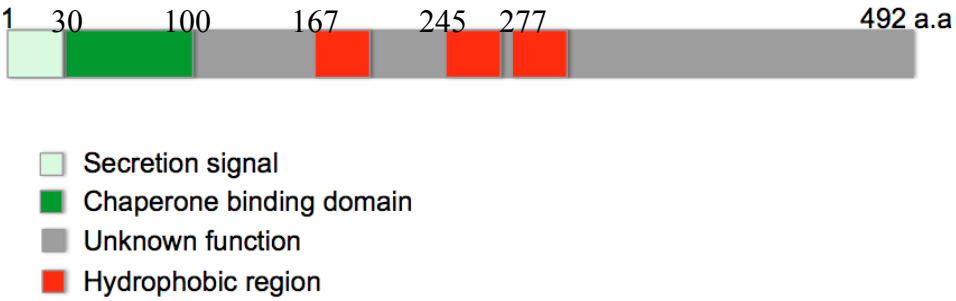
1
30
100
167
245
277
492 a.a
Secretion signal
Chaperone binding domain
Unknown function
Hydrophobic region

**B**

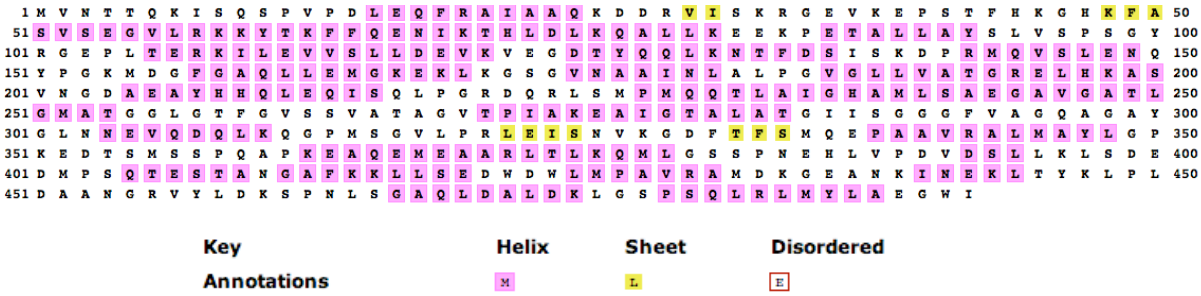
1 M V N T T Q K I S Q S P V P D L E Q F R A I A A Q K D D R V I S K R G E V K E P S T F H K G H K F A 50
51 S V S E G V L R K K Y T K F F Q E N I K T H L D L K Q A L L K E E K P E T A L L A Y S L V S P S G Y 100
101 R G E P L T E R K I L E V V S L L D E V K V E G D T Y Q Q L K N T F D S I S K D P R M Q V S L E N Q 150
151 Y P G K M D G F G A Q L L E M G K E K L K G S G V N A A I N L A L P G V G L L V A T G R E L H K A S 200
201 V N G D A E A Y H H Q L E Q I S Q L P G R D Q R L S M P M Q Q T L A I G H A M L S A E G A V G A T L 250
251 G M A T G G L G T F G V S S V A T A G V T P I A K E A I G T A L A T G I I S G G G F V A G Q A G A Y 300
301 G L N N E V Q D Q L K Q G P M S G V L P R L E I S N V K G D F T F S M Q E P A A V R A L M A Y L G P 350
351 K E D T S M S S P Q A P K E A Q E M E A A R L T L K Q M L G S S P N E H L V P D V D S L L K L S D E 400
401 D M P S Q T E S T A N G A F K K L L S E D W D W L M P A V R A M D K G E A N K I N E K L T Y K L P L 450
451 D A A N G R V Y L D K S P N L S G A Q L D A L D K L G S P S Q L R L M Y L A E G W I
Key
Helix
Sheet
Disordered
Annotations
M
L
E

**C**

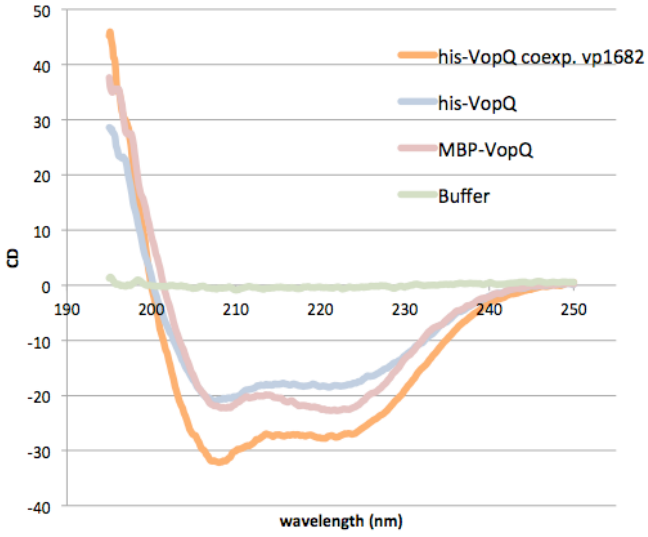
50
40
30
20
10
0
-10
-20
-30
-40
CD
190
200
210
220
230
240
250
wavelength (nm)
his-VopQ coexp. vp1682
his-VopQ
MBP-VopQ
Buffer

**Figure 25. VopQ primary and secondary structure**. (**A**) VopQ domain architecture. Encoded in light green is the secretion signal from amino acids 1-30, in dark green is the CBD from amino acids 31-100, in red is the hydrophobic patch from amino acids 167-198 and 245-297. (**B**) VopQ secondary structure prediction using psiPred (*128*). (**C**) CD spectra of purified recombinant VopQ indicate that the protein is predominantly α-helical. His tagged VopQ was expressed with or without its chaperone, vp1682. MBP-VopQ denotes VopQ tagged with both a polyhistidine tag and Maltose Binding Protein (MBP), which increases solubility of the protein.

**Results**

*Analysis of truncation mutants for VopQ*

Truncation mutants were made by deleting 100 amino acids from the N or C terminal of VopQ. Several of the truncated proteins are not stably expressed or readily purified (**Figure 26 A-C**). Stable proteins, Δ100 VopQ and Δ200 VopQ, were used in two different assays, the liposome leakage assay and the vacuole fusion assay, to define which regions are contributing the activities defined for VopQ.

The mutant proteins were first tested in the liposome dye release assay at pH 5.5 to test for pore forming activity. As there are no proteins in the liposomes, this assay can test for pore activity but not V-ATPase-dependent targeting of VopQ. Based on our deletion mutants, the N-terminal 200 amino acids and C-terminal 92 amino acids were dispensable for pore formation in this assay (**Figure 27A**). Next, we wanted to test these truncation mutants in the alkaline phosphatase vacuolar fusion assay. The fusion assay can test for both targeting and pore activity because VopQ binds to the V-ATPase to localize and form a channel on the vacuolar membrane. This assay, however, has two major disadvantages. First, many mutants cannot be tested in the assay due to the duration required for stability of the protein over the 1-hour time frame of the assay. Second, the targeting activity is epistatic to the pore activity in this assay. This means that the mutant protein will not form a channel if it does not bind to the V-ATPase on the vacuolar membrane. The fusion assay revealed that deletion of the first 100 amino acids abrogated VopQ-mediated fusion inhibition (**Figure 27B**), as does deletion of the first 28 amino acids (**Figure 27C**). This latter deletion reduces the binding of VopQ to the V-ATPase as seen in the pulldown experiment (**Figure 27D**). Therefore, we tested if

targeting VopQ to the membrane can restore the fusion inhibition. Addition of a membrane-binding domain, Phox to Δ28 VopQ recapitulated the fusion inhibition (**Figure 27C**). This indicates that the N terminal of VopQ aids in targeting to the membrane and this targeting is required for fusion inhibition. In summary, the liposome assay along with the fusion assay suggests that amino acids 200-400 are required for channel activity and that the N terminal is required for targeting.

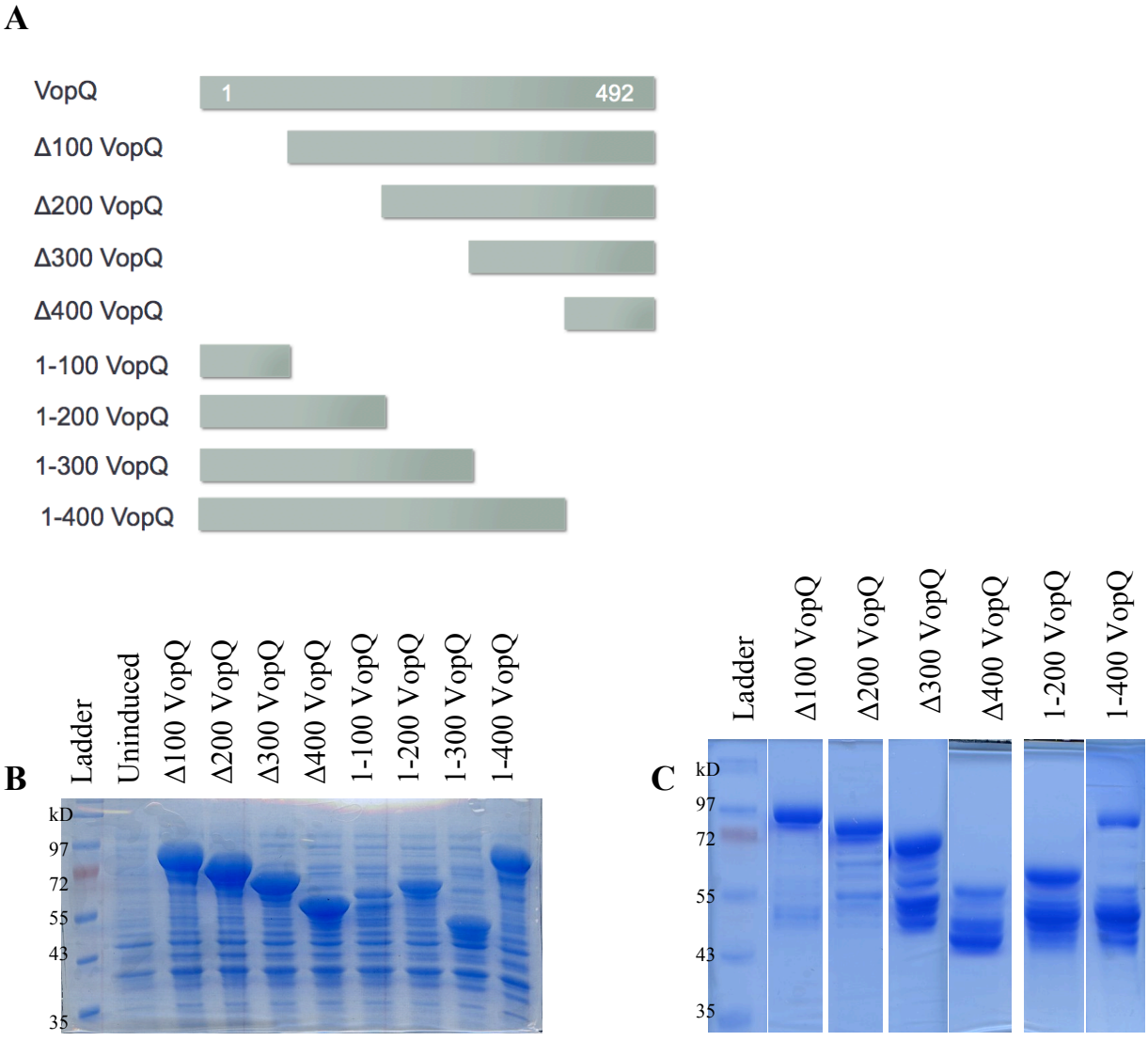


**Figure 26. Purification of truncation mutants**. (**A**) Schematic of truncation mutants (**B**) Expression profile of N terminal and C terminal truncations of VopQ tagged with MBP-his. All truncation mutants express upon induction with IPTG except for 1-100aa and 1-300aa MBP-VopQ (**C**) Stability of eluted proteins from nickel affinity chromatography

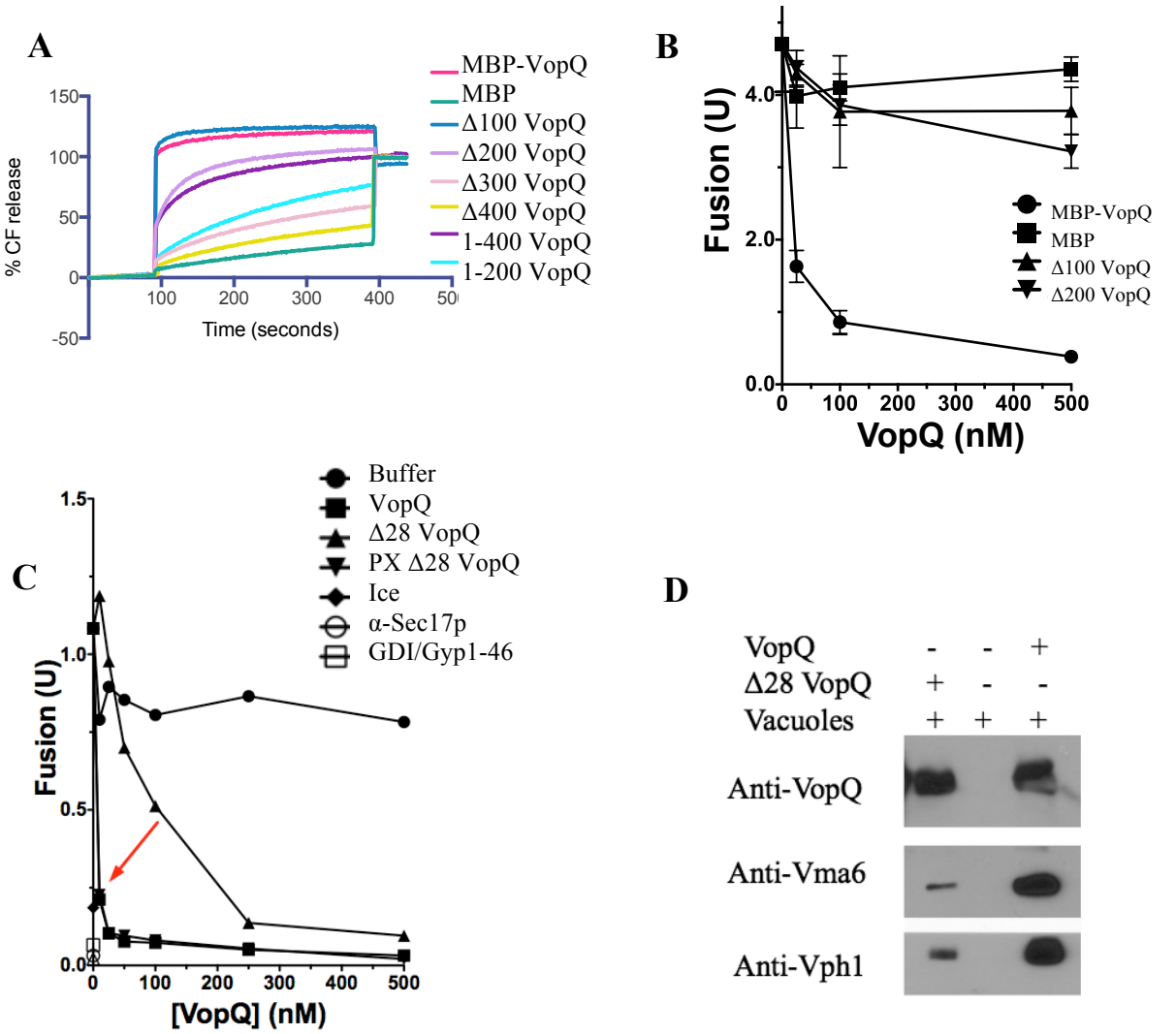


**Figure 27. Functional assays of truncation mutants** (**A**) Liposome leakage assay with truncation mutants (**B**) Vacuole fusion assay with truncation mutants. (**C**) Targeting sequence of VopQ can be substituted with PI3P binding domain, phox (PX), to target VopQ to the vacuolar membrane. Red arrow denotes Δ28 VopQ vs. PX Δ28 VopQ fusion inhibition (**D**) Immunoblot analysis of VopQ-associated proteins from yeast vacuoles.

*Analysis of point mutants for VopQ*

In order to find conserved domains and to delineate the dual function of VopQ, I made point mutations based on putative domains. Bioinformatics analysis of VopQ reveals the presence of a glycine zipper motif (**Figure 28A**, Lisa Kinch). Glycine zippers are common motifs found in membrane proteins especially homoligomeric channel proteins. They consist of the consensus sequence GXXXGXXXG and form tetramers, pentamers, hexamers and heptamers (*129*). Approximately 25% of membrane proteins contain this domain and mutations result in diminished channel activity (*129*). These sequences are found in bacterial pore toxins such as VacA as well as Alzheimer's Aβ protein. The glycine motif in VopQ is found in the second putative transmembrane helix. Therefore, I mutated G244A, G247A, G251A, G258A found in the putative VopQ glycine zipper motif. Unfortunately, none of the single point mutations altered the ability of VopQ to induce liposome dye release (**Figure 28B**).

Next, we used random mutagenesis to identify a non-toxic VopQ mutant in a yeast survival screen. VopQ plasmid was transformed into the error-prone *E. coli* strain, XL1-Red, to create a library of mutants. This library was then transformed into yeast cells and screened for viable yeast clones. The screen yielded one strong candidate, $VopQ^{S200P,F292I}$ (**Figure 28C**). Unfortunately, $VopQ^{S200P,F292I}$ protein did not express well in *E. coli*. To study the point mutations independently, we created single mutants $VopQ^{S200P}$ and $VopQ^{F292I}$. These point mutants expressed well in *E. coli* (**Figure 28D**). Analysis of these mutants in a yeast toxicity assay showed that $VopQ^{S200P,F292I}$ and $VopQ^{S200P}$ had reduced toxicity, while $VopQ^{F292I}$ exhibited wild-type toxicity (**Figure 28C)**. Therefore, the $VopQ^{S200P}$ mutant

protein was used for the liposome dye release and vacuole fusion inhibition assays (**Figure 28E and F**, respectively). VopQ$^{S200P}$ formed pores on liposomes but did not inhibit fusion. Similar to Δ28 VopQ, we hypothesized that the reduced fusion inhibition may be due the reduced affinity of VopQ$^{S200P}$ for the V-ATPase. Pulldown assays showed that VopQ$^{S200P}$ has reduced binding to the V-ATPase (**Figure 28G**). Current studies are focused on examining the interaction of VopQ$^{S200P}$ with the $V_o$ domain of the V-ATPase. Additional insight into the interaction of VopQ with the V-ATPase would probably be gained through crystallographic studies.

**A**

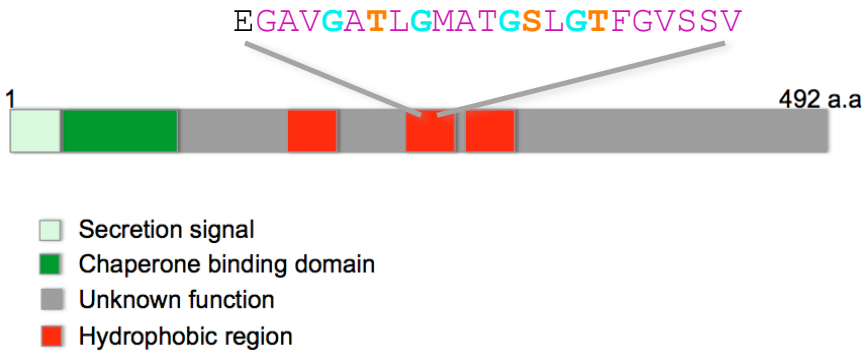
EGAVGATLGMATGSLGTFGVSSV
1
492 a.a
Secretion signal
Chaperone binding domain
Unknown function
Hydrophobic region

**B**

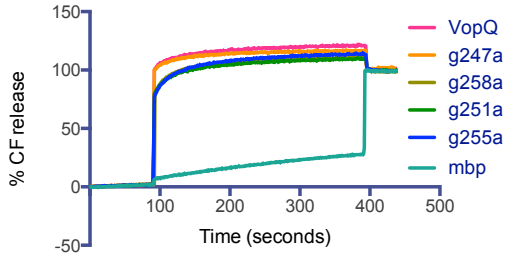
% CF release
Time (seconds)
VopQ
g247a
g258a
g251a
g255a
mbp

**C**

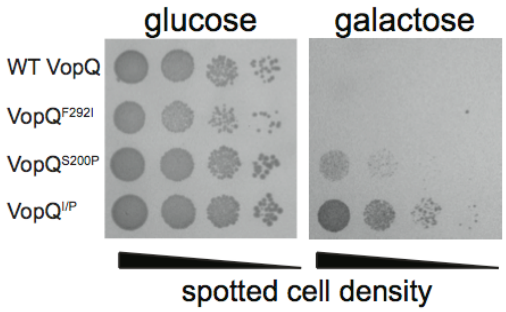
glucose
galactose
WT VopQ
VopQF292I
VopQS200P
VopQI/P
spotted cell density

**D**

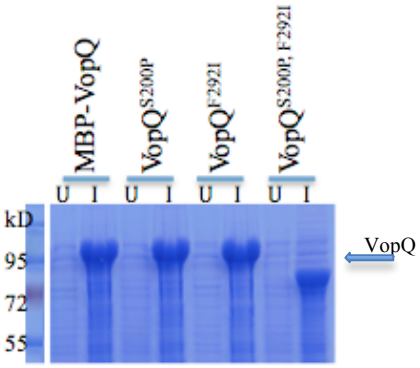
MBP-VopQ
VopQS200P
VopQF292I
VopQS200P, F292I
U I
kD
95
72
55
VopQ

**E**

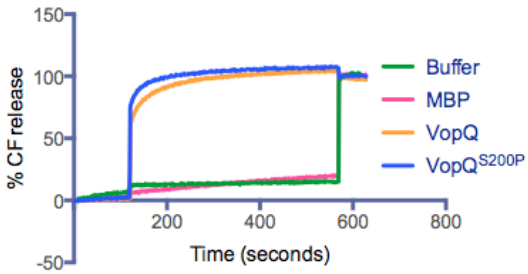
% CF release
Time (seconds)
Buffer
MBP
VopQ
VopQS200P

**F**

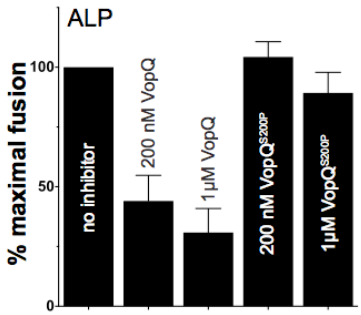
ALP
% maximal fusion
no inhibitor
200 nM VopQ
1 µM VopQ
200 nM VopQS200P
1µM VopQS200P

**G**

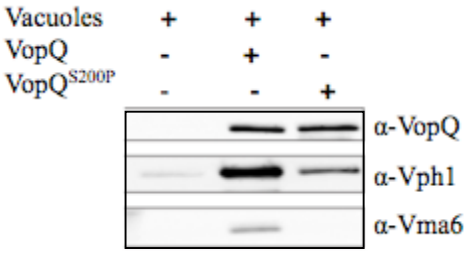
Vacuoles
VopQ
VopQS200P
α-VopQ
α-Vph1
α-Vma6

**Figure 28. Analysis of VopQ point mutants**. (**A**) VopQ glycine zipper motif (**B**) Liposome leakage assay with glycine mutants (**C**) Yeast dilution plating shows that the S200P, F292I mutation diminishes the wild type toxicity (**D**) Expression profile of VopQ mutants. I : VopQ protein expression induced; U: uninduced. (**E**) $VopQ^{S200P}$ forms pores in liposomes (**F**) $VopQ^{S200P}$ does not inhibit fusion. (**G**) Immunoblot analysis of $VopQ^{S200P}$ interacting proteins from yeast vacuoles.

*Limited proteolysis of soluble VopQ reveals a stable fragment*

VopQ consists of several disordered regions that may prevent protein crystallization (**Figure 25B**). Initially, VopQ was co-expressed and purified with its chaperone, vp1682 (**Figure 29A**). To determine the stable core of the protein bound to its chaperone, I used various proteases to digest the accessible disordered regions of the protein (**Figure 29B**). Increasing concentrations of proteases yielded two stable products (**Figure 29B**). However, because full length VopQ bound to the chaperone was relatively resistant to protease cleavage (**Figure 29B, lane 1,2,4,5 and 7**), we did not use the 25 kD for further studies. Full length VopQ bound to the chaperone was used instead for crystallography trials.

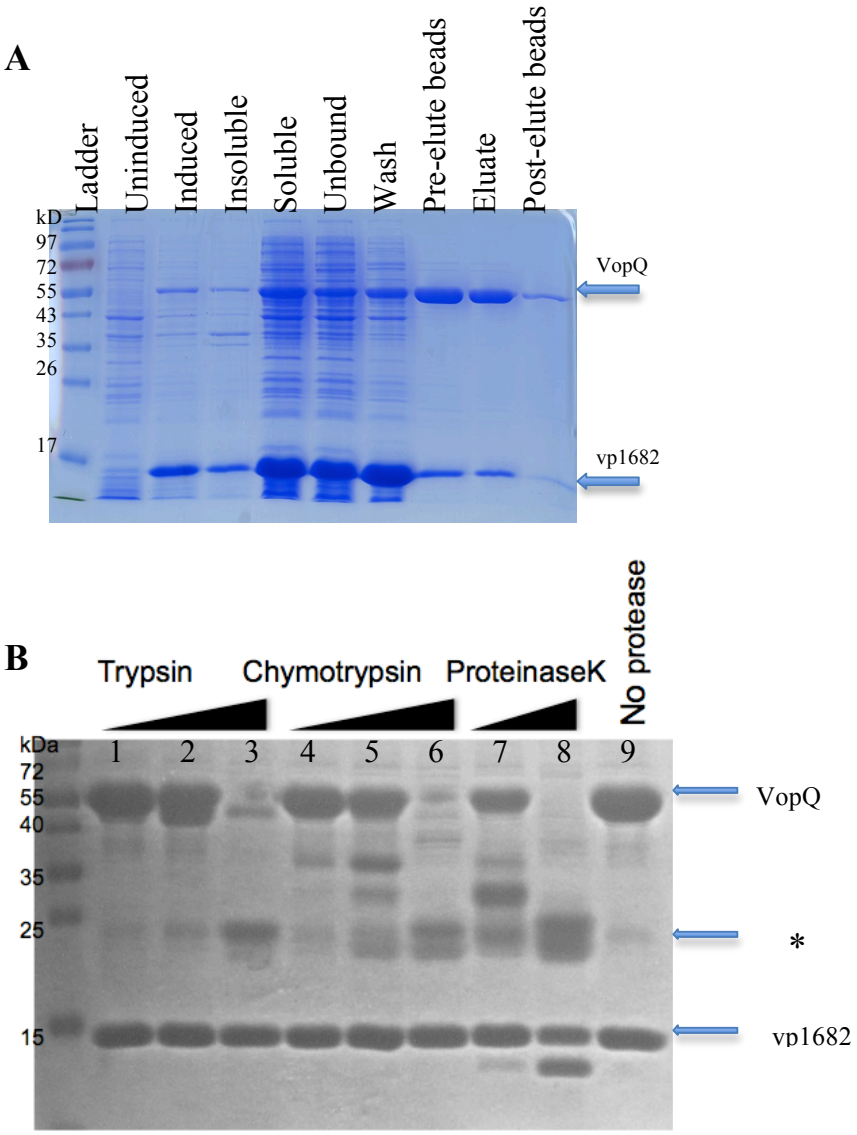


**Figure 29. Purification of soluble VopQ. (A)** Purification of $His_6$VopQ co-expressed with its chaperone vp1682, using nickel affinity chromatography. **(B)** Limited proteolysis of full length VopQ (55kD) bound to its chaperone, vp1682 (17kd) was subject to proteolysis by proteases with varying specificity. Protease digestion resulted in an unknown fragment denoted by * .

*Initial Screening of VopQ-vp1682 produces crystals of degradation product*

In order to obtain VopQ bound to vp1682 for crystallography, his tagged VopQ was co-expressed with untagged vp1682. The complex was then purified using nickel affinity chromatography followed by gel filtration (**Figure 30A**). VopQ bound to chaperone was highly soluble (>40mg/mL) and moderately stable (**Figure 30B**). This protein complex was used to screen a range of conditions varying in chemical compositions, concentrations and pH for crystal formation. Crystals formed in about 2 weeks at room temperature and diffracted to approximately 20 Å (**Figure 30C**). VopQ co-expressed with vp1682 produced reproducible crystals in 0.1M KCl, 5% glycerol, 13% PEG3350. Hence, this condition was used to optimize the crystal quality. First, I altered the PEG and salt concentration to improve crystal resolution. These trials resulted in crystals that diffracted to about 5-6 Å. Unfortunately, better resolution is needed to solve the structure. Secondly, I used the additive screen to check for any chemical additives that would improve crystal quality. Additives did not improve crystal resolution. After exhaustive optimization with no improvement in resolution, the crystals were harvested and checked for protein degradation (**Figure 30D**). N-terminal protein sequencing revealed that VopQ crystals were made up of a degradation product, Δ243 VopQ. VopQ stored at room temperature for about 2 weeks degrades to a similar fragment as was observed with the crystals. Current studies focus on expression and purification of Δ243 VopQ for crystallography.

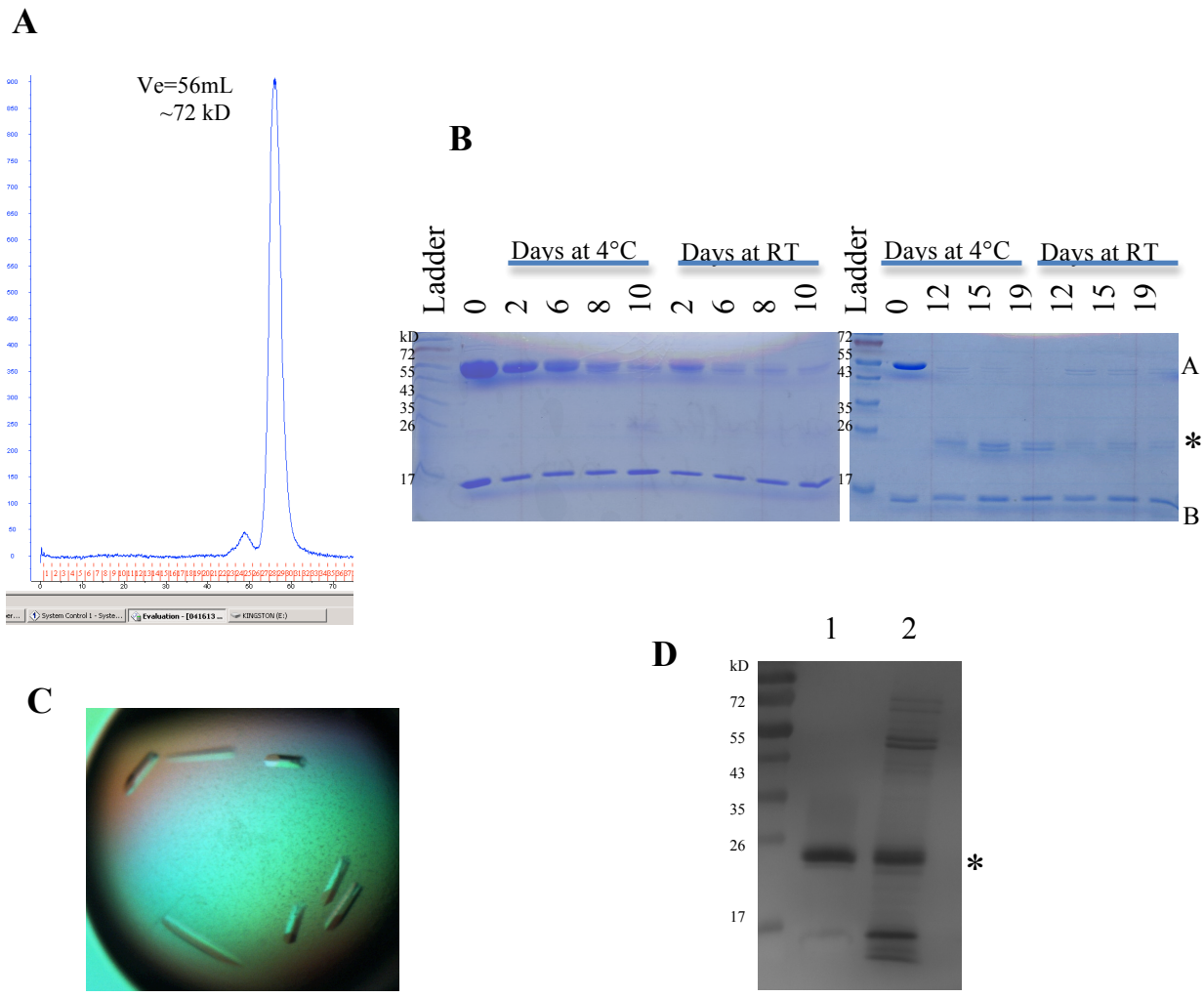


**Figure 30. VopQ purification and stability test for crystallography**. (**A)** Superdex75 trace of $His_6$VopQ purified using nickel affinity column as seen in **Figure 29A** (**B**) Stability of VopQ co-expressed with vp1682 at 4°C or room temperature.* denotes the degradation product, "A" denotes VopQ, "B" denotes vp1682 (**C**) VopQ crystals formed in 0.1M KCl, 5% glycerol, 13% PEG 3350. (**D**) Lane 1: Crystals harvested and run on SDS-PAGE gel reveal degradation product, Δ243 VopQ. Lane 2: VopQ stored at room temperature for two weeks.

VopQ bound to vp1682 produced crystals of a degradation product indicating that the complex was unstable. A common technique used to improve stability is to slightly vary the construct by using structural mutants or homologues of the protein (*130*). The homologue of VopQ in *Vibrio campbellii* is a fusion protein of the effector and chaperone eliminating the need for the chaperone-binding domain (**Figure 31A**). I attempted to use a similar fusion protein of VopQ and the chaperone, Δ100VopQ fusion Δc10vp1682, for crystallography. This construct was previously used by Phi Luong in our lab to obtain reproducible crystals; however, they diffracted poorly. The protein was very stable and crystals formed in one day (**Figure 31 B and C**). However, these crystals diffracted to >20 angstroms; optimization trials did not yield better crystals.

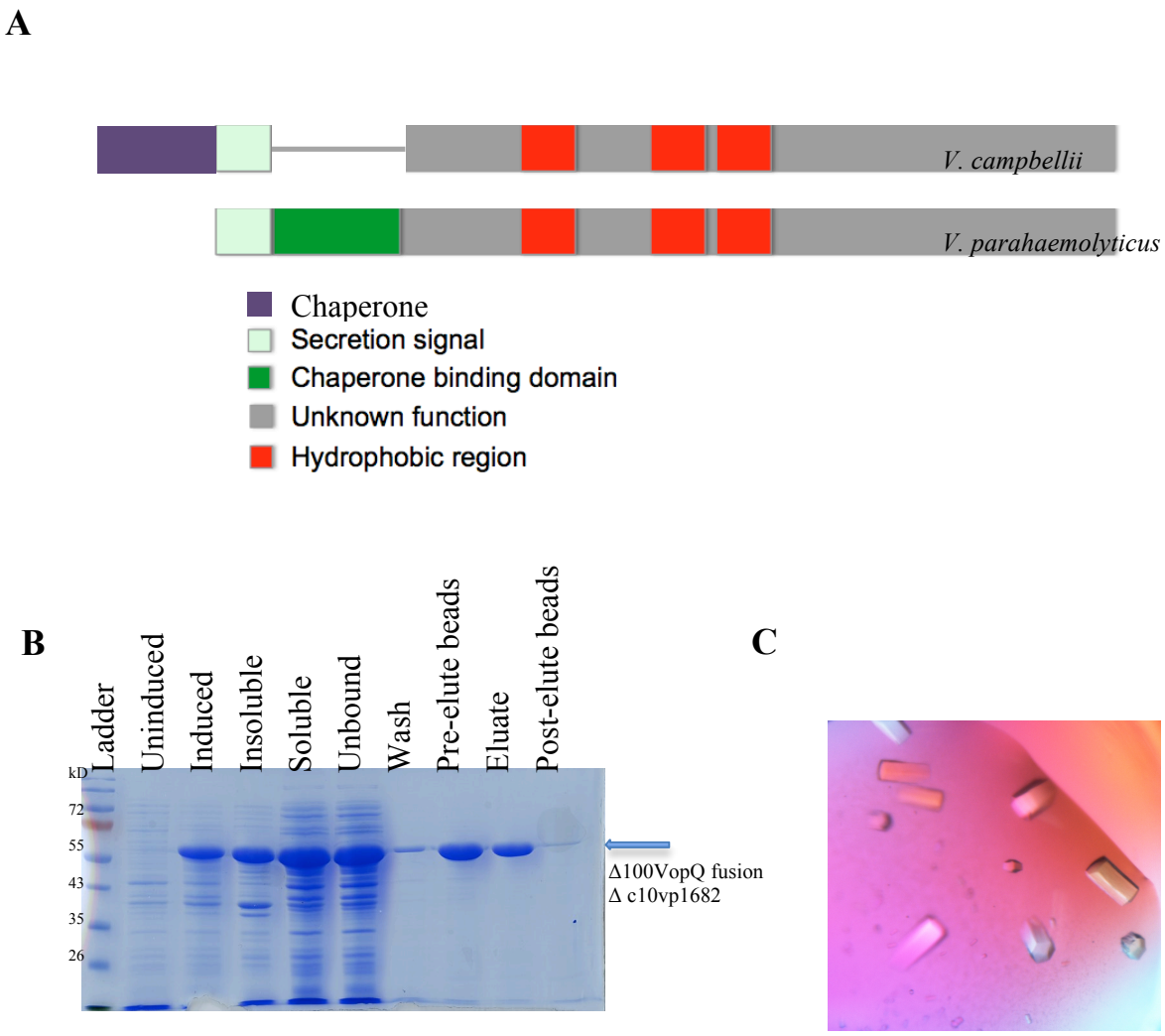


**Figure 31. Purification and crystals of Δ100VopQ fusion Δ c10vp1682** (**A**) Cartoon alignment of VopQ from *Vibrio parahaemolyticus* and *Vibrio campbellii*. *V. campbellii* lacks the chaperone binding domain, amino acids 31-100. However, *V. campbellii* VopQ is fused to the chaperone making the CBD unnecessary. (**B**) His tagged Δ100VopQ fusion Δc10vp1682 purification (**C**) Δ100VopQ fusion Δ c10vp1682 crystals.

*VopQ inserts into the vacuolar membrane*

VopQ inserts into lipid bilayers to form a voltage-gated channel (*31*). In order to characterize the VopQ channel further, we used a protease-protection assay to determine the membrane topology of VopQ. The protease-protection assay is based on the inaccessibility of a protease to parts of the protein that are inserted into the membrane or lumen of the organelle. We used the assay to determine the fragment of VopQ that inserts into the membrane. VopQ was incubated with purified yeast vacuolar membranes and then digested with proteinase K. In the absence of vacuoles, VopQ was completely digested by proteinase K (**Figure 32, lane 3 and 10)**. PMSF efficiently inhibited digestion by proteinase K (**Figure 32, lane 4)**. In the presence of vacuoles, VopQ was almost completely protected from protease digestion (**Figure 32, lane 5, 6 and 7)**. This protection is eliminated when the vacuolar membrane is dissolved with Triton X-100 (**Figure 32, lane 8 and 9)**. This assay shows that VopQ almost completely inserts into the membrane or translocates into the lumen of the vacuole.

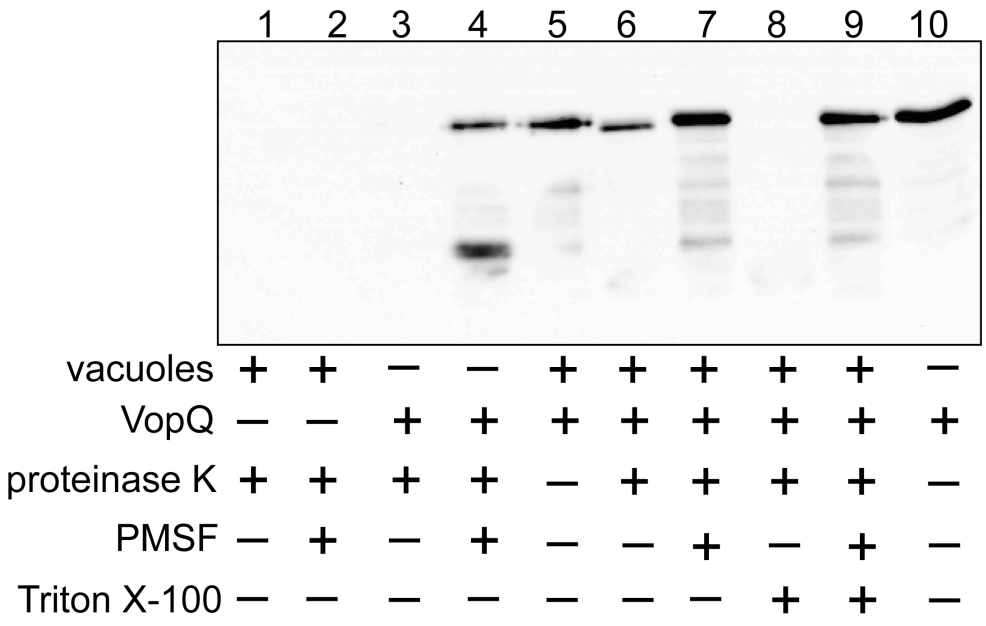


**Figure 32**. **Analysis of proteinase K treated VopQ**. VopQ was incubated in the presence or absence of vacuoles, PMSF and Triton X-100 for 15 minutes at room temperature. The reaction was then treated with proteinase K for 1 hour at 4°C. After incubation time, PMSF was added to stop the reaction. Samples were then separated using SDS-PAGE and immunoblotted with α-VopQ antibody.

*Incubation of VopQ with DDM yields a oligomeric complex*

Proteinase K digestion shows that VopQ inserts into membrane to form a channel. In order to characterize the oligomeric state of this channel, I used full length VopQ to screen for detergents that may stabilize an oligomeric form of VopQ (**Figure 33A**). Detergents are commonly used for membrane protein crystallography as they mimic the lipidic natural environment of membrane proteins (*131*). Although most detergents caused aggregation of VopQ, n-dodecyl β-D maltoside (DDM) induced the formation of an oligomer when incubated overnight with MBP tagged VopQ (**Figure 33B and C**). MBP-VopQ was incubated with DDM and subjected to a Superdex200 size-exclusion column. Based on the elution volume estimate of the complex, VopQ may form a tetrameric complex in the presence of DDM (**Figure 34A**). This fraction was then used for crystallography. Unfortunately, no crystals were observed during initial screening. I hypothesized that the lack of crystals may be due to the bulky 43 kD MBP tag on VopQ. Therefore, I used his tagged or untagged VopQ with DDM but the complex was unstable and the protein immediately precipitated. Next, I incubated MBP-VopQ with DDM and cleaved the tag at 4°C in the presence of DDM (**Figure 34B**). This produced an oligomeric VopQ that was stable at 4°C. However, this complex did not yield any crystals upon initial screening.

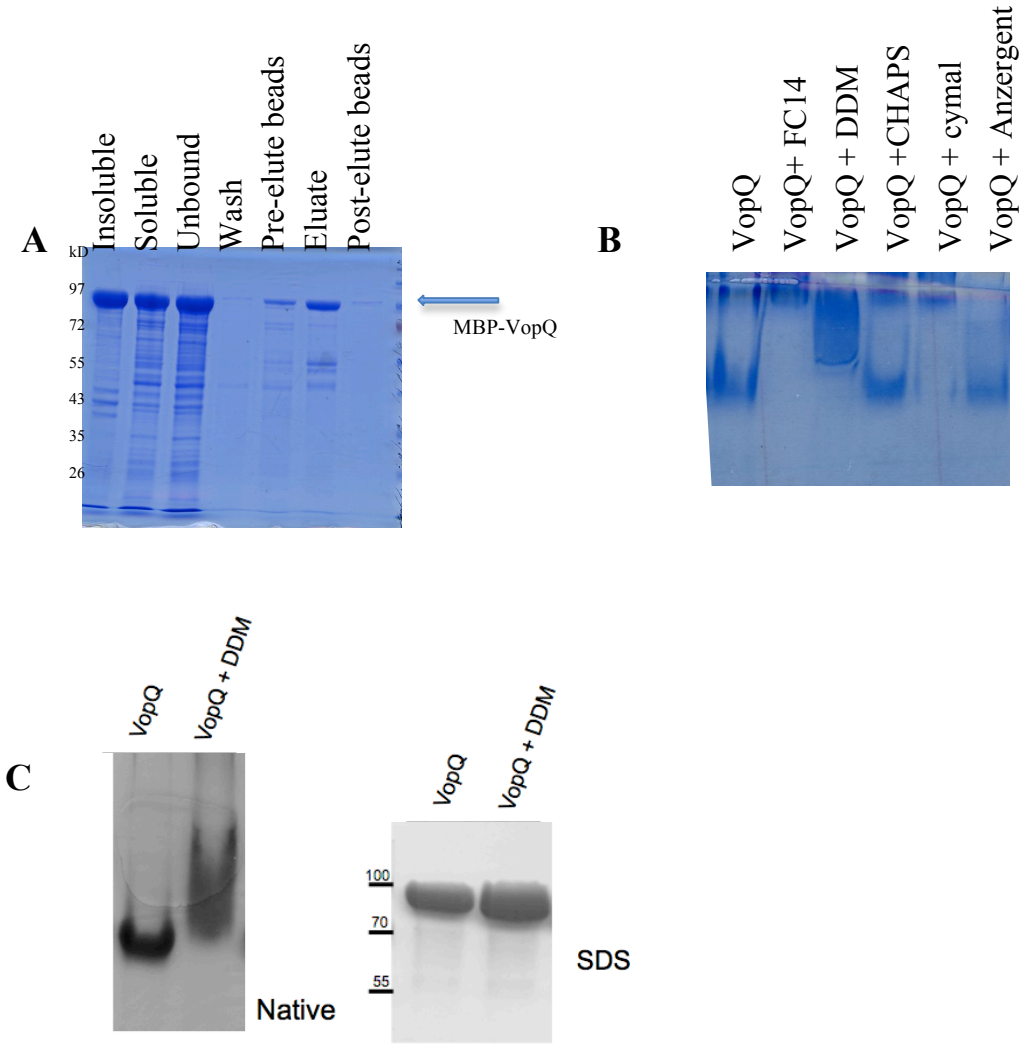


**Figure 33. Detergent screen for oligomeric VopQ.** (**A**) Nickel affinity purification of MBP-VopQ (**B**) VopQ detergent screen. VopQ incubated with detergents and run on native gel to reveal oligomeric state. FC14: zwitterionic detergent; DDM: non-ionic detergent; CHAPS: zwitterionic detergent; Cymal: non-ionic detergent; Anzergent: zwitterionic detergent (**C**) Native and SDS-PAGE gel of VopQ incubated with DDM.

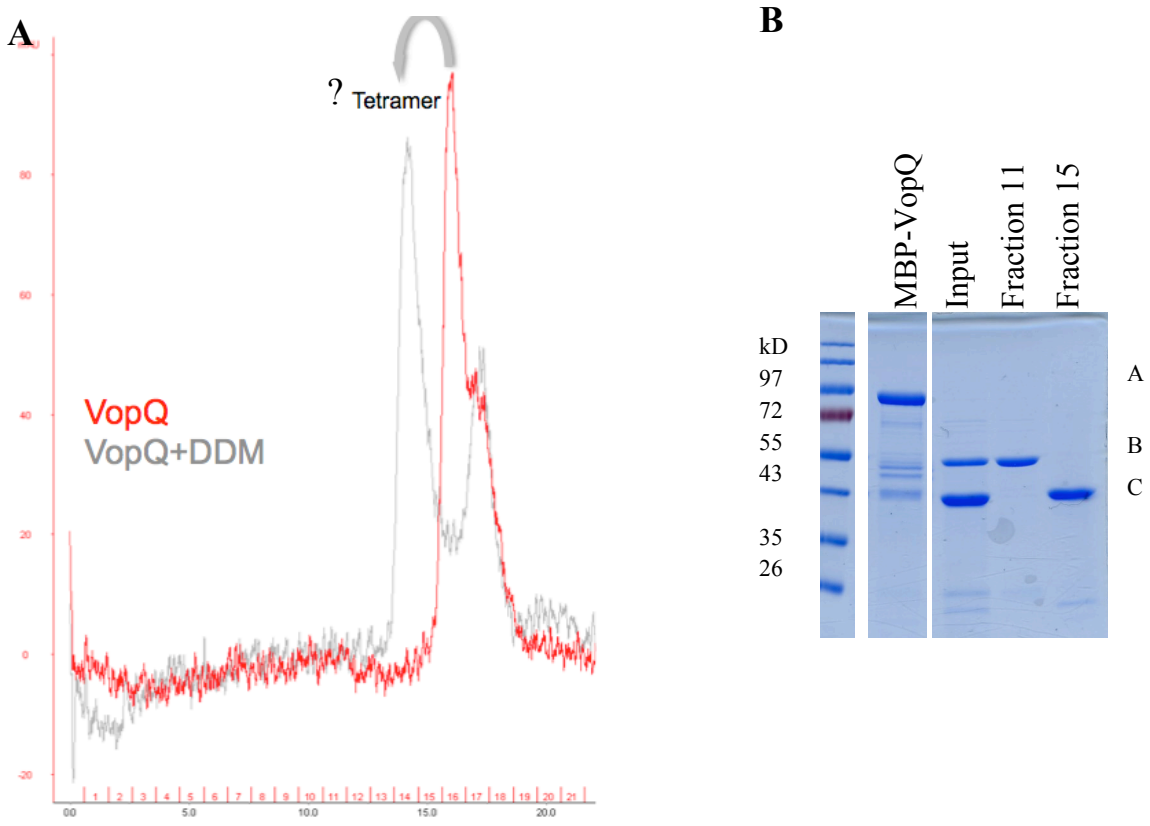


**Figure 34. VopQ forms a oligomeric complex in the presence of DDM. (A)** VopQ oligomerizeration as observed on gel filtration column. **(B)** Lane 1: MBP-VopQ purified by nickel affinity chromatography. Lane 2: MBP-VopQ incubated with TEV protease and DDM overnight. Input into Superdex200. Lane 3: Fraction 11 corresponds to oligomeric VopQ. Lane 4: Fraction 15 corresponds to the MBP tag. "A" denotes MBP-VopQ, "B" denotes VopQ, "C" denotes MBP.

**Discussion**

VopQ binds to the V-ATPase to form channels in adjacent membranes and inhibit vacuole fusion. The purpose of the structural studies is to map the channel and fusion inhibition activity of VopQ. Previous studies delineated the chaperone binding site to amino acids 31-100 (*126*). In order to delineate the two functions, I constructed truncation and point mutants based on putative domains to test in the liposome leakage and vacuole fusion assay. Mutational studies using yeast vacuoles indicate that the first 100 amino acids aid in V-ATPase binding and that this interaction is required for fusion inhibition. The first 100 amino acids may be important for protein folding or direct binding to the V-ATPase. Due to the instability of the fragment, I was not able to test if the first 100 amino acids are sufficient for binding and fusion inhibition. Liposome leakage assays reveal that the N terminal 100 amino acids and C terminal 92 amino acids are not required for pore formation in liposomes. These studies along with the bioinformatics suggest that the N-terminal is involved in targeting to the V-ATPase while the hydrophobic core, amino acids 200-400, is involved in the channel formation. To further understand the structure-function relationship of VopQ, we attempted to crystallize VopQ bound to its chaperone and the oligomer membrane bound VopQ. Crystallography trials with VopQ bound to its chaperone revealed a more stable degradation product, Δ243 VopQ. In future work this fragment will be used for crystallographic screening and optimization. Next, I focused on biochemical characterization of the membrane bound VopQ for crystallography. Protease protection assays indicate that VopQ is almost completely protected from digestion by insertion or translocation though the membrane. In the presence of DDM, full length VopQ forms an oligomer that approximately

corresponds with the elution volume of a tetrameric complex. Initial studies have focused on homogeneity and stability of the protein complex. Future studies will aim to stabilize the protein complex at room temperature and try additional detergents and chemical stabilizers.

# CHAPTER SIX

## Conclusions and Recommendations

### Summary of Research findings

We recently characterized the biochemical activity of the virulence factor VopQ, a novel *V. parahaemolyticus* protein with no homology to any proteins outside of *Vibrios*. One of these Gram-negative marine bacterium, *Vibrio parahaemolyticus,* is a major cause of gastroenteritis due to the consumption of contaminated raw or undercooked seafood, which may be life threatening in immune-compromised patients. In clinical isolates, each of the two chromosomes of *V. parahaemolyticus* harbor a type three secretion system (T3SS), designated T3SS1 and T3SS2, enabling the translocation of bacterial proteins, or effectors, into the eukaryotic host. T3SS1 orchestrates a temporally regulated cell death mediated by the induction of autophagy, followed by cell rounding, and eventual lysis of the host cell. The T3SS1 effector VopQ disrupts autophagic flux during infection, and elucidating its molecular mechanism not only provides a better understanding of *V. parahaemolyticus* pathology, but also offers new insights into the mechanism of eukaryotic autophagy.

Previously, recombinant VopQ was shown to be necessary and sufficient to induce rapid autophagosomal accumulation in HeLa cells. In order to understand the activity of VopQ, we sought to find interacting proteins in eukaryotic model systems. Using pulldown assays, we show that VopQ interacts with at least one $V_o$ subunit of the conserved V-ATPase proton pump, the main electrogenic proton pump responsible for the acidification of

intracellular organelles such as the lysosome. The V-ATPase consists of two distinct and separable domains: the $V_1$ ATP-hydrolyzing domain and the $V_o$ proton translocation domain. In order to understand how VopQ affects V-ATPase activity, we isolated yeast vacuoles and tested V-ATPase activity in the presence of VopQ in vitro. Surprisingly, VopQ immediately deacidifies the vacuole at low nanomolar concentrations, without hindering ATP hydrolysis activity. This phenotype was consistent during *V. parahaemolyticus* infections where VopQ is necessary to induce deacidification of lysosomes. Using the pH-dependent dye LysoTracker, we also show that VopQ is sufficient to immediately deacidify lysosomes upon microinjection of recombinant VopQ.

Due to the rapid deacidification observed with VopQ, we hypothesized that VopQ either inhibits the $V_o$ proton channel or antagonizes it by forming a lysosomal pore. With synthetic liposomes encapsulating fluorescent dyes of differing molecular weights, we showed that VopQ forms a pore independent of the V-ATPase structure and does not translocate molecules larger than 3 kDa. Consistent with this observation, we confirmed that VopQ does not allow large molecules, such as a 10-kDa dextran or proteases, to escape the lysosome during an infection. Furthermore, electrophysiology experiments using lipid bilayers showed that VopQ forms a gated channel with an approximate pore size of 18Å, in agreement with our liposome dye release assays.

The ability of VopQ to form pores in liposomes by a V-ATPase-independent mechanism suggests that the activity of VopQ is not specific to the lysosomal membrane. The ability of VopQ to bind liposomes, however, is based purely on electrostatics: in the

liposome assay at pH 5.5, VopQ is positively charged due to its pI of 6, and binds to negatively charged liposomes made of POPC/DOPS. Raising the reaction pH or eliminating negatively charged lipids from the liposome completely abrogates VopQ pore-forming activity. When using purified yeast vacuolar membranes, we found that the association of VopQ with the vacuolar membrane is completely dependent upon the V-ATPase at physiological pH (7.5). Therefore, VopQ required the V-ATPase to identify, bind, and form pores on eukaryotic endolysosomal membranes. This is the first example of a targeted bacterial effector that forms pores on lysosomal membranes to alter ion homeostasis and autophagic flux. We show that VopQ, similar to lysosomotropic agents such as chloroquine, equilibrated the concentration of small ions in and out of the lysosome and caused autophagosomal accumulation through inhibiting the turnover of autophagosomes.

Bacterial effectors often mimic eukaryotic activities and in this case, VopQ may function similarly to the lysosomal mTOR-dependent ATP-sensitive sodium channel. This channel senses the metabolic state of the cell, alters lysosomal membrane potential accordingly, and regulates autophagic recycling of nutrients (*91*). Similarly, VopQ forms a gated ion channel in a strategic location to collapse membrane potentials, thereby directly altering autophagic flux. Furthermore, VopQ binds directly to the V-ATPase $V_o$ domain, which plays a key role in the regulation of autophagy through amino acid sensing, and even more directly in membrane fusion (*64, 102, 132*). Therefore, we next studied the effect of VopQ on homotypic vacuolar fusion using the well-established model system of *Saccharomyces cerevisiae*.

Expression of VopQ in yeast induces extensive vacuolar fragmentation indicative of a defect in vacuole fusion *in vivo*. To test if VopQ is an authentic inhibitor of fusion *in vitro*, we used vacuolar lipid- and content-mixing assays. We show that VopQ is a potent inhibitor of fusion even at nanomolar amounts. In order to characterize how VopQ inhibits fusion, we analyzed the kinetics of fusion inhibition. Fusion occurs in three distinct steps: priming, docking and fusion of the vacuoles. By monitoring the kinetics of each step, we show that VopQ inhibits the docking step of fusion. Concomitantly, VopQ inhibits SNARE pair formation at the docking step of fusion. We hypothesize that VopQ binds to the $V_o$ subunit of the V-ATPase and inhibits $V_o$-SNARE interactions to inhibit fusion. Future studies will focus on using VopQ as a tool in understanding the interplay between V-ATPase and SNAREs in fusion.

VopQ is the first bacterial effector that disrupts endolysosomal proton gradient and inhibits membrane fusion by a direct interaction with the $V_o$ domain. In order to delineate these two functions, I use mutational and crystallographic studies. VopQ is a 492 amino acid protein with an N terminal T3S signal, chaperone binding region and three putative hydrophobic transmembrane helices. Using truncation mutants in the liposome leakage assay, we show that the N terminal 100 amino acids and C terminal 92 amino acids are not necessary for pore formation. Using the truncation mutants in the fusion assay, we show that the N-terminous is required for targeting of VopQ to the V-ATPase containing membranes. The N-terminous may facilitate targeting by directly binding to the V-ATPase or by enabling proper folding for the tertiary structure. To gain insight into the structure of VopQ, I attempted to crystallize soluble VopQ bound to its chaperone, vp1682. Crystallization trials

resulted in reproducible but poorly diffracting crystals. Further analysis of the crystals revealed that VopQ bound to vp1682 is unstable and degrades to a smaller fragment, Δ243 VopQ. Next, I tried to characterize and crystallize the membrane bound VopQ. Protease protection assays show that VopQ almost completely inserts or translocates into the membrane. Therefore, full length VopQ was used to screen for detergents that induce pore oligomer formation by mimicking the natural lipid environment. DDM, a nonionic detergent with low critical micelle concentration (CMC), induced the formation of a oligomeric complex of VopQ. This complex was used in initial crystallography screening with no positive results potentially due to instability of the oligomeric complex.

**Future directions**

In summary, the studies presented in this thesis show how a bacterial effector, VopQ, binds to the conserved V-ATPase to form a lysosomal-gated channel and inhibit fusion. This novel finding opens the door for several questions regarding the activity of VopQ.

*How does VopQ alter autophagy?*

mTOR is a master regulator of growth and is deregulated in many disease states such cancer, diabetes and neurodegeneration (*133*). It acts by sensing the energy and nutrient status of the cell and coupling it to the cellular metabolism. Upon nutrient deprivation, mTOR becomes inactive and autophagy is turned on to provide energy for the starving cell. Upon nutrient replenishment, mTOR is activated by the nutrient sensing machinery and autophagy is turned off. The nutrient sensing machinery consists of Rag GTPases, V-ATPase

and the ragulator (**Figure 35A**)(*134*). The V-ATPase detects the amino acid levels in the lysosomal lumen and binds the ragulator complex (*132*). The ragulator complex acts as the link between the V-ATPase and the Rag GTPases. Through its GEF activity, the ragulator complex relays the nutrient status signal to the Rag GTPases (*135*). The GTP bound Rag GTPase binds to mTOR to localize it to the lysosome where it stays active (*134*). Active mTOR phosphorylates S6K and ULK kinase to promote protein synthesis and prevent autophagosome formation respectively (*136*). Therefore, in the presence of amino acids, active mTOR localizes to the lysosome and inhibits autophagy (**Figure 35A**) (*132*).

The V-ATPase plays a major role in nutrient sensing and induction of autophagy. Zoncu et al. showed that the ATP hydrolysis of the pump is necessary for amino acid sensing by the V-ATPase (*132*). Inhibitors of the V-ATPase inhibit mTOR activation and localization to the lysosome thereby uncoupling autophagy and amino acid levels. Several V-ATPase subunits including $V_oD$ and $V_oC$ were shown to interact with the regulator (*132*). These same subunits also interact with VopQ, warranting the question if VopQ acts similar to the V-ATPase inhibitors that lead to mTOR inactivation and induction of autophagy. The massive accumulation of autophagosomes seen in the short time frame of VopQ microinjection and *V. parahaemolyticus* infection could be due to the additive affects of inducing the formation and blocking the degradation of autophagosomes.

I speculate that VopQ binds to the V-ATPase to prevent binding of the ragulator complex to the V-ATPase. This hypothesis can be tested using immunoprecipitation assays. Cells expressing flag-tagged ragulator protein can be used to pulldown V-ATPase subunits in the presence or absence of recombinant VopQ. I speculate that VopQ will bind to the V-

ATPase and hinder the interaction of the V-ATPase with the ragulator. This will uncouple nutrient sensing from autophagy leading to the constitutive induction of autophagy. Localization and activity of mTOR can be used to monitor induction of autophagy. Immunofluorescence can be used to examine mTOR localization to the lysosome during a *V. parahaemolyticus* infection and VopQ microinjection. If VopQ binds to the V-ATPase and prevents binding of the ragulator, then inactive mTOR will be delocalized from the lysosome leading to induction of autophagy. Phosphorylation of mTOR substrates such as S6K can be detected using antibodies to check for mTOR kinase activation during an infection with *V. parahaemolyticus*. Preliminary data suggests that *V. parahaemolyticus* T3SS1 induces VopQ-independent autophagy (**Figure 35B**). In uninfected cells, active mTOR phosphorylates S6K and inhibits autophagy (**Figure 35B lane 1**). Inhibition of mTOR with rapamycin leads to a change in the phosphorylation state of S6K and induction of autophagy (**Figure 35B lane 2**). Infection with POR3 also leads to inactivation of mTOR and induction of autophagy, independent of VopQ (**Figure 35B lane 3-11**). These results suggest the presence of another virulence factor from *V. parahaemolyticus* that induces autophagy.

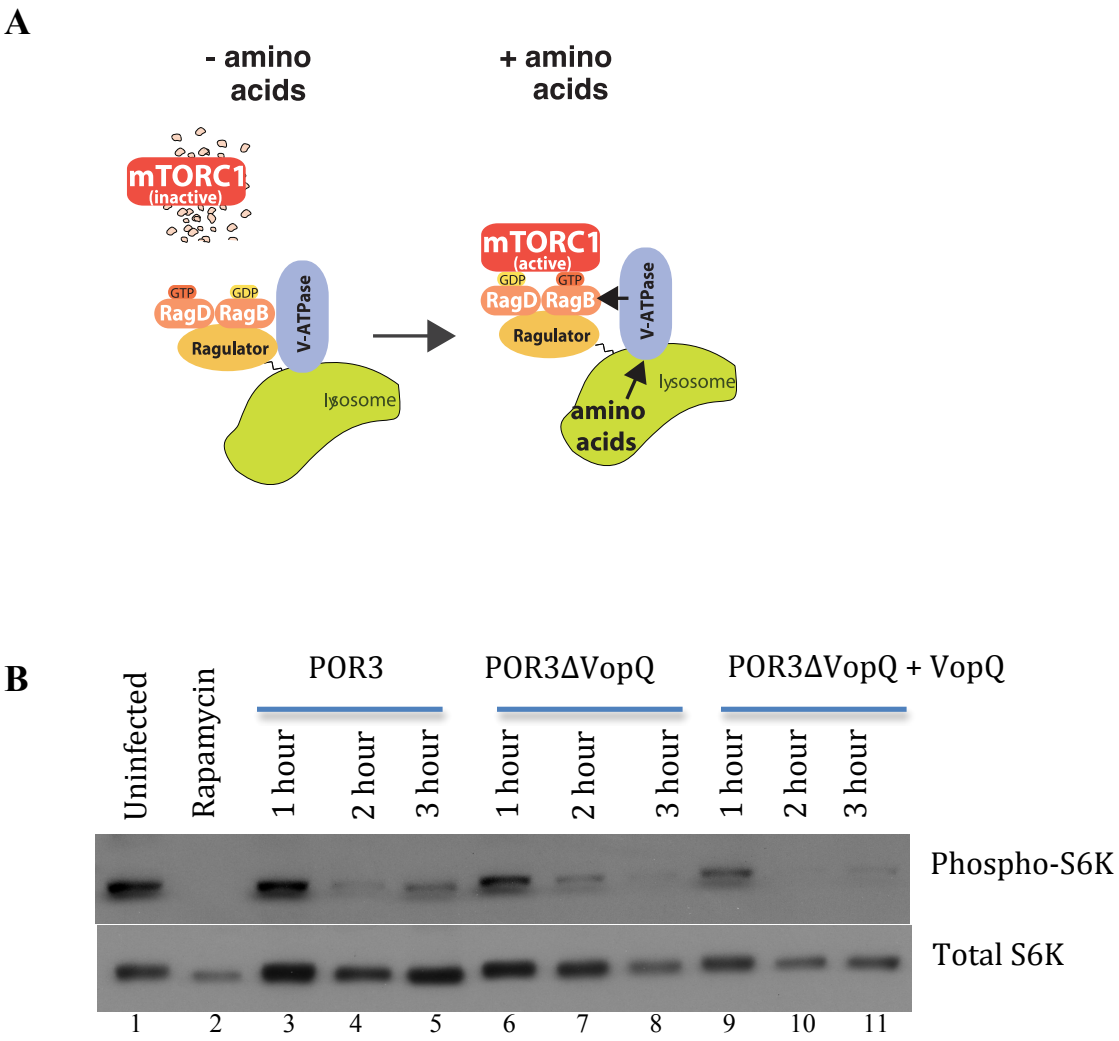


**Figure 35. The role of the V-ATPase in autophagy.** (**A**) V-ATPase uses an inside-out mechanism to sense amino acids and couples nutrient status to autophagy. Figure reproduced from (*132*) (**B**) HeLa cells were left untreated, treated with 100 μM rapamycin or infected with the indicated *V. parahaemolyticus* strains. At the indicated time points, cells were harvested and cell lysates were separated via SDS-PAGE and immunoblotted for phosphorylated-S6K and total S6K.

*How does VopQ inhibit fusion?*

VopQ inhibits fusion at nanomolar levels but the mechanism of inhibition is unknown. VopQ binds to the V-ATPase that is composed of two domains. The $V_1$ domain hydrolyzes ATP to provide energy for the translocation of protons across the membrane through the $V_o$ channel. Several lines of evidence support an acidification independent role of the $V_o$ domain of the V-ATPase. For example, $V_o$ mutants have a more severe phenotype than $V_I$ mutants (*63*). Additionally, subunits of the $V_o$ domain have been shown to directly interact with SNARE proteins to facilitate exocytosis (*102*). I hypothesize that VopQ binds to the $V_o$ subunit and inhibits $V_o$-SNARE interaction. To test this hypothesis, I propose to pull down the SNARE protein, synaptobrevin, with the $V_o$C subunit in the presence and absence of VopQ. I predict that VopQ inhibits $V_o$C–SNARE interaction. VopQ may inhibit this interaction through steric hindrance by binding to the $V_o$ domain. Pulldown assay using Δ28 VopQ truncation mutant suggests that the N-terminal is required for targeting of VopQ to the $V_o$ domain. Therefore, I could test if the N-terminal fragment, 1-28 amino acids, is sufficient to bind to the V-ATPase. If VopQ inhibits fusion by binding to the V-ATPase then 1-28 amino acids may be sufficient to inhibit fusion without forming a channel on the membrane.

*Therapeutic potential of VopQ*

The V-ATPase is found on lysosomes and late endosomes in most eukaryotic cells. However, specialized cells such as kidney cells, as well as some tumor cells, have the V-ATPase present on the plasma membrane in addition to acidic compartments (**Figure 36**)

(*99*). It is reasonable to assume that VopQ can act as a potent cytotoxin to form pores on the plasma membrane of these cells. Thus VopQ has potential as an anti-metastasis drug by killing tumor cells and preventing metastasis. By the same idea, the N-terminal V-ATPase targeting domain in VopQ can be swapped with a targeting sequence that is specific to certain pathogens or cells for selection. Further studies are required to test how VopQ can be engineered to target cell of interest.

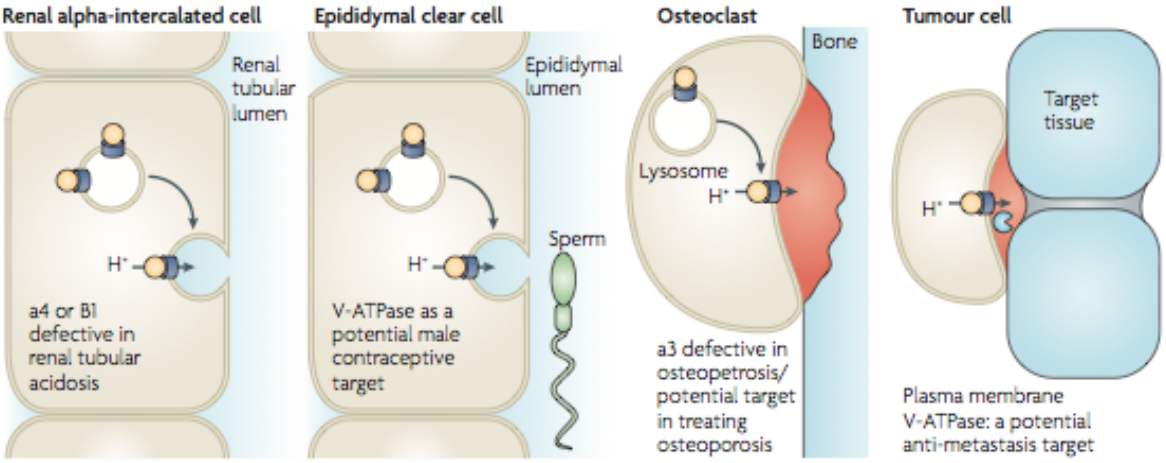


**Figure 36. V-ATPase as a drug target in renal tubular acidosis, sperm maturation, osteoporosis and cancer.** The V-ATPase is the main electrogenic pump that is involved in acidification of intracellular organelles. Defects in the V-ATPase can lead various disease states such as renal tubular acidosis, a condition where kidney cells fail to acidify the urine resulting in lower blood pH (*137*). The V-ATPase also acidifies the epididymal lumen for sperm maturation (*138*). These examples highlight the importance of the V-ATPase in acid-base homeostasis. However, the V-ATPase can also play a detrimental role in some disease states such as osteoporosis and cancer. In osteoclasts, the V-ATPase decreases the extracellular pH leading to bone demineralization (*139*). In tumor cells, the V-ATPase plays an important role in metastasis. Inhibitors of the V-ATPase, such as bafilomycin, have been shown to decrease invasiveness of certain breast cancer cells (*140*). VopQ can be engineered to antagonize the detrimental role of the V-ATPase and increase the extracellular pH. Figure reproduced from (*99*)

*Screen for small molecule inhibitors*

In addition to structural studies, inhibitors can be used to delineate the two functions of VopQ. In order to find small molecule inhibitors of VopQ, I propose to do a high-throughout screen using two functional assays. The alkaline phosphatase vacuole fusion assay can be used to screen for fusion inhibitors. Next, these inhibitors can be used in the liposome leakage assay to test pore formation. The vacuole and liposome assays provide dynamic colorometric and fluorescent readout allowing for fast screening. The latter will identify molecules that disrupt channel activity by plugging the pore or dissociating the protein complex. The vacuole fusion assay will identify molecules that disrupt channel activity in addition to molecules that inhibit binding to the V-ATPase.

*Solve the crystal structure of VopQ*

The Protein Data Bank (PDB) consists of structural data of more than 80, 000 proteins. Membrane proteins represent only 1% of these, highlighting the difficulty in studying these challenging proteins (*131*). The major challenge lies in reconstituting the protein in its natural environment while preserving its activity, stability and homogeneity (*141*). The first step is to obtain the protein of interest from its natural source or through over expression in *E. Coli*. The next step is to extract the protein from the membrane and purify the protein to homogeneity. Finally, a large number of conditions must be screened to determine optimal crystallization conditions. There are two methods used to crystallize membrane proteins: “in surfo” method and “in cubo“ method (*131*). “In surfo” is a detergent-based method in which the protein is incorporated into detergent micelles that mimic the lipid

environment. The two major challenges in this method are controlling the protein flexibility and homogeneity. "In cubo" is a lipid-based method in which the protein is incorporated into lipidic phases such as a lipid bilayer. Proteins that are unstable in detergents maybe crystallized using the "in cubo" method. While the VopQ oligomer has been successfully purified to homogeneity, no crystals have been observed using the "in surfo" method. This may be due to the instability of VopQ in detergents. Two approaches can be taken to solve this problem. A detergent screen can be used to assay a larger number of detergents for VopQ oligomerization. Secondly, the "in cubo" method can be used to crystallize VopQ.

To the best of my knowledge, the structure of a full-length bacterial effector bound to its chaperone has not been solved. However, the chaperone-binding domain bound to its chaperone has been solved (*142*). While this provides information on how the chaperone binds to the effector, it does not shed light on the state of the effector. In fact, the N-terminus of many of the effectors is disordered in the solved crystal structures. Hence, the first step in such crystallographic studies is to determine the stable fragment that associates with the chaperone. Crystals of VopQ with its chaperone vp1682 are formed with a stable fragment, Δ243 VopQ. I propose to clone, purify and set up screens with this construct. If this protein yields poorly diffracting crystal, I propose to optimize the conditions using the MORPHEUS screen (*143*). The MORPHEUS screen was developed by statistical analysis of crystallization conditions of proteins in the PDB. It consists of a mix of components most likely to produce good quality crystals. However, components of this screen may have deleterious effects on VopQ crystals. Solving the structure of VopQ bound to its chaperone and the oligomeric channel may help us understand the targeting and channel gating mechanism of the VopQ.

Overall the discovery of the activity of VopQ has provided novel insight into *V. parahaemolyticus* pathogenesis as well as host signaling. *V. parahaemolyticus* uses a V-ATPase targeted pore forming effector, VopQ, to immediately collapse host ion gradients and inhibit SNARE dependent vesicle fusion.

# BIBLIOGRAPHY


1. P. A. Blake, R. E. Weaver, D. G. Hollis, Diseases of humans (other than cholera) caused by vibrios. *Annual review of microbiology* **34**, 341 (1980).

2. CDC. ( Centers for Disease Control and Prevention, 2013).

3. Y. C. Su, C. Liu, Vibrio parahaemolyticus: a concern of seafood safety. *Food microbiology* **24**, 549 (Sep, 2007).

4. K. Fujino, [Pathogenic Vibrio]. *Nihon saikingaku zasshi. Japanese journal of bacteriology* **21**, 389 (Aug, 1966).

5. K. Fujino, [Discovery of Vibrio parahaemolyticus]. *Nihon saikingaku zasshi. Japanese journal of bacteriology* **21**, 373 (Aug, 1966).

6. T. Fujino, T. Miwatani, Y. Takeda, S. Shinoda, A. Yoshihara, Characterization of Vibrio parahaemolyticus isolated in the USA. *Biken journal* **15**, 223 (Dec, 1972).

7. CDC, "National Enteric Disease Surveillance" (Centers for Disease Control and Prevention, Atlanta, GA).

8. CDC. (Centers for Disease Control and Prevention, 2012), vol. 2014.

9. Y. Nakaguchi, Contamination by Vibrio parahaemolyticus and Its Virulent Strains in Seafood Marketed in Thailand, Vietnam, Malaysia, and Indonesia. *Tropical medicine and health* **41**, 95 (Sep, 2013).

10. L. Tran *et al.*, Determination of the infectious nature of the agent of acute hepatopancreatic necrosis syndrome affecting penaeid shrimp. *Diseases of aquatic organisms* **105**, 45 (Jul 9, 2013).

11. K. Sadok, S. Mejdi, S. Nourhen, B. Amina, Phenotypic characterization and RAPD fingerprinting of Vibrio parahaemolyticus and Vibrio alginolyticus isolated during Tunisian fish farm outbreaks. *Folia microbiologica* **58**, 17 (Jan, 2013).

12. K. Makino *et al.*, Genome sequence of Vibrio parahaemolyticus: a pathogenic mechanism distinct from that of V cholerae. *Lancet* **361**, 743 (Mar 1, 2003).

13. Y. Miyamoto *et al.*, In vitro hemolytic characteristic of Vibrio parahaemolyticus: its close correlation with human pathogenicity. *Journal of bacteriology* **100**, 1147 (Nov, 1969).

14. K. S. Park *et al.*, Cytotoxicity and enterotoxicity of the thermostable direct hemolysin-deletion mutants of Vibrio parahaemolyticus. *Microbiology and immunology* **48**, 313 (2004).

15. H. Shirai *et al.*, Molecular epidemiologic evidence for association of thermostable direct hemolysin (TDH) and TDH-related hemolysin of Vibrio parahaemolyticus with gastroenteritis. *Infection and immunity* **58**, 3568 (Nov, 1990).

16. T. Fukui *et al.*, Thermostable direct hemolysin of Vibrio parahaemolyticus is a bacterial reversible amyloid toxin. *Biochemistry* **44**, 9825 (Jul 26, 2005).

17. T. Lynch *et al.*, Vibrio parahaemolyticus disruption of epithelial cell tight junctions occurs independently of toxin production. *Infection and immunity* **73**, 1275 (Mar, 2005).

18. C. A. Broberg, T. J. Calder, K. Orth, Vibrio parahaemolyticus cell biology and pathogenicity determinants. *Microbes and infection / Institut Pasteur* **13**, 992 (Nov, 2011).

19. K. S. Park *et al.*, Functional characterization of two type III secretion systems of Vibrio parahaemolyticus. *Infection and immunity* **72**, 6659 (Nov, 2004).

20. T. Ono, K. S. Park, M. Ueta, T. Iida, T. Honda, Identification of proteins secreted via Vibrio parahaemolyticus type III secretion system 1. *Infection and immunity* **74**, 1032 (Feb, 2006).

21. H. Hiyoshi, T. Kodama, T. Iida, T. Honda, Contribution of Vibrio parahaemolyticus virulence factors to cytotoxicity, enterotoxicity, and lethality in mice. *Infection and immunity* **78**, 1772 (Apr, 2010).

22. N. Okada *et al.*, Identification and characterization of a novel type III secretion system in trh-positive Vibrio parahaemolyticus strain TH3996 reveal genetic lineage and diversity of pathogenic machinery beyond the species level. *Infection and immunity* **77**, 904 (Feb, 2009).

23. T. Kodama *et al.*, Identification and characterization of VopT, a novel ADP-ribosyltransferase effector protein secreted via the Vibrio parahaemolyticus type III secretion system 2. *Cellular microbiology* **9**, 2598 (Nov, 2007).

24. J. E. Trosky *et al.*, VopA inhibits ATP binding by acetylating the catalytic loop of MAPK kinases. *The Journal of biological chemistry* **282**, 34299 (Nov 23, 2007).

25. S. Mukherjee, Y. H. Hao, K. Orth, A newly discovered post-translational modification--the acetylation of serine and threonine residues. *Trends in biochemical sciences* **32**, 210 (May, 2007).

26. A. D. Liverman *et al.*, Arp2/3-independent assembly of actin by Vibrio type III effector VopL. *Proceedings of the National Academy of Sciences of the United States of America* **104**, 17117 (Oct 23, 2007).

27. J. A. Zahm *et al.*, The bacterial effector VopL organizes actin into filament-like structures. *Cell* **155**, 423 (Oct 10, 2013).

28. S. Namgoong *et al.*, Mechanism of actin filament nucleation by Vibrio VopL and implications for tandem W domain nucleation. *Nature structural & molecular biology* **18**, 1060 (Sep, 2011).

29. B. Yu, H. C. Cheng, C. A. Brautigam, D. R. Tomchick, M. K. Rosen, Mechanism of actin filament nucleation by the bacterial effector VopL. *Nature structural & molecular biology* **18**, 1068 (Sep, 2011).

30. L. Zhang *et al.*, Type III effector VopC mediates invasion for Vibrio species. *Cell reports* **1**, 453 (May 31, 2012).

31. A. Sreelatha *et al.*, Vibrio effector protein, VopQ, forms a lysosomal gated channel that disrupts host ion homeostasis and autophagic flux. *Proceedings of the National Academy of Sciences of the United States of America* **110**, 11559 (Jul 9, 2013).

32. M. L. Yarbrough *et al.*, AMPylation of Rho GTPases by Vibrio VopS disrupts effector binding and downstream signaling. *Science* **323**, 269 (Jan 9, 2009).

33. D. Salomon *et al.*, Effectors of animal and plant pathogens use a common domain to bind host phosphoinositides. *Nature communications* **4**, 2973 (2013).

34. C. A. Broberg, L. Zhang, H. Gonzalez, M. A. Laskowski-Arce, K. Orth, A Vibrio effector protein is an inositol phosphatase and disrupts host cell membrane integrity. *Science* **329**, 1660 (Sep 24, 2010).

35. D. L. Burdette, M. L. Yarbrough, A. Orvedahl, C. J. Gilpin, K. Orth, Vibrio parahaemolyticus orchestrates a multifaceted host cell infection by induction of autophagy, cell rounding, and then cell lysis. *Proceedings of the National Academy of Sciences of the United States of America* **105**, 12497 (Aug 26, 2008).

36. D. L. Burdette, J. Seemann, K. Orth, Vibrio VopQ induces PI3-kinase-independent autophagy and antagonizes phagocytosis. *Molecular microbiology* **73**, 639 (Aug, 2009).

37. N. Mizushima, B. Levine, A. M. Cuervo, D. J. Klionsky, Autophagy fights disease through cellular self-digestion. *Nature* **451**, 1069 (Feb 28, 2008).

38. D. J. Klionsky, Autophagy: from phenomenology to molecular understanding in less than a decade. *Nature reviews. Molecular cell biology* **8**, 931 (Nov, 2007).

39. H. Abeliovich, D. J. Klionsky, Autophagy in yeast: mechanistic insights and physiological function. *Microbiology and molecular biology reviews : MMBR* **65**, 463 (Sep, 2001).

40. D. J. Klionsky, The autophagy connection. *Developmental cell* **19**, 11 (Jul 20, 2010).

41. N. Mizushima, Y. Ohsumi, T. Yoshimori, Autophagosome formation in mammalian cells. *Cell Struct Funct* **27**, 421 (Dec, 2002).

42. A. Orvedahl, B. Levine, Eating the enemy within: autophagy in infectious diseases. *Cell death and differentiation* **16**, 57 (Jan, 2009).

43. M. G. Gutierrez *et al.*, Autophagy is a defense mechanism inhibiting BCG and Mycobacterium tuberculosis survival in infected macrophages. *Cell* **119**, 753 (Dec 17, 2004).

44. K. A. Rich, C. Burkett, P. Webster, Cytoplasmic bacteria can be targets for autophagy. *Cellular microbiology* **5**, 455 (Jul, 2003).

45. M. I. Colombo, Pathogens and autophagy: subverting to survive. *Cell death and differentiation* **12 Suppl 2**, 1481 (Nov, 2005).

46. G. J. Howell, Z. G. Holloway, C. Cobbold, A. P. Monaco, S. Ponnambalam, Cell biology of membrane trafficking in human disease. *International review of cytology* **252**, 1 (2006).

47. C. A. Kaiser, R. Schekman, Distinct sets of SEC genes govern transport vesicle formation and fusion early in the secretory pathway. *Cell* **61**, 723 (May 18, 1990).

48. P. Novick, R. Schekman, Secretion and cell-surface growth are blocked in a temperature-sensitive mutant of Saccharomyces cerevisiae. *Proceedings of the National Academy of Sciences of the United States of America* **76**, 1858 (Apr, 1979).

49. W. E. Balch, W. G. Dunphy, W. A. Braell, J. E. Rothman, Reconstitution of the transport of protein between successive compartments of the Golgi measured by the coupled incorporation of N-acetylglucosamine. *Cell* **39**, 405 (Dec, 1984).

50. T. Sollner *et al.*, SNAP receptors implicated in vesicle targeting and fusion. *Nature* **362**, 318 (Mar 25, 1993).

51. Y. Hata, C. A. Slaughter, T. C. Sudhof, Synaptic vesicle fusion complex contains unc-18 homologue bound to syntaxin. *Nature* **366**, 347 (Nov 25, 1993).

52. M. S. Perin, V. A. Fried, G. A. Mignery, R. Jahn, T. C. Sudhof, Phospholipid binding by a synaptic vesicle protein homologous to the regulatory region of protein kinase C. *Nature* **345**, 260 (May 17, 1990).

53. J. Armstrong, Yeast vacuoles: more than a model lysosome. *Trends in cell biology* **20**, 580 (Oct, 2010).

54. C. Ungermann, B. J. Nichols, H. R. Pelham, W. Wickner, A vacuolar v-t-SNARE complex, the predominant form in vivo and on isolated vacuoles, is disassembled and activated for docking and fusion. *The Journal of cell biology* **140**, 61 (Jan 12, 1998).

55. J. P. Luzio, P. R. Pryor, N. A. Bright, Lysosomes: fusion and function. *Nature reviews. Molecular cell biology* **8**, 622 (Aug, 2007).

56. K. M. Collins, W. T. Wickner, Trans-SNARE complex assembly and yeast vacuole membrane fusion. *Proceedings of the National Academy of Sciences of the United States of America* **104**, 8755 (May 22, 2007).

57. A. Mayer, W. Wickner, Docking of yeast vacuoles is catalyzed by the Ras-like GTPase Ypt7p after symmetric priming by Sec18p (NSF). *The Journal of cell biology* **136**, 307 (Jan 27, 1997).

58. C. Stroupe, K. M. Collins, R. A. Fratti, W. Wickner, Purification of active HOPS complex reveals its affinities for phosphoinositides and the SNARE Vam7p. *EMBO J* **25**, 1579 (Apr 19, 2006).

59. T. Nishi, M. Forgac, The vacuolar (H+)-ATPases--nature's most versatile proton pumps. *Nature reviews. Molecular cell biology* **3**, 94 (Feb, 2002).

60. D. Mijaljica, M. Prescott, R. J. Devenish, V-ATPase engagement in autophagic processes. *Autophagy* **7**, 666 (Jun, 2011).

61. B. Strasser, J. Iwaszkiewicz, O. Michielin, A. Mayer, The V-ATPase proteolipid cylinder promotes the lipid-mixing stage of SNARE-dependent fusion of yeast vacuoles. *The EMBO journal* **30**, 4126 (Oct 19, 2011).

62. C. Peters *et al.*, Trans-complex formation by proteolipid channels in the terminal phase of membrane fusion. *Nature* **409**, 581 (Feb 1, 2001).

63. M. J. Bayer, C. Reese, S. Buhler, C. Peters, A. Mayer, Vacuole membrane fusion: V0 functions after trans-SNARE pairing and is coupled to the Ca2+-releasing channel. *The Journal of cell biology* **162**, 211 (Jul 21, 2003).

64. W. R. Williamson, D. Wang, A. S. Haberman, P. R. Hiesinger, A dual function of V0-ATPase a1 provides an endolysosomal degradation mechanism in Drosophila melanogaster photoreceptors. *The Journal of cell biology* **189**, 885 (May 31, 2010).

65. A. M. Krachler, A. R. Woolery, K. Orth, Manipulation of kinase signaling by bacterial pathogens. *The Journal of cell biology* **195**, 1083 (Dec 26, 2011).

66. K. Matlawska-Wasowska *et al.*, The Vibrio parahaemolyticus Type III Secretion Systems manipulate host cell MAPK for critical steps in pathogenesis. *BMC microbiology* **10**, 329 (2010).

67. T. Shimohata *et al.*, Vibrio parahaemolyticus infection induces modulation of IL-8 secretion through dual pathway via VP1680 in Caco-2 cells. *The Journal of infectious diseases* **203**, 537 (Feb 15, 2011).

68. S. Matsuda, N. Okada, T. Kodama, T. Honda, T. Iida, A cytotoxic type III secretion effector of Vibrio parahaemolyticus targets vacuolar H+-ATPase subunit c and ruptures host cell lysosomes. *PLoS Pathog* **8**, e1002803 (2012).

69. B. Turk, V. Turk, Lysosomes as "suicide bags" in cell death: myth or reality? *The Journal of biological chemistry* **284**, 21783 (Aug 14, 2009).

70. H. Ham, A. Sreelatha, K. Orth, Manipulation of host membranes by bacterial effectors. *Nature reviews. Microbiology* **9**, 635 (Sep, 2011).

71. D. L. Burdette, J. Seemann, K. Orth, Vibrio VopQ induces PI3-kinase-independent autophagy and antagonizes phagocytosis. *Molecular microbiology* **73**, 639 (Aug, 2009).

72. P. Slusarewicz, Z. Xu, K. Seefeld, A. Haas, W. T. Wickner, I2B is a small cytosolic protein that participates in vacuole fusion. *Proc Natl Acad Sci U S A* **94**, 5582 (May 27, 1997).

73. L. Wang, A. J. Merz, K. M. Collins, W. Wickner, Hierarchy of protein assembly at the vertex ring domain for yeast vacuole docking and fusion. *The Journal of cell biology* **160**, 365 (Feb 3, 2003).

74. V. J. Starai, Y. Jun, W. Wickner, Excess vacuolar SNAREs drive lysis and Rab bypass fusion. *Proceedings of the National Academy of Sciences of the United States of America* **104**, 13551 (Aug 21, 2007).

75. N. Perzov, V. Padler-Karavani, H. Nelson, N. Nelson, Characterization of yeast V-ATPase mutants lacking Vph1p or Stv1p and the effect on endocytosis. *J Exp Biol* **205**, 1209 (May, 2002).

76. C. J. Roberts, C. K. Raymond, C. T. Yamashiro, T. H. Stevens, Methods for studying the yeast vacuole. *Methods Enzymol* **194**, 644 (1991).

77. D. Arac *et al.*, Close membrane-membrane proximity induced by Ca(2+)-dependent multivalent binding of synaptotagmin-1 to phospholipids. *Nat Struct Mol Biol* **13**, 209 (Mar, 2006).

78. X. Chen *et al.*, SNARE-mediated lipid mixing depends on the physical state of the vesicles. *Biophysical journal* **90**, 2062 (Mar 15, 2006).

79. S. M. Mumby, Subcellular localization of G protein subunits. *Methods Enzymol* **344**, 383 (2002).

80. H. Zheng, W. Liu, L. Y. Anderson, Q. X. Jiang, Lipid-dependent gating of a voltage-gated potassium channel. *Nat Commun* **2**, 250 (2011).

81. A. Haas, A quantitative assay to measure homotypic fusion in vitro. *Methods Cell Sci* **17**, 283 (1995).

82. Y. Jun, W. Wickner, Assays of vacuole fusion resolve the stages of docking, lipid mixing, and content mixing. *Proceedings of the National Academy of Sciences of the United States of America* **104**, 13010 (Aug 7, 2007).

83. B. Ma, Y. Xiang, L. An, Structural bases of physiological functions and roles of the vacuolar H(+)-ATPase. *Cell Signal* **23**, 1244 (Aug, 2011).

84. Y. Kabeya *et al.*, LC3, a mammalian homologue of yeast Apg8p, is localized in autophagosome membranes after processing. *Embo J* **19**, 5720 (Nov 1, 2000).

85. E. Iwai-Kanai *et al.*, A method to measure cardiac autophagic flux in vivo. *Autophagy* **4**, 322 (Apr, 2008).

86. I. G. Ganley *et al.*, ULK1.ATG13.FIP200 complex mediates mTOR signaling and is essential for autophagy. *The Journal of biological chemistry* **284**, 12297 (May 1, 2009).

87. L. Zhang *et al.*, Requirements for the formation of membrane pores by the reovirus myristoylated micro1N peptide. *J Virol* **83**, 7004 (Jul, 2009).

88. H. Zheng, W. Liu, L. Y. Anderson, Q. X. Jiang, Lipid-dependent gating of a voltage-gated potassium channel. *Nat Commun* **2**, 250 (2011).

89. B. Hille, *Ion Channels of Excitable Membranes*. (Sinauer Associates, Inc., Sunderland, MA, USA, 2001), vol. 3rd Ed.

90. H. Ham, A. Sreelatha, K. Orth, Manipulation of host membranes by bacterial effectors. *Nat Rev Microbiol* **9**, 635 (Sep, 2011).

91. C. Cang *et al.*, mTOR regulates lysosomal ATP-sensitive two-pore Na(+) channels to adapt to metabolic state. *Cell* **152**, 778 (Feb 14, 2013).

92. A. Efeyan, D. M. Sabatini, mTOR and cancer: many loops in one pathway. *Curr Opin Cell Biol* **22**, 169 (Apr, 2010).

93. K. Matlawska-Wasowska *et al.*, The Vibrio parahaemolyticus Type III Secretion Systems manipulate host cell MAPK for critical steps in pathogenesis. *BMC Microbiol* **10**, 329 (2010).

94. T. Shimohata *et al.*, Vibrio parahaemolyticus infection induces modulation of IL-8 secretion through dual pathway via VP1680 in Caco-2 cells. *J Infect Dis* **203**, 537 (Feb 15, 2011).

95. D. Chuderland, R. Seger, Calcium regulates ERK signaling by modulating its protein-protein interactions. *Commun Integr Biol* **1**, 4 (2008).

96. F. Stavru, F. Bouillaud, A. Sartori, D. Ricquier, P. Cossart, Listeria monocytogenes transiently alters mitochondrial dynamics during infection. *Proceedings of the National Academy of Sciences of the United States of America* **108**, 3612 (Mar 1, 2011).

97. P. R. Hiesinger *et al.*, The v-ATPase V0 subunit a1 is required for a late step in synaptic vesicle exocytosis in Drosophila. *Cell* **121**, 607 (May 20, 2005).

98. W. Wickner, Yeast vacuoles and membrane fusion pathways. *The EMBO journal* **21**, 1241 (Mar 15, 2002).

99. M. Forgac, Vacuolar ATPases: rotary proton pumps in physiology and pathophysiology. *Nature reviews. Molecular cell biology* **8**, 917 (Nov, 2007).

100. F. G. van der Goot, J. Gruenberg, Intra-endosomal membrane traffic. *Trends in cell biology* **16**, 514 (Oct, 2006).

101. S. Poea-Guyon *et al.*, The V-ATPase membrane domain is a sensor of granular pH that controls the exocytotic machinery. *The Journal of cell biology* **203**, 283 (Oct 28, 2013).

102. J. Di Giovanni *et al.*, V-ATPase membrane sector associates with synaptobrevin to modulate neurotransmitter release. *Neuron* **67**, 268 (Jul 29, 2010).

103. A. Kawai, H. Uchiyama, S. Takano, N. Nakamura, S. Ohkuma, Autophagosome-lysosome fusion depends on the pH in acidic compartments in CHO cells. *Autophagy* **3**, 154 (Mar-Apr, 2007).

104. Y. Lu *et al.*, Two pore channel 2 (TPC2) inhibits autophagosomal-lysosomal fusion by alkalinizing lysosomal pH. *The Journal of biological chemistry* **288**, 24247 (Aug 16, 2013).

105. I. G. Ganley, P. M. Wong, N. Gammoh, X. Jiang, Distinct autophagosomal-lysosomal fusion mechanism revealed by thapsigargin-induced autophagy arrest. *Molecular cell* **42**, 731 (Jun 24, 2011).

106. A. Grotemeier *et al.*, AMPK-independent induction of autophagy by cytosolic Ca2+ increase. *Cellular signalling* **22**, 914 (Jun, 2010).

107. A. Sreelatha, K. Orth, V. J. Starai, The pore-forming bacterial effector, VopQ, halts autophagic turnover. *Autophagy* **9**, 2169 (Dec, 2013).

108. T. A. Vida, S. D. Emr, A new vital stain for visualizing vacuolar membrane dynamics and endocytosis in yeast. *The Journal of cell biology* **128**, 779 (Mar, 1995).

109. A. Haas, D. Scheglmann, T. Lazar, D. Gallwitz, W. Wickner, The GTPase Ypt7p of Saccharomyces cerevisiae is required on both partner vacuoles for the homotypic fusion step of vacuole inheritance. *The EMBO journal* **14**, 5258 (Nov 1, 1995).

110. A. Mayer, W. Wickner, A. Haas, Sec18p (NSF)-driven release of Sec17p (alpha-SNAP) can precede docking and fusion of yeast vacuoles. *Cell* **85**, 83 (Apr 5, 1996).

111. G. Eitzen, E. Will, D. Gallwitz, A. Haas, W. Wickner, Sequential action of two GTPases to promote vacuole docking and fusion. *The EMBO journal* **19**, 6713 (Dec 15, 2000).

112. L. Wang, A. J. Merz, K. M. Collins, W. Wickner, Hierarchy of protein assembly at the vertex ring domain for yeast vacuole docking and fusion. *The Journal of cell biology* **160**, 365 (Feb 3, 2003).

113. L. Wang, E. S. Seeley, W. Wickner, A. J. Merz, Vacuole fusion at a ring of vertex docking sites leaves membrane fragments within the organelle. *Cell* **108**, 357 (Feb 8, 2002).

114. A. J. Merz, W. T. Wickner, Trans-SNARE interactions elicit Ca2+ efflux from the yeast vacuole lumen. *The Journal of cell biology* **164**, 195 (Jan 19, 2004).

115. C. Peters, A. Mayer, Ca2+/calmodulin signals the completion of docking and triggers a late step of vacuole fusion. *Nature* **396**, 575 (Dec 10, 1998).

116. C. Ungermann, W. Wickner, Vam7p, a vacuolar SNAP-25 homolog, is required for SNARE complex integrity and vacuole docking and fusion. *The EMBO journal* **17**, 3269 (Jun 15, 1998).

117. C. Ungermann, W. Wickner, Z. Xu, Vacuole acidification is required for trans-SNARE pairing, LMA1 release, and homotypic fusion. *Proceedings of the National Academy of Sciences of the United States of America* **96**, 11194 (Sep 28, 1999).

118. S. O. Sorensen, H. B. van den Hazel, M. C. Kielland-Brandt, J. R. Winther, pH-dependent processing of yeast procarboxypeptidase Y by proteinase A in vivo and in vitro. *European journal of biochemistry / FEBS* **220**, 19 (Feb 15, 1994).

119. C. Reese, F. Heise, A. Mayer, Trans-SNARE pairing can precede a hemifusion intermediate in intracellular membrane fusion. *Nature* **436**, 410 (Jul 21, 2005).

120. E. M. Coonrod *et al.*, Homotypic vacuole fusion in yeast requires organelle acidification and not the V-ATPase membrane domain. *Developmental cell* **27**, 462 (Nov 25, 2013).

121. W. Wickner, Membrane fusion: five lipids, four SNAREs, three chaperones, two nucleotides, and a Rab, all dancing in a ring on yeast vacuoles. *Annual review of cell and developmental biology* **26**, 115 (2010).

122. F. Peri, C. Nusslein-Volhard, Live imaging of neuronal degradation by microglia reveals a role for v0-ATPase a1 in phagosomal fusion in vivo. *Cell* **133**, 916 (May 30, 2008).

123. J. Mima, W. Wickner, Phosphoinositides and SNARE chaperones synergistically assemble and remodel SNARE complexes for membrane fusion. *Proceedings of the National Academy of Sciences of the United States of America* **106**, 16191 (Sep 22, 2009).

124. C. Stroupe, C. M. Hickey, J. Mima, A. S. Burfeind, W. Wickner, Minimal membrane docking requirements revealed by reconstitution of Rab GTPase-dependent membrane fusion from purified components. *Proceedings of the National Academy of Sciences of the United States of America* **106**, 17626 (Oct 20, 2009).

125. H. Xu, W. Wickner, Phosphoinositides function asymmetrically for membrane fusion, promoting tethering and 3Q-SNARE subcomplex assembly. *The Journal of biological chemistry* **285**, 39359 (Dec 10, 2010).

126. Y. Akeda *et al.*, Identification and characterization of a type III secretion-associated chaperone in the type III secretion system 1 of Vibrio parahaemolyticus. *FEMS microbiology letters* **296**, 18 (Jul, 2009).

127. J. Kyte, R. F. Doolittle, A simple method for displaying the hydropathic character of a protein. *Journal of molecular biology* **157**, 105 (May 5, 1982).

128. D. T. Jones, Protein secondary structure prediction based on position-specific scoring matrices. *Journal of molecular biology* **292**, 195 (Sep 17, 1999).

129. S. Kim *et al.*, Transmembrane glycine zippers: physiological and pathological roles in membrane proteins. *Proceedings of the National Academy of Sciences of the United States of America* **102**, 14278 (Oct 4, 2005).

130. A. Savchenko *et al.*, Strategies for structural proteomics of prokaryotes: Quantifying the advantages of studying orthologous proteins and of using both NMR and X-ray crystallography approaches. *Proteins* **50**, 392 (Feb 15, 2003).

131. A. M. Seddon, P. Curnow, P. J. Booth, Membrane proteins, lipids and detergents: not just a soap opera. *Biochimica et biophysica acta* **1666**, 105 (Nov 3, 2004).

132. R. Zoncu *et al.*, mTORC1 senses lysosomal amino acids through an inside-out mechanism that requires the vacuolar H(+)-ATPase. *Science* **334**, 678 (Nov 4, 2011).

133. A. Efeyan, R. Zoncu, D. M. Sabatini, Amino acids and mTORC1: from lysosomes to disease. *Trends in molecular medicine* **18**, 524 (Sep, 2012).

134. Y. Sancak *et al.*, Ragulator-Rag complex targets mTORC1 to the lysosomal surface and is necessary for its activation by amino acids. *Cell* **141**, 290 (Apr 16, 2010).

135. L. Bar-Peled, L. D. Schweitzer, R. Zoncu, D. M. Sabatini, Ragulator is a GEF for the rag GTPases that signal amino acid levels to mTORC1. *Cell* **150**, 1196 (Sep 14, 2012).

136. C. H. Jung *et al.*, ULK-Atg13-FIP200 complexes mediate mTOR signaling to the autophagy machinery. *Molecular biology of the cell* **20**, 1992 (Apr, 2009).

137. F. E. Karet *et al.*, Mutations in the gene encoding B1 subunit of H+-ATPase cause renal tubular acidosis with sensorineural deafness. *Nature genetics* **21**, 84 (Jan, 1999).

138. W. W. Shum *et al.*, Regulation of V-ATPase recycling via a RhoA- and ROCKII-dependent pathway in epididymal clear cells. *American journal of physiology. Cell physiology* **301**, C31 (Jul, 2011).

139. F. L. Yuan *et al.*, The vacuolar ATPase in bone cells: a potential therapeutic target in osteoporosis. *Molecular biology reports* **37**, 3561 (Oct, 2010).

140. S. R. Sennoune *et al.*, Vacuolar H+-ATPase in human breast cancer cells with distinct metastatic potential: distribution and functional activity. *American journal of physiology. Cell physiology* **286**, C1443 (Jun, 2004).

141. Z. E. Newby *et al.*, A general protocol for the crystallization of membrane proteins for X-ray structural investigation. *Nature protocols* **4**, 619 (2009).

142. J. Phan, J. E. Tropea, D. S. Waugh, Structure of the Yersinia pestis type III secretion chaperone SycH in complex with a stable fragment of YscM2. *Acta crystallographica. Section D, Biological crystallography* **60**, 1591 (Sep, 2004).

143. F. Gorrec, The MORPHEUS protein crystallization screen. *Journal of applied crystallography* **42**, 1035 (Dec 1, 2009).